Chromatic Dispersion Monitoring for Next Generation Optical Networks

Liu Ning

School of Electrical and Electronic Engineering

A thesis submitted to the Nanyang Technological University
in fulfillment of the requirement for the degree of
Doctor of Philosophy

2008

Statement of Originality

I hereby declare that the work embodied in this thesis is the result of original research and has not been submitted for a higher degree to any other university or institution, except where due reference or acknowledgement has been made in the text of the thesis.

_____ _____

Date Liu Ning

Abstract

Chromatic dispersion (CD) is one of the major factors limiting optical transmission distance. Therefore, it is essential to monitor the residual CD of individual wavelength channels so as to ensure that the residual CD does not exceed the designed tolerance. This thesis documents the investigations of cost-effective and high performance CD monitoring techniques.

Different techniques for CD monitoring are thoroughly reviewed in the thesis. Among them, tracking the power of radio frequency (RF) tones is relatively simple and effective for CD monitoring. However, this technique may be influenced by the power loss or gain of optical transmission links. To address this issue, an improved CD monitoring method based on the RF power ratio is proposed. It is shown that, with an inserted dispersion offset, the CD monitoring range and accuracy (or sensitivity) can be greatly improved by selecting appropriate RF frequencies and dispersion offsets. Adequate modulation index of the RF tone should be chosen so as to acquire a large monitoring range with a small power penalty. By employing an RF tone removal scheme, the power penalty induced by the RF tones can be further reduced.

Polarization mode dispersion (PMD), self-phase modulation (SPM), cross-phase modulation (XPM) and chirp parameter of external modulator may influence the accuracy of the CD monitoring. The effects of PMD, SPM, XPM and chirp on CD monitoring are investigated in the thesis. It is shown that the presence of these effects induces significant CD monitoring errors. To tackle this problem, a new CD

monitoring technique is proposed, which can effectively suppress the impacts due to PMD, SPM, XPM and chirp. Both experiments and simulations show that the PMD, SPM, and XPM effects can be eliminated or suppressed by optically sideband filtering and DSB/SSB RF power ratio detection, and the monitoring error induced by the small chirp fluctuation can be suppressed using two RF tones and a CD offset. Other degradation effects on the CD monitoring are also discussed.

Furthermore, the thesis presents a new CD monitoring technique for DPSK signals by detecting the power of the clock tone as well as an added RF tone. A new transmitter configuration is proposed for simultaneous generation of an RF tone and a DPSK data signal using only a single dual electrode Mach-Zehnder modulator (DE-MZM). The RF tone induced power penalty to the DPSK signal is investigated. By introducing one bit delay interferometer (DI) used for DPSK demodulation, the RF tone influence can be suppressed. Experimental and simulation results show that the technique can significantly improve the CD monitoring capability and the DI can greatly suppress the RF tone induced power penalty if the RF tone has a frequency close to the half data bit-rate. The proposed transmitter configuration is applied to optical label switching systems, and it is shown that the use of the proposed transmitter can simultaneously generate a DPSK payload and an SCM label. This SCM label can be exploited for CD monitoring. Investigations on the impacts of the subcarrier frequency, label bit-rate, and modulation index on both the DPSK payload and the label demonstrate that the technique provides good transmission performance for both the DPSK payload and the label signal without requiring an additional label eraser.

Acknowledgements

I would like to thank everybody who contributed in so many ways, great and small, to my ideas and work during my Ph. D. studies.

My first thanks go to my supervisor, Associate Professor Zhong Wen-De. The beneficial discussions with him always help me out of difficulties and bring ideas to solve the problems. This dissertation cannot be completed without his guidance and encouragement. Dr. Wen Yang Jing also deserves great acknowledgement for all the expertise instructions. He unselfishly shared his experience and views on my studies and I definitely benefited a lot from them. I would also like to thank and acknowledge Associate Professor Cheng Tee Hiang, Professor Lu Chao, Associate Professor Shum Ping and Dr. Wang Yixin for their continuous support during the past several years.

I am fortunate enough to know and work with many talented students and staff at NTU. I wish to thank Dr. Li Zhaohui, Dr. Cheng Linghao, Dr. Tang Ming, and Dr. Fu Songnian, for many valuable discussions and collaborations. Appreciation is also extended to all students and staff in NTRC and all the other friends in Singapore for their care and friendship in my joyful life here.

Finally yet importantly, I would like to appreciate my family. In spite of enduring many difficulties, they have been always there with their encouragement and support, without which I would not be where I am today. The thesis is dedicated to my father, Liu Yongyi and my grandfather, Liu Heyan, who have left me during my Ph. D. studies. Hope the thesis can comfort their soul.

Table of Contents

List of Acronyms

AC	alternating current
AM	amplitude modulation
ASE	amplified spontaneous emission
ASK	amplitude shift keying
AWG	arrayed waveguide grating
BER	bit-error-rate
BERT	bit-error-rate tester
BPF	bandpass filter
CD	chromatic dispersion
CDR	clock data recovery
CNR	carrier-to-noise ratio
CW	continuous wave
DC	direct current
DCF	dispersion compensating fiber
DE-MZM	dual electrode Mach-Zehnder modulator
DGD	differential group delay
DI	delay interferometer
DPSK	differential phase-shift keying
DQPSK	differential quadrature phase-shift keying
DSB	double sideband
DWDM	dense wavelength division multiplexing

EDFA	erbium-doped fiber amplifier
ETDM	electrical time-division multiplexing
FBG	fiber Bragg grating
FM	frequency modulation
FSR	free spectral range
FTTH	fiber-to-the-home
GVD	group velocity dispersion
LPF	low pass filter
LSB	lower sideband
MMF	multimode fiber
MSK	minimum-shift keying
MZI	Mach-Zehnder interferometer
MZM	Mach-Zehnder modulator
NRZ	nonreturn-to-zero
NZDSF	nonzero dispersion shifted fiber
OBPF	optical band-pass filter
OLS	optical label switching
OOK	on-off-keying
OPM	optical performance monitoring
OSNR	optical signal-to-noise ratio
OTDM	optical time-division multiplexing
OXC	optical crossconnect
PM	phase modulation
PMD	polarization mode dispersion

PPG	pulse pattern generator
PRBS	pseudo-random bit series
PSP	principal states of polarization
PZT	piezoelectric transducer
RF	radio frequency
RFSA	radio frequency spectrum analyzer
ROADM	reconfigurable optical add-drop multiplexer
RZ	return-to-zero
SBS	stimulated Brillouin scattering
SCM	subcarrier multiplexing
SMF	single-mode fiber
SPM	self-phase modulation
SRS	stimulated Raman scattering
SSB	single sideband
TDC	tunable dispersion compensator
TDM	time-division multiplexing
TPA	two-photon absorption
USB	upper sideband
VNA	vector network analyzer
VOA	variable optical attenuator
VSB	vestigial-sideband
WDM	wavelength division multiplexing
XGM	cross-gain modulation
XPM	cross-phase modulation

List of Figures

List of Tables

Chapter 1

Introduction

1.1 Background and Motivations

The use of optical carrier for telecommunications purpose can be traced back to more than one hundred years ago, when Alexander Graham Bell reported the experiment in which the speech was transmitted by using a beam [1]. Modern optical communications originated with the invention of the laser in 1960s [1]. The development of optical fiber communication systems began in the 1970s with the appearance of low loss optical fibers [1], and continued with the advent of optical amplifiers [2] in the late 1980s and early 1990s. From the late 1990s, with the explosive and continuous growth of the Internet and related services, the demand for telecommunications capacity has been continuously increasing. The Internet traffic volume has been growing exponentially (around 50% or more per annum), and this growth is expected to continue with the wide deployment of new triple play (voice, data and video) high-speed services and increasing penetration of fiber-to-the-home

(FTTH) and other emerging broadband services to end-users in the future [3-6]. Therefore, new components and transmission technologies are required for the increasing demand for the transmission capacities.

High-speed time-division multiplexing (TDM) technology has been planned to meet the growth in capacity demanded by the Internet. 40-Gb/s electrical time-division multiplexing (ETDM) systems have been studied for replacement of the current 10-Gb/s systems [7]. Recently, 107-Gbit/s ETDM transmitter has been presented for 100G Ethernet transport [8]. Moreover, transmission experiments with channel rates above 640 Gb/s have been demonstrated using optical time-division multiplexing (OTDM) techniques [9]. Nevertheless, the approach of increasing channel rate is only expandable to a certain level. Fortunately, the development of wavelength division multiplexing (WDM) technology has dramatically increased transmission capacities. This is the technology to send many independent optical channels with different carrier wavelengths on a single fiber. Presently, more than 300 wavelengths can be transmitted simultaneously [10] and the wavelength spacing is as narrow as 12.5 GHz [11]. With the dense wavelength division multiplexing (DWDM) technology, 3.2-Tb/s (40 channel × 85 Gb/s) systems with 1.6-b/s/Hz spectrally efficient have been achieved over 1,700-km standard single-mode fiber (SMF) transmission [12].

However, these evolutions also lead to the increased significance and complexity for network management. In long haul high capacity optical fiber communication systems, the signal quality in an optical channel can be affected by various factors of increasing importance. For the efficient network management and establishment of protection and restoration, it is vitally important to monitor the quality of transported

signals. In addition, it is also important to identify the sources leading to signal degradation for effective compensation. These new requirements make the optical performance monitoring (OPM) become more and more important for next generation WDM networks [13].

There are various sources that may cause optical signal transmission impairments, including attenuation, dispersion and fiber nonlinearity. With the realization of optical amplifiers, fiber attenuation is no longer a major limiting factor for optical communication systems. However, the chromatic dispersion (CD) induced degradation of the transmitted signals accumulates over cascaded optically amplified transmission spans. By keeping the launched optical power reasonably low, the fiber nonlinearity can be well controlled. As a result, chromatic dispersion of optical channels will limit the attainable distance in optical fiber communication systems.

Chromatic dispersion occurs due to the fact that different frequency components of the light travel through fiber at different speeds. Any information-bearing signal is composed of a range of frequency components. As a light pulse travels through a length of SMF, some frequencies arrive before others. In particular, for a digital signal that is intensity modulated to an optical carrier, chromatic dispersion causes the broadening of signal pulses and leads to overlapping of adjacent pulses, resulting in erroneous signal transmission. With the dispersion only, the extent of pulse broadening increases linearly with transmission distance. This will limit the maximum transmission distance.

Although it is possible to manufacture fibers that induce zero chromatic dispersion, the effects of chromatic dispersion still exist in most optical communication systems. On the one hand, this is because that most of today's optical communication systems are working near 1.55 μm and transmitting on the installed standard SMF cables whose zero dispersion wavelengths are 1.31 μm. The chromatic dispersion of standard SMFs is about 17 ps/(nm·km) at 1.55 μm. On the other hand, when the fiber dispersion is near zero in a DWDM system, different channels travel at almost the same speed. This would strengthen the fiber nonlinear effects (such as four wave mixing (FWM)) which would in turn degrade the transmitted signals. Therefore, although the zero dispersion wavelength can be shifted to 1.55-μm region by designed fiber refractive-index profile, the fiber with zero dispersion value is undesired for the deployment of DWDM systems.

The dispersion tolerances of optical communication systems decrease with the bit rate. Chromatic dispersion limits a 2.5-Gb/s channel to roughly 900 km (1-dB power penalty), and a 10-Gb/s and 40-Gb/s channel to approximately 60 km and 4 km, respectively [14]. As a result, for upgrading the data rate of existing fiber cables, chromatic dispersion compensation is necessary. Traditionally, chromatic dispersion compensation can be achieved by using dispersion compensating fiber (DCF). However, as reported in [15, 16], the statistically distributed chromatic dispersion of optical fiber results in residual dispersion in the channels using only the DCF module. The chromatic dispersion can also vary with changes in environmental conditions such as ambient temperature, pressure, and strain [17]. Furthermore, daily maintenance and future upgrade of an optical system may change the accumulated chromatic dispersion. In addition, with the introduction of network elements such as

optical crossconnects (OXCs) and reconfigurable optical add-drop multiplexers (ROADMs), a given channel's accumulated chromatic dispersion may change with dynamic reconfigurations of the network. Therefore, it is essential to monitor the accumulated chromatic dispersion of individual optical channels so as to ensure that the accumulated chromatic dispersion would not exceed the specified value and cause severe degradation to optical signals.

1.2 Objectives

Although extensive works have been carried out for monitoring chromatic dispersion, the existing techniques exhibit some disadvantages such as low monitoring sensitivity and narrow monitoring range, complex and costly system configuration, susceptible to other effects (see Chapter 2 for details, where a detailed review of the existing techniques is presented). The main objectives of this work are:

- To propose novel and practical optical performance monitoring techniques capable of in-line measuring accumulated chromatic dispersion of individual optical channels in WDM systems. The methods should not affect data signals while the data are being transmitted through the optical network. Moreover, they should be simple to implement, that is, simple and cost-effective.

- To investigate and improve the monitoring capability of chromatic dispersion monitoring technique. The monitoring capability includes the monitoring sensitivity and range. For providing fault diagnosis and network protection to

avoid communication service interruption, the monitoring method should have high sensitivity to track the dispersion variation before CD causes severe transmission errors. The monitoring range should be as large as possible to acquire the effective and strong dispersion compensation ability.

- To analyze the accuracy of chromatic dispersion monitoring technique. The results of chromatic dispersion monitoring may suffer from various optical transmission impairments such as polarization mode dispersion (PMD), modulator chirp, self-phase and cross-phase modulation. To reduce chromatic dispersion monitoring errors, a technique which can isolate chromatic dispersion from other impairments is desirable.

- To extend this monitoring technique into more advanced modulation formats. In long-haul high-capacity WDM systems, the use of advanced modulation formats has been demonstrated as an effective scheme to manage signal impairments and attracted significant attention recently. However, little work has been done on chromatic dispersion monitoring for those advanced modulation formats. Therefore, another objective is to present a chromatic dispersion monitoring scheme for advanced modulation formats.

1.3 Major Contributions of the Thesis

The main contributions of this thesis are listed below:

- The proposal of an optical performance monitoring technique with improved monitoring range and accuracy. The proposed technique is capable of in-line measuring the accumulated chromatic dispersion of separated optical channels in WDM systems. It is based on the radio frequency (RF) power ratio detection and dispersion offset insertion. The theoretical analysis of RF power is conducted by considering the modulator's chirp, chromatic dispersion, fiber attenuation and the components' gain or loss. Using the RF power ratio, the dispersion monitoring errors induced by the attenuation or gain of the optical channel can be eliminated, and the insertion of the dispersion offset greatly improves the monitoring capability, i.e., higher sensitivity and wider monitoring range. Furthermore, an RF tone removal scheme is presented to reduce the power penalty induced by the added RF tones.

- The analysis and investigation of the impacts of other signal degradation effects on RF tone based chromatic dispersion monitoring. An expression for the power fading of an RF signal is derived by considering not only CD, but also PMD. A novel and practical double sideband (DSB) / single sideband (SSB) RF power ratio detection technique with an optical sideband filtering and inserted dispersion offset is proposed. A general expression for the sideband filtering and DSB/SSB power ratio detection is given. Experiments and simulations show that the monitoring errors induced by other optical transmission impairments are greatly suppressed using the proposed method.

- The proposal of an RF tone based dispersion monitoring for differential phase-shift keying (DPSK) signal and a new transmitter configuration using a single dual electrode Mach-Zehnder modulator (DE-MZM) for generating DPSK signal and RF tone simultaneously. With only a single DE-MZM, the dispersion monitoring of DPSK signals is achieved with significantly improved monitoring capability. Moreover, the theoretical analysis and experimental investigation demonstrate that with the introduction of the one-bit delay interferometer (DI) suited for DPSK demodulation, the RF tone influence can be suppressed by selecting the RF tone frequency close to the half data bit-rate.

- The application of the new transmitter configuration to optical label switching (OLS) systems. DPSK payload and subcarrier multiplexing (SCM) label are generated simultaneously using this transmitter. The RF power of the label is explored for CD monitoring together with the regenerated clock tone in DPSK OLS systems. Without any additional label eraser, the SCM label influence can be greatly removed by selecting the subcarrier frequency at the half payload bit-rate.

1.4 Thesis Organization

The rest of the thesis is organized as follows. Chapter 2 first gives an overview of chromatic dispersion and dispersion compensation. Several main techniques for chromatic dispersion measurement and monitoring are surveyed.

Chapter 3 presents an improved chromatic dispersion monitoring technique based on the RF power ratio detection and dispersion offset insertion. The operational principle of this technique is introduced and discussed. The experimental results show that the RF power ratio technique can eliminate the dispersion monitoring errors induced by the loss or gain of the optical channel, and the insertion of the dispersion offset greatly improves the monitoring capability. Moreover, the system power penalty induced by the added RF tones is investigated and an RF tone removal scheme is presented to reduce the power penalty.

Chapter 4 offers a DSB/SSB RF power ratio detection technique with an optical sideband filtering and inserted dispersion offset for suppressing the CD monitoring errors induced by other impairments. Both theoretical and experimental studies show that the RF tone based CD monitoring technique experiences large errors when PMD, modulator chirp, as well as fiber nonlinear effects exist. To tackle this issue, a novel and practical DSB/SSB RF power ratio detection technique with an optical sideband filtering and inserted dispersion offset is proposed. Experiments and simulations show that the monitoring errors induced by other optical transmission impairments are greatly suppressed by this method.

In Chapter 5, the chromatic dispersion monitoring for DPSK systems are studied. Adding an RF tone to the DPSK data and detecting its power together with the regenerated clock tone, a new dispersion monitoring method is proposed for DPSK systems. Its monitoring capability, and the relationship between the RF tone induced power penalty and the RF tone frequency are discussed. A new transmitter configuration for simultaneous DPSK signal and RF tone generation is proposed for

the RF power based dispersion monitoring. This part is followed by an extended application to OLS systems. For this application, a similar DE-MZM configuration is proposed for generating DPSK payload and label simultaneously. By measuring the RF power of both the SCM label and the clock tone, dispersion can be monitored in DPSK OLS systems with good monitoring capability.

Finally, the thesis is concluded in Chapter 6 with recommendations for future research.

Chapter 2

Review of Chromatic Dispersion Monitoring

In this chapter, the chromatic dispersion (CD) and its compensation, measurement, and monitoring are reviewed. The origin of chromatic dispersion is first introduced. Then the fixed and tunable CD compensation is discussed for illustrating the necessity of CD monitoring. In Section 2.3, two conventional CD measurement methods are presented. Their operational principles are useful for exploring CD monitoring. Finally, a survey for some existing CD monitoring techniques is given in detail.

2.1 Chromatic Dispersion

With the advent of optical amplifiers, fiber loss is no longer a major limiting factor for optical communication systems. However, dispersion-induced degradation of the transmitted signal accumulates over multiple amplified fiber transmission spans. As a

result, the chromatic dispersion of the channel becomes the major factor limiting the attainable distance in high-speed transmission systems.

There are two different types of dispersion in optical fibers: intermodal dispersion and intramodal dispersion. Intermodal dispersion only occurs in multimode fibers (MMFs). Multimode fiber may support hundreds of modes traveling in it. The light energy distributed among the modes is delayed by different amounts because each mode propagates along the fiber at different speeds. The intermodal dispersion in multimode fibers leads to considerable broadening of optical pulses.

When the injected pulses are transported by a single-mode fiber (SMF), intermodal dispersion would not take place. However, pulse broadening does not disappear all together. This is because a sequence of optical light pulses contains a band of frequencies, and different frequency components of the light pulses travel through a SMF at different speeds. This leads to pulse broadening and signal energy overlapping. Such a dispersion mechanism is called as intramodal dispersion, or chromatic dispersion (CD).

As a specific spectral component at the frequency ω_0 propagates along a single-mode waveguide, the group velocity v_g is defined as:

$$v_g = \left(\frac{d\beta}{d\omega}\right)^{-1} \tag{2.1}$$

where β is the propagation constant at ω_0.

Then the group delay τ_g in the direction of propagation for a distance L is given by:

$$\tau_g = \frac{L}{v_g} = \frac{d\beta}{d\omega} L \tag{2.2}$$

If a signal pulse contains a small spread of frequencies around a carrier frequency ω_0, the propagation constant $\beta(\omega)$ varies with wavelength. Expanding $\beta(\omega)$ in a Taylor series:

$$\begin{aligned}\beta(\omega) = \beta(\omega_0) + \frac{d\beta}{d\omega}\Big|_{\omega=\omega_0}(\omega-\omega_0) + \frac{1}{2}\frac{d^2\beta}{d\omega^2}\Big|_{\omega=\omega_0}(\omega-\omega_0)^2 \\ + \frac{1}{6}\frac{d^3\beta}{d\omega^3}\Big|_{\omega=\omega_0}(\omega-\omega_0)^3 + \cdots\end{aligned} \tag{2.3}$$

Then Eq.(2.2) is written as:

$$\tau_g = \beta_1 L + \beta_2(\omega-\omega_0)L + \frac{1}{2}\beta_3(\omega-\omega_0)^2 L + \cdots \tag{2.4}$$

where β_1, β_2 and β_3 are the first, second and third derivative of the propagation constant with respect to the frequency at ω_0.

If the spectral width of the pulse is $\Delta\omega$, the extent of pulse broadening $\Delta\tau$ is written as:

$$\Delta\tau = \beta_2 L \cdot \Delta\omega + \frac{1}{2}\beta_3 L \cdot (\Delta\omega)^2 + \cdots \tag{2.5}$$

The factors β_2 and β_3 are known as the group velocity dispersion (GVD) parameter and third order dispersion (TOD) parameter. Usually, GVD determines how much an optical pulse will broaden on propagation inside the waveguide. TOD and higher dispersion terms are very small and can be neglected.

In some optical communication systems, the frequency spread $\Delta\omega$ is determined by the spectral width of modulated light $\Delta\lambda$. By using $\omega = 2\pi c/\lambda$, $\Delta\omega = (-2\pi c/\lambda^2)\cdot\Delta\lambda$ and neglecting high order dispersion, Eq.(2.5) can be written as:

$$\Delta\tau = DL\Delta\lambda \tag{2.6}$$

where $D = -2\pi c\beta_2/\lambda^2$ is designated as the dispersion coefficient and is expressed in units of ps/(nm·km).

CD is a result of material dispersion and waveguide dispersion. Material dispersion occurs because the refractive index of silica being used changes slightly with the optical wavelength. Some wavelengths therefore have higher group velocities and travel faster than others. Different wavelengths of a light pulse enter a fiber at the same time and leave the fiber at different time. The material dispersion equals zero when the wavelength is 1.276 μm for pure silica. This wavelength is called zero-material dispersion wavelength. It varies from 1.27 μm to 1.29 μm for optical fibers with different doped materials [2]. The material dispersion is negative below the zero-material dispersion wavelength and becomes positive above that.

Waveguide dispersion occurs because the shape and the profile of the fiber have a very significant effect on the group velocity. Each wavelength component of a pulse will have a different propagation constant β and travel at a different velocity because β is a function of a/λ (here a is the core radius) [18]. Waveguide dispersion is normally very small, yet this does not mean it can always be neglected in practical waveguides. For example, in the vicinity of the zero-material dispersion wavelength in a single-mode waveguide, waveguide dispersion plays a dominant role. If the

material dispersion and waveguide dispersion have different signs, a careful design of the waveguide dispersion can be used to cancel the material dispersion.

Although it is possible to manufacture fibers that induce zero chromatic dispersion, the effects of chromatic dispersion still exist in most optical communication systems. On the one hand, this is because that most of today's optical communication systems are working near 1.55 μm and transmitting on the installed standard single-mode fiber cables whose zero dispersion wavelengths are 1.31 μm. The chromatic dispersion of a standard single-mode fiber is about 17 ps/(nm·km) at 1.55 μm. On the other hand, when the chromatic dispersion is near zero in a DWDM system, different channels travel at almost the same speed. Thus operating at zero dispersion wavelength will strengthen the nonlinear fiber effects which tend to degrade the signal. Therefore, the fiber with zero dispersion value is not desirable for the deployment of DWDM systems.

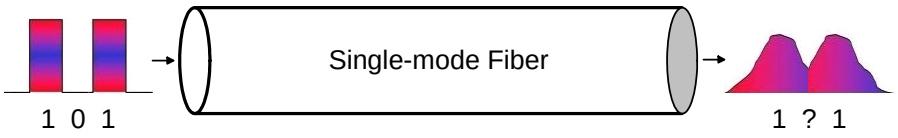

Fig. 2.1 Chromatic dispersion induced signal pulses broadening and energy overlapping.

Any information-bearing signal is composed of many different frequency components which travel at different speeds along a single-mode waveguide. In particular, for digital signal intensity modulated on an optical carrier, chromatic dispersion causes broadening of signal pulses and leads to overlapping of adjacent pulses, resulting in erroneous signal transmission, as shown in Fig. 2.1. From Eq. (2.6), the extent of

pulse broadening increases linearly with transmission distance. This will limit the maximum transmission distance at a constant bit rate of the data signal.

The conventional criterion for the effect of dispersion on distance L at bit rate B is to consider the broadening of a pulse smaller than the bit time period, that is, $\Delta\tau < 1/B$ [2]. By using $\Delta\tau$ from Eq. (2.6), the dispersion-limited distance L_D is given by:

$$L_D = \frac{1}{D \cdot B \cdot \Delta\lambda} \tag{2.7}$$

Eq.(2.7) shows that the dispersion-limited distance L_D is inversely proportional to the bit rate B. Note that the spectral width $\Delta\lambda$ is directly proportional to the bit rate B. It is because that the frequency bandwidth of a data signal is roughly of the same order of magnitude as the bit rate of the signal. For the nonreturn-to-zero (NRZ) format, the bandwidth Δf roughly equals half of the bit rate B, i.e., $\Delta f \approx B/2$ [2]. The increased bit rate will extend the Fourier-transformed frequency spectrum of the signal. Using the relation $\Delta\lambda = \frac{c}{f^2}\Delta f = \frac{\lambda^2}{c}\Delta f$, the lower limit to spectral width $\Delta\lambda$ of NRZ signal is set by the bit rate B [19]:

$$\Delta\lambda \approx \frac{\lambda^2}{2c} B \tag{2.8}$$

Substituting this into Eq. (2.7), the dispersion-limited distance L_D is expressed as follows:

$$L_D \approx \frac{2c}{DB^2\lambda^2} \tag{2.9}$$

Therefore, the dispersion-limited distance of an optical communication system decreases quadratically with the bit rate. The signal distortion induced by dispersion is crucial in high bit rate systems. A detailed calculation shows, whereas dispersion limits a 2.5-Gb/s channel to roughly 900 km (1-dB power penalty), a 10-Gb/s and 40-Gb/s channel will be limited to approximately 60 km and 4 km, respectively [14].

2.2 Dispersion Compensation

For those existing fiber cables that normally consist of standard SMF, to upgrade channel data rates, it is usually essential to employ certain type of chromatic dispersion compensation. Moreover, a small non-zero chromatic dispersion is beneficial for WDM systems because the walk-off between different wavelength channels can reduce fiber nonlinearities, especially the four wave mixing (FWM) and cross phase modulation (XPM). Therefore, although it is possible to manufacture fibers that induce zero chromatic dispersion, chromatic dispersion management is vital for high data-rate WDM systems. Fixed chromatic dispersion compensation can be used if the dispersion value of each fiber link is known and will not change with time.

The use of dispersion compensating fiber (DCF) is one of the fixed chromatic dispersion compensation approaches. Its basic principle is that inserting a length of a fiber with a negative dispersion characteristic can compensate the positive dispersion of the standard SMF. After the compensation, the total dispersion of the link will be almost zero. To achieve a DCF with a high negative-dispersion coefficient, it is

necessary to maneuver the waveguide dispersion, i.e. modify the refractive-index profile and the relative index value. It tends to have a small effective area and a high-index difference between core and cladding. Typically, a designer lowers the refractive index of the inner part of the cladding by doping fluorine [2]. The cladding trench's radius is 2.5 times larger than the core's. Fig. 2.2 shows the typical refractive index profile of DCF, where Δn is defined as refractive index relative to the cladding [14], i.e., $\Delta n = (n - n_{clad})/n_{clad}$. Here, n is the refractive index of the fiber core and n_{clad} is the refractive index of the cladding. Moreover, slope match DCF modules have been designed and fabricated for compensating many WDM channels simultaneously [20, 21]. DCF fabrication is a relatively mature technology in the fiber industry. Large-volume manufacturing of DCFs is a growing trend. However, DCF experiences some disadvantages. The negative dispersion value of DCF is not very high (its absolute value is normally five times of the one of standard SMF). To compensate the dispersion of standard SMF, a long DCF is required. Therefore, the DCF module is quite heavy and bulky, and also induces a large insertion loss. Additionally, the cross section of DCF (about 19 μm^2) is much smaller than that of SMF (about 80 μm^2) [14]. The small cross section and the long propagation length will lead to higher nonlinear fiber effects.

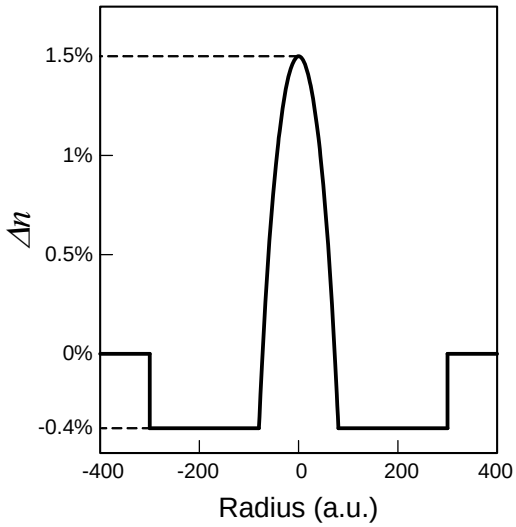

Fig. 2.2 Refractive index profile of dispersion compensating fiber.

Fiber Bragg gratings (FBGs) written with ultraviolet (UV) light into the core of an optical fiber have become important and useful components for many applications in optical fiber communication and sensor systems [22-24]. They are also widely explored in the application of dispersion compensation [23, 25].

The phase mask technique is popular for fabrications of FBGs [26]. By exposure of a fiber through a spatially periodic mask, the periodic refractive index modulation in the core of the fiber can be achieved, as shown in Fig. 2.3.

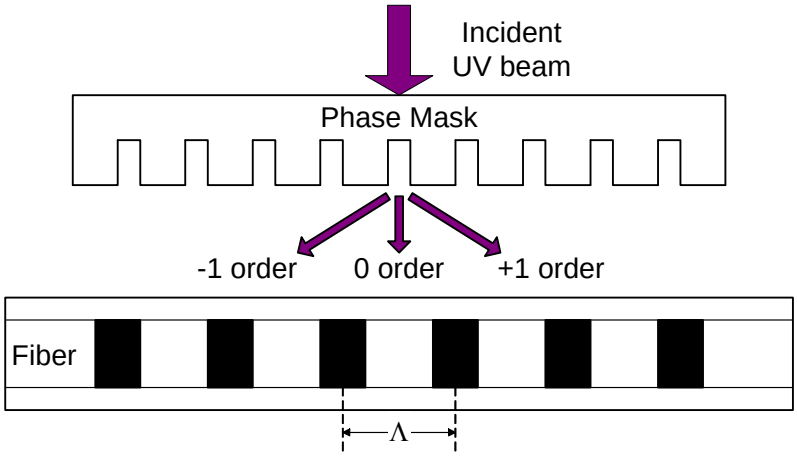

Fig. 2.3 FBG fabrication based on phase mask technique.

In Fig. 2.3, Λ is the grating pitch. The Bragg condition of the fiber grating is represented as

$$\lambda_B = 2n_{eff}\Lambda \tag{2.10}$$

where the Bragg wavelength, λ_B, is the free space center wavelength of the input light that will be back-reflected from the Bragg grating, and n_{eff} is the effective refractive index of the fiber core at the free space center wavelength. Light, guided along the core of an optical fiber, will be scattered by each grating plane. If the Bragg condition is not satisfied, the reflected light from each of the subsequent planes becomes progressively out of phase and will eventually cancel out. Thus, the light experiences very weak reflection at each of the grating planes. When the Bragg condition is satisfied, contributions of reflected light from each grating plane add constructively in the backward direction and then form a back-reflected peak with a center wavelength defined by the grating parameters.

When the optical period $n_{eff}\Lambda$ of FBG changes along the fiber length, the FBG is called chirped FBG. According Eq. (2.10), the Bragg wavelength of a chirped FBG is a function of the position along the grating, i.e., the signals with different wavelength are reflected at different positions of the FBG. It will induce a wavelength dependent time delay in the reflected optical signal. Consequently, a well-designed chirped FBG can be used to compensate CD, as shown in Fig. 2.4.

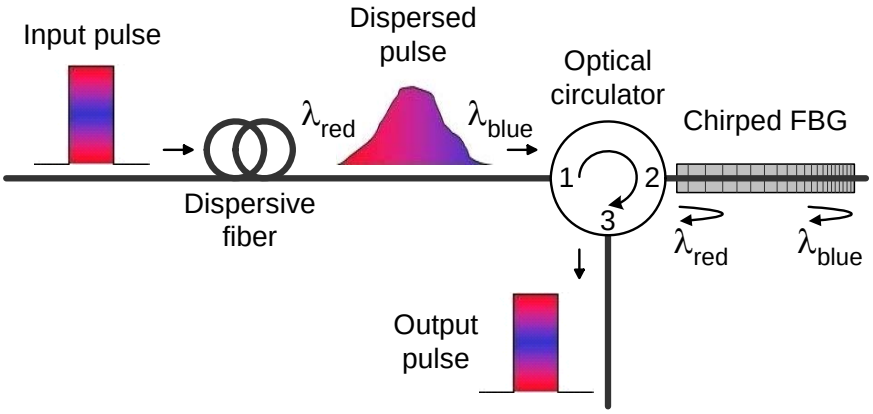

Fig. 2.4 Chirped FBG for dispersion compensation.

Compared with the DCF module, a small piece of dispersion compensating chirped FBG could compensate a large accumulated CD because of its high dispersion value. Its short length guarantees low loss, small size and low nonlinear effects at high optical power.

From the viewpoint that the periodicity of the FBG changes with the position linearly or nonlinearly, chirped FBG can be classified as two categories: linearly chirped FBG and nonlinearly chirped FBG. For a linearly chirped FBG, its relative time delay is linearly dependent on the wavelength. Then its dispersion (i.e., the slope of the time delay curve) is constant. Therefore, similar with the DCF module, linear chirped FBG

can be used in fixed dispersion compensation only when the dispersion value of each fiber link is known and will not change with time. As reported in [15, 16], the CD of optical fiber is statistically distributed instead of a fixed known value. Furthermore, a given channel's CD may change with dynamic reconfigurations of the network and variations in environmental conditions such as ambient temperature [17, 27]. Therefore, tunable dispersion compensation is essential to ensure that the accumulated CD would not exceed the specified value and cause severe degradation of optical signals anywhere and anytime.

Together with an external mechanical stretcher, nonlinearly chirped FBG is presented for tunable dispersion compensation [28]. Fig. 2.5 shows the concept. The relative time delay of a nonlinearly chirped FBG is nonlinearly dependent on the wavelength, i.e., the induced dispersion varies with the wavelength. Once such a nonlinearly chirped FBG is uniformly stretched by an external mechanical stretcher, the time delay curve is shifted uniformly toward longer wavelength. Because the time delay curve is nonlinear, the slope of the shifted curve changes at the certain wavelength, i.e., the induced dispersion changes with the external mechanical stretch. By mounting the nonlinearly chirped FBG on a piezoelectric transducer (PZT) and stretching the FBG via PZT, the dispersion can be tuned for tunable dispersion compensation.

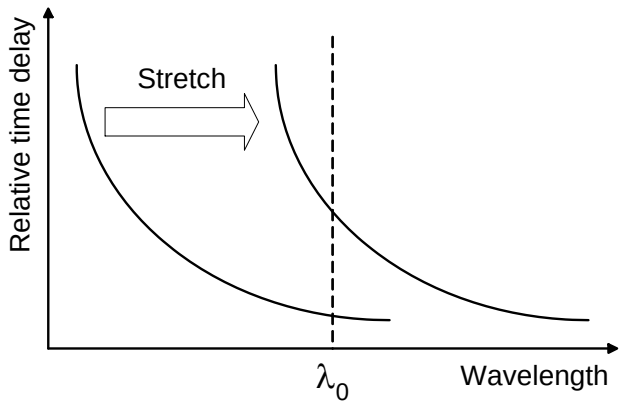

Fig. 2.5 Dispersion variation of a nonlinearly chirped FBG due to the external mechanical stretch.

Some other techniques such as virtually imaged phased array (VIPA) [29] have been proposed recently for tunable dispersion compensation. However, for controlling those tunable dispersion compensators, a dynamic feedback loop is required. Thus, an on-line chromatic dispersion monitoring subsystem is necessary for tracking the accumulated dispersion that the signal experiences and tuning the tunable dispersion compensators (TDCs).

2.3 Chromatic Dispersion Measurement

Conventionally, chromatic dispersion measurements are performed by fiber researchers and manufacturers. Most of those existing chromatic dispersion measurement methods require that the signal source and destination must be at the same location. Therefore, they are only suitable for factory and laboratory testing in which a loop-back fiber is under test. Nevertheless, their operational principles are

useful for exploring chromatic dispersion monitoring. This section gives a brief review of existing chromatic dispersion measurement techniques.

2.3.1 Modulation Phase-shift Method

Modulation phase-shift method is widely used in chromatic dispersion measurement [18, 30]. Fig. 2.6 shows the schematic of the setup.

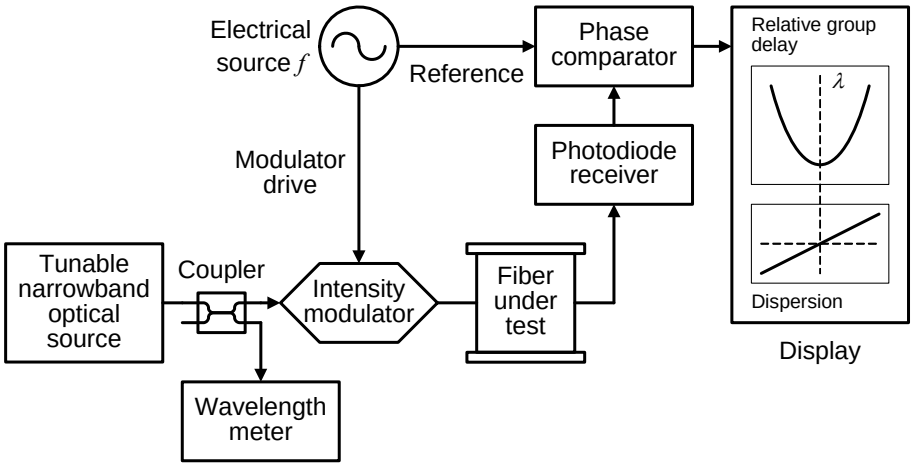

Fig. 2.6 Schematic diagram of modulation phase-shift method.

An electrical signal is used to modulate a tunable laser source with small linewidth through an external intensity modulator. The modulated optical signal propagates along a fiber or device under test and then is detected by a photodetector. A vector voltmeter is used as a phase comparator to measure the phase shift between the electrical signal source and the signal after transmission. By tuning the laser source with a small wavelength interval $\Delta\lambda$ and reiterating the phase measurement, the change of group delay of the wavelength interval $\Delta\lambda$ can be given by [18, 30]:

$$\Delta\tau_{\lambda} = \frac{\phi_{\lambda+\frac{\Delta\lambda}{2}} - \phi_{\lambda-\frac{\Delta\lambda}{2}}}{2\pi f} \tag{2.11}$$

where λ is the wavelength at the center of the interval, f is the modulation frequency and ϕ is the phase of the measured modulation.

These procedures should be repeated across the interested spectral band. The relative group delay curve can be plotted as shown in Fig. 2.6. The dispersion can be calculated by Eq. (2.6).

2.3.2 Baseband AM Response Method

Chromatic dispersion changes the relative phase of the two sidebands of amplitude modulated (AM) signals, where each sideband suffers different delays proportional to the frequency separation and the dispersion value. This effect gives the RF response a characteristic shape that can be analyzed to determine the dispersion coefficient at a given operating wavelength [31, 32]. The setup of this scheme is given in Fig. 2.7(a). A dispersive fiber of length L has been tested to verify the system performance. As shown in Fig. 2.7(a), an RF signal generated by a scalar network analyzer is used to drive an optical modulator which intensity modulates the lightwave signal from a tunable laser. After propagating through the dispersive fiber, the modulated signal is detected by the photodetector. When the two sidebands of the modulated RF signal are in counterphase and cancelled each other, the received RF signal will be very small (RF fading). Therefore, as the modulated frequency is swept, the baseband AM

response exhibits a series of dips, as shown in Fig. 2.7(b). The dispersion coefficient of fiber under test D can be calculated from these frequencies according to [31, 32]:

$$D = \frac{\left(n - \frac{1}{2}\right)c}{\lambda^2 f_n^2 L} \qquad n = 0,1,2\ldots \tag{2.12}$$

where f_n and c are the center frequency of the n-th dip in the baseband AM response, and the speed of light in vacuum, respectively.

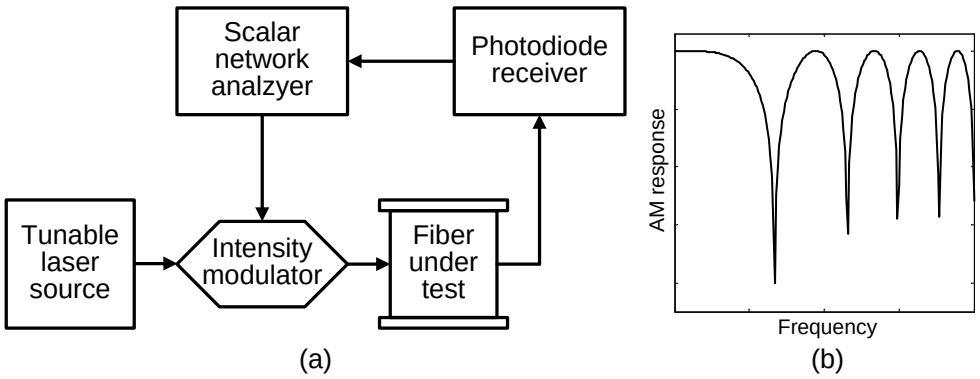

Fig. 2.7 (a) Configuration of the baseband AM response method;
(b) Baseband AM response of the swept RF signal.

2.4 Chromatic Dispersion Monitoring

For next generation high capacity all optical WDM networks, it is essential to monitor the residual CD of individual channels to ensure that the residual CD does not exceed the designed tolerance. Several CD monitoring methods have been reported. In this section, some of these methods will be reviewed.

2.4.1 Phase Shift Techniques

Because of the frequency dependent transmission speed, chromatic dispersion causes the phase shift between different frequency components. This characteristic is widely exploited in various CD monitoring techniques.

2.4.1.1 The method of phase shift between spacing-fixed WDM signals

This method makes use of the relative phase shift between spacing-fixed WDM signals [33]. Its system configuration is depicted in Fig. 2.8.

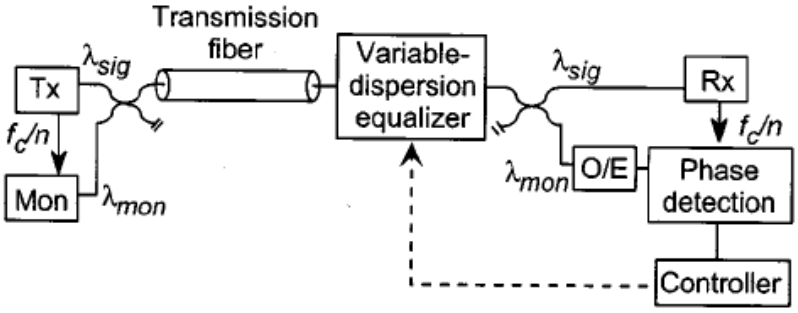

Fig. 2.8 System configuration of the relative phase shift between spacing-fixed WDM signals technique [33].

As shown in Fig. 2.8, a monitor wavelength λ_{mon} is added to the signal wavelength λ_{sig}. The monitor wavelength is intensity modulated by a clock signal which is synchronized with the clock for signal wavelength. The two wavelengths are wavelength-division multiplexed and passed through the same fiber, and demultiplexed at the receiver side. By measuring the phase shift between the extracted signal clock and monitor clock of the two channels, the relative phase

difference between the monitor wavelength and the signal wavelength is detected. Therefore, this technique can monitor the dispersion change due to the temperature variation. However, an additional wavelength is required just for CD monitoring.

2.4.1.2 Phase delay of DSB SCM method

This technique makes use of the phase delay between two sidebands of a subcarrier multiplexed (SCM) signal. With this method, a modulated double sideband (DSB) subcarrier signal is added to the baseband data at the transmitter and the phase delay between the two sidebands is measured [34, 35]. Fig. 2.9 shows a setup of this method.

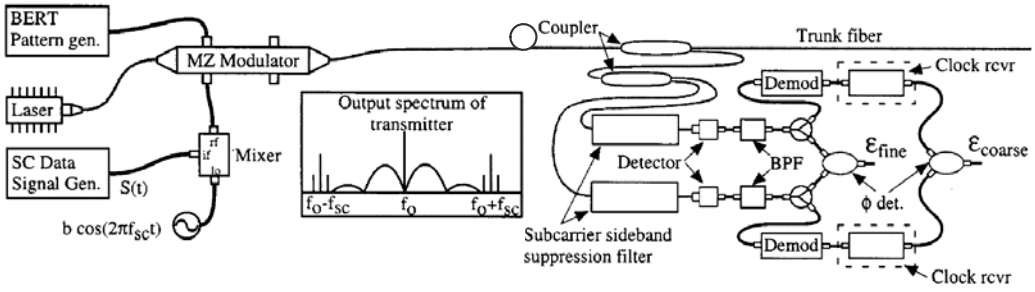

Fig. 2.9 Schematic diagram of phase delay of DSB SCM method [34, 35].

When this modulated signal propagates through a dispersive fiber, the dispersion induces a relative time delay between the two subcarrier sidebands. The delay is given by [34, 35]:

$$\Delta\tau = f_{SC} D L \lambda^2 / c \tag{2.13}$$

where λ is the optical carrier wavelength, c is the vacuum light speed, f_{SC} is the subcarrier frequency, D is the dispersion coefficient, and L is the length of fiber.

By measuring the phase difference between the two sidebands, it is possible to determine the amount of dispersion (*DL* product) the baseband signal has experienced. The shortcomings of this method are that the monitoring accuracy greatly depends on the rejection of the optical filters that separate the two sidebands, and an added subcarrier modifies the transmitter configuration, which would cause power penalty to the baseband data signal.

2.4.1.3 VSB clock phase-shift detection method

Another CD monitoring technique, which uses VSB clock phase-shift detection, does not need to add a subcarrier at the transmitter [36, 37]. It involves an optical filter that selects upper and lower vestigial-sideband (VSB) signals in the data of return-to-zero (RZ) or NRZ format, then monitors the relative clock phase-shift caused by dispersion. Either NRZ or RZ format has two optical sidebands that carry the same data information. Hence, each sideband can be selected by tuning an optical filter apart from the spectral center of the optical signal. Since these two optical sidebands occupy different wavelength ranges, fiber chromatic dispersion induces a relative group delay, which results in a clock phase-shift between the lower and upper VSB signals. Fig. 2.10 below shows the schematic diagram of this dispersion monitoring technique.

The clock phase-shift can be expressed by [36, 37]:

$$\Delta\phi = 2\pi R_b (DL)\eta \frac{\lambda^2}{c} \tag{2.14}$$

and

$$\eta = \frac{1}{2\Delta f}\int f\left[S_{USB}(f) - S_{LSB}(f)\right]df \tag{2.15}$$

where R_b is the data bit rate, and $S_{USB}(f)$ and $S_{LSB}(f)$ are the power-spectral-density functions of the upper and lower VSB signals, respectively. From equations (2.14) and (2.15), with the measured clock phase-shift $\Delta\phi$, the accumulated chromatic dispersion DL can be calculated. Note that the clock that is recovered by the receiver is used as a reference signal for phase-sensitive detection.

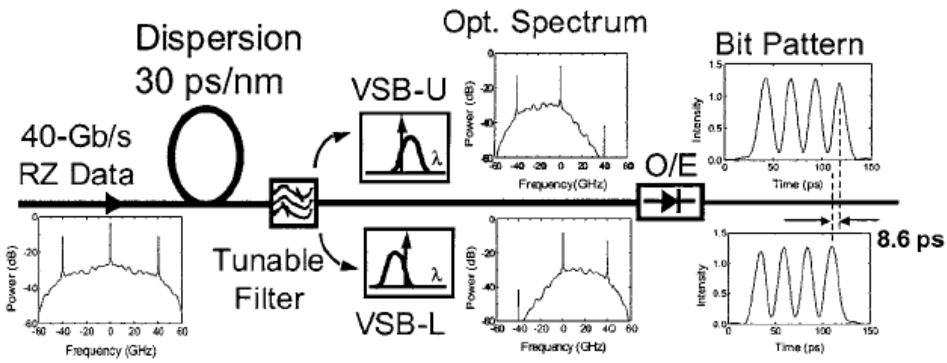

Fig. 2.10 Schematic diagram of VSB clock phase-shift detection [36, 37].

Similar to the VSB clock phase-shift detection method, some other techniques have also been proposed by comparing the phase-shift between different frequency components of the clock or data signal [38, 39].

2.4.1.4 Coherent detection method

All of the above mentioned phase shift methods utilize optical filter to extract some frequency components for monitoring purpose. More recently, a coherent detection method is proposed for CD monitoring where the filtering is implemented in the RF

domain, instead of the optical domain [40]. It combines coherent heterodyne optical detection and RF signal processing. Fig. 2.11 shows the experimental setup for this method.

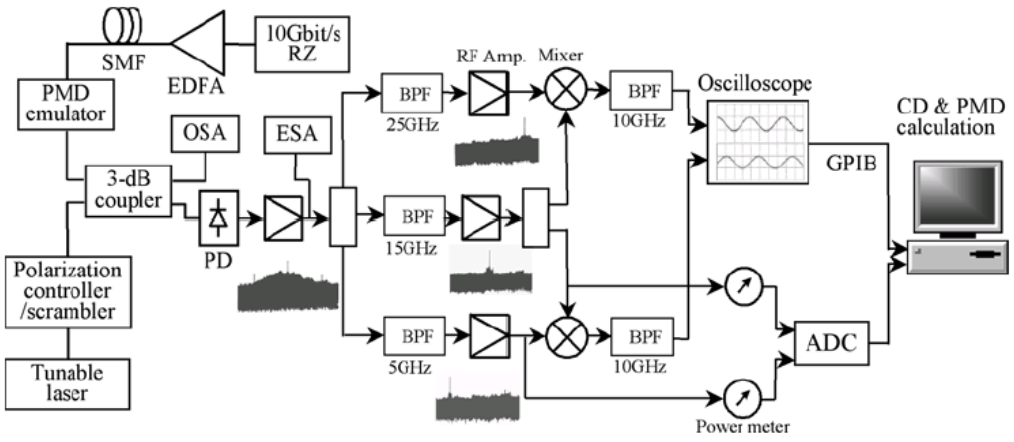

Fig. 2.11 Experimental setup for coherent detection method [40].

In this method, the light with 10-Gb/s signal transmits through fiber and combines with a light emitted from a tunable laser which has about 15-GHz frequency spacing with the signal light. The coherent detection down converts the spectrum of the optical signal into RF domain. Using a wide-band photodiode, the relative phase-delay information is preserved. In RF domain, the carrier (15 GHz) and two sidebands clocks (5 GHz and 25 GHz) are selected separately by three bandpass filters (BPFs). The carrier component is further split into two and used to mix with the upper and lower sidebands independently to generate two independent clocks. Chromatic dispersion is then evaluated from the relative time delay Δt between these two recovered clocks by [40]

$$\Delta t = \frac{DL\lambda^2 R_b}{c} \tag{2.16}$$

where D is the chromatic dispersion coefficient of the fiber, L is the fiber length, λ is the signal wavelength, c is the speed of light and R_b is the data rate. The coherent detection method is beneficial from the mature RF signal processing technique. However, this method is more useful for systems with moderate data-rates. For very high data rate, more expensive electronics will have to be used.

2.4.2 RF Power Techniques

When a modulate light propagates through a dispersive channel, CD induces the phase difference between different frequency components. Beating at a square-law photodetector, the phase difference may cause the power variation in the RF domain. Therefore, CD can be monitored by measuring the RF power at some specific frequencies, as introduced below.

2.4.2.1 Regenerated clock power method

It is well known that the power spectrum of an NRZ signal has no or weak clock component. The clock component will be regenerated when an NRZ signal propagates through a length of dispersive fiber (i.e., the transmission of 10-Gb/s data signal generates a power spectrum at 10 GHz). The regenerated clock frequency is due to the chromatic dispersion [41]. Within a range of accumulated dispersion, the clock power increases with the dispersion. Beyond this dispersion value, the clock power fades, but will continue to increase and decrease periodically with accumulated dispersion. Similarly, RZ signal experiences the faded power at the clock frequency

after the CD distortion. Fig. 2.12 depicts RF spectra and eye diagrams of NRZ and RZ signals with different dispersions [42].

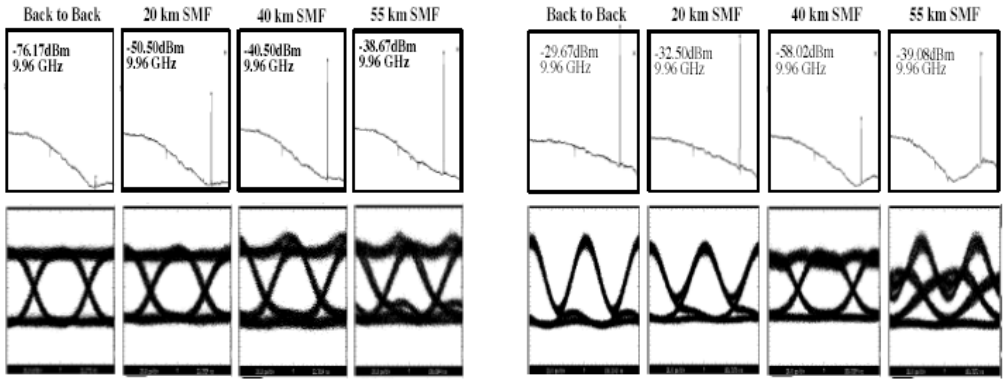

(a) Clock regeneration of NRZ signal (b) Clock fading of RZ signal

Fig. 2.12 RF spectra and eye diagrams of NRZ and RZ signals at different dispersions [42].

This phenomenon of clock regeneration or fading has been exploited for monitoring the accumulated CD without the addition of extraneous signals to the baseband data [42, 43]. The efficient clock extraction methods of NRZ signal have also been presented by Kim et al [44]. However, because the monitoring sensitivity and range depend on the regenerated clock tone, the monitoring method is greatly limited by the data bit-rate and data format.

2.4.2.2 PM-AM conversion method

This method is to add a phase modulation at the transmitter and subsequently measure the phase modulation (PM) to amplitude modulation (AM) converted signal at the receiver [45, 46]. Fig. 2.13 shows a setup of this method.

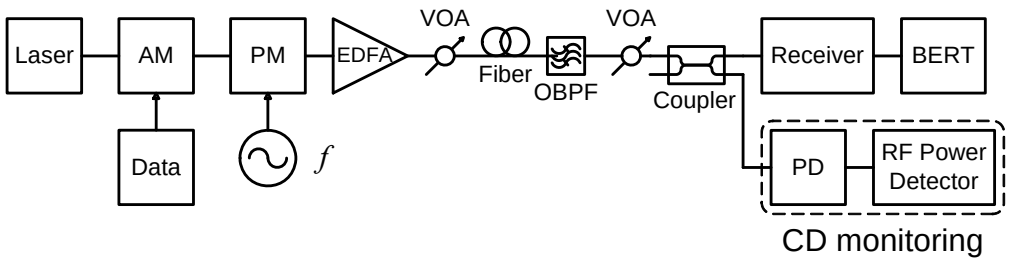

Fig. 2.13 Schematic diagram of PM-AM conversion method.

When a phase modulated optical signal propagates along an optical fiber, the dispersion changes the phase difference between the optical carrier and its sidebands. Thus, the amplitude of the transmitted signal becomes modulated. Consequently, the chromatic dispersion that an optical signal experiences can be monitored by measuring the AM component.

The AM power of the received PM pilot tone caused by the PM-AM conversion can be described as [45, 46]:

$$P = AJ_0^2(m)J_1^2(m)\sin^2\left(\pi DL\lambda^2 f^2/c\right) \tag{2.17}$$

where m is the depth of phase modulation, J_0 and J_1 are Bessel functions of the first kind of order 0 and 1, D is the fiber dispersion coefficient, L is the fiber length, f is the RF modulating signal frequency, λ is the optical carrier wavelength, c is the speed of light in vacuum, and A is an constant whose value is influenced by the loss or gain that the signal experiences.

This method needs an additional phase modulator, which adds complexity to the transmitter. Furthermore, the accuracy of the measured accumulated CD is influenced by the power loss or gain of the optical transmission link.

2.4.2.3 RF power fading method

The RF power fading method is to insert an RF tone at the transmitter and subsequently monitor the RF power fading at the receiver [47]. Fig. 2.14 shows a setup of this method.

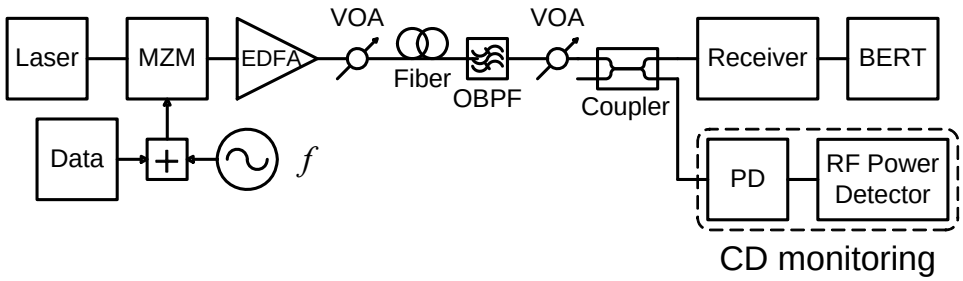

Fig. 2.14 Schematic diagram of RF power fading method.

When an RF modulated optical signal propagates along an optical link, the dispersion creates a phase difference between the two sidebands. This will generate a destructive interference and then result in the RF power fading at the photodetector. The detected RF power at the photodetector is given by [47]:

$$P = Am^2 \cos^2\left(\pi DL\lambda^2 f^2 / c\right) \tag{2.18}$$

where m is the modulation index.

This method is relatively simple. However, like that of PM-AM conversion method, the accuracy of the measured accumulated CD is influenced by the power loss or gain of the optical transmission link.

2.4.2.4 Subcarrier ratio method

The subcarrier ratio method is proposed for dealing with the link loss or gain dependence problem of the RF power fading method by inserting two RF tones, instead of one RF tone, at the transmitter and monitoring the power ratio of the RF tones at the receiver [35]. Fig. 2.15 shows a setup of this method.

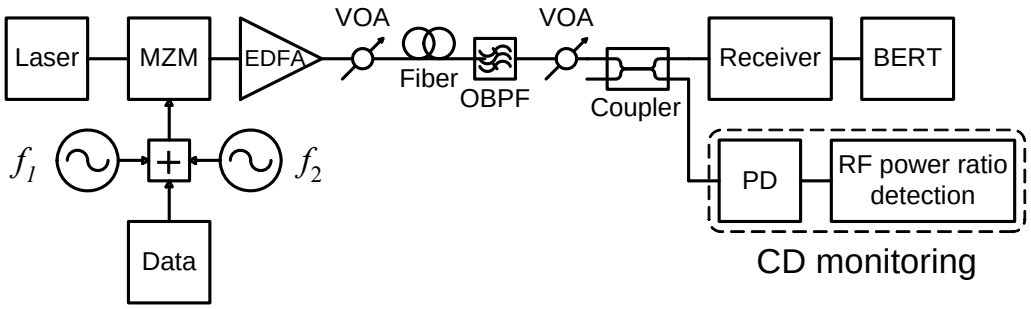

Fig. 2.15 Schematic diagram of subcarrier ratio method [35].

The fundamental principle of this method is the same as that of the RF power fading method. Two RF signals at frequencies f_1 and f_2 are added to the baseband data signal at the transmitter. The factor A in Eq.(2.18) can be cancelled by taking the ratio of the RF power at f_1 to that at f_2, since the two RF signals propagate through the same optical elements. The power ratio between the two RF signals at the receiver is given by [35]:

$$R = \frac{\cos^2\left(\pi DL\lambda^2 f_1^2/c\right)}{\cos^2\left(\pi DL\lambda^2 f_2^2/c\right)}, \quad f_1 < f_2 \tag{2.19}$$

This method eliminates the influence of power loss and gain in the RF power fading method. However, the monitoring range is quite small and sensitivity is low.

2.4.3 Amplitude Histogram Techniques

Amplitude histogram has emerged as an attractive scheme for optical performance monitoring. It has been demonstrated for optical signal-to-noise ratio (OSNR) monitoring, bit-error-rate (BER) estimation, and eye pattern reconstruction [48-52]. In these methods, digital signals are sampled synchronously or asynchronously so as to obtain their amplitude histograms. Asynchronous sampling attracts more attentions for high bit-rate system because no synchronization between data and the sampling clock is required and hence no clock recovery is necessary. Recently, a few asynchronous amplitude histogram methods have been reported for CD monitoring. These will be reviewed in the following subsections.

2.4.3.1 Cross-point count method

When an optical pulse travels through a length of fiber, dispersion induces the pulse broadening and prolongs the pulse rise and fall time. Chen et al. [53] monitored the pulse rise and fall time by using the cross-point count of the asynchronous amplitude histogram. Then the monitored pulse rise and fall time can be used to estimate the accumulated CD. Fig. 2.16 shows the eye diagram and histogram that were acquired by asynchronous sampling.

With asynchronous sampling, due to the absence of the clock signal, the sampling occurs randomly. The amplitude histogram obtained by asynchronous sampling can represent the pulse amplitude distribution in a bit period if a sufficient number of

samplings are acquired. With the asynchronous amplitude histogram, despite of two dark lines at the mark and space levels, there are a lot of cross-points between the mark and space levels which represent the pulse rise and fall. The cross-point count is roughly linear related to the pulse rise and fall time. Hence, the in-service CD monitoring can be expected by measuring the cross-point count. However, this method is susceptible to the noise effect and nonlinear pulse edge. Moreover, the monitoring capability will be affected when it is used in NRZ data transmission systems with a long sequence of consecutive data "1's".

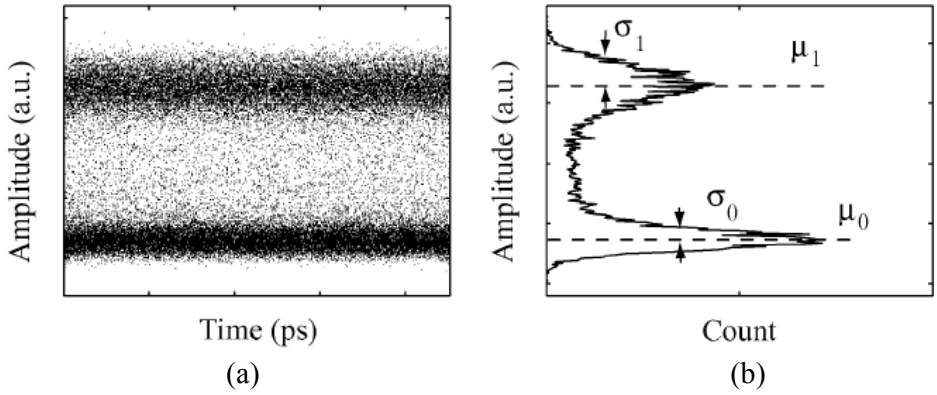

Fig. 2.16 (a) Eye diagram with asynchronous sampling;
(b) histogram with asynchronous sampling [53].

2.4.3.2 Statistical moments of asynchronous amplitude histogram method

Another approach is to apply the *N*th-order statistical moment of the asynchronous amplitude histogram to CD monitoring [54]. In principle, the asymmetry of the histogram can be reflected by the third-order statistical moment and higher order odd ones. Since the histogram of NRZ-based waveforms becomes most symmetric at zero CD and accordingly the odd moments become minimum. On the other hand, the

fourth-order statistical moments and higher order even ones reflect unsharpness, and they increase as the histogram becomes dull with a large CD. Therefore, the statistical moments of asynchronous amplitude histograms can be exploited for CD monitoring. Fig. 2.17 plots the experimental and simulated normalized *N*th-order statistical moments against chromatic dispersion for 10-Gb/s NRZ modulations.

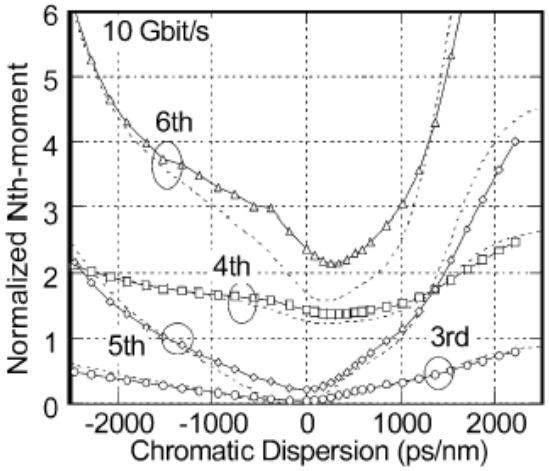

Fig. 2.17 Normalized *N*th-order moments versus chromatic dispersion for 10-Gb/s NRZ modulations [54].

The advantage of this method is that it is suitable for monitoring a wide range of CD with a wide range of data rates. However, the drawbacks of this method are low monitoring sensitivity, and high monitoring errors.

2.4.3.3 Delay tap asynchronous sampling method

Recently, Dods et al. proposed a novel asynchronous sampling technique which resolves the power variation within each bit and can be used to estimate the accumulated CD [55]. Different from those conventional asynchronous sampling

techniques which normally measure once for each sampling point, this technique obtains two measurement results for each sampling point by sampling with a two tap delay line. Fig. 2.18(a) shows the sampling process for three sample points. The two measurements (x and y) are separated by a fixed time Δt corresponding to the delay line. The two-tap scatter plot with a delay corresponding to 1/8 of a bit period is shown in Fig. 2.18(b).

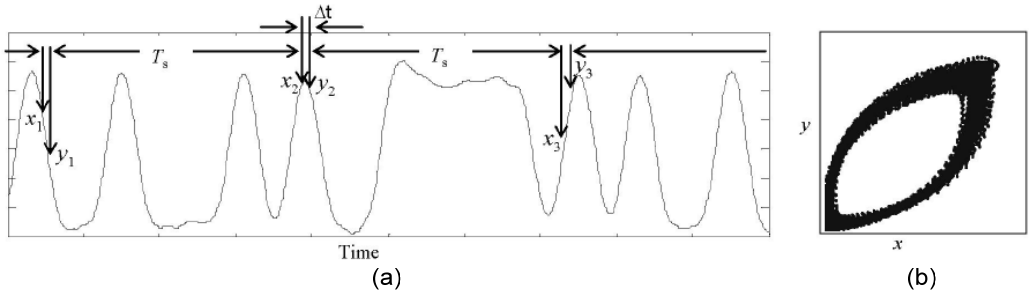

Fig. 2.18 (a) Delay-tap asynchronous sampling process for three sample points, where T_s is the sampling period and Δt is the time offset within each sample. (b) The two-tap scatter plot with a delay corresponding to 1/8 of a bit period [55].

For delays of less than half a bit, the two-tap scatter plot represents the power evolution within each bit. It contains information about the pulse shape, in particular the rise and fall times, which are useful pointers of the various impairments, including CD. Consequently, CD can be monitored by reading the two-tap scatter plot. However, as a new rising technology, the delay tap asynchronous sampling technique requires further investigations. It lacks a vernier which can represent CD directly and quantitatively. Moreover, the accuracy and stability of the delay line may affect the CD monitoring. Its impact needs further studies.

2.4.3.4 Asynchronous amplitude histogram with PM-AM conversion method

The PM-AM conversion is a well-known phenomenon [56]. After propagating through a length of dispersive channel, the PM-AM conversion may lead to intensity ripple for NRZ-DPSK and RZ-DPSK signals [57-59]. Consequently, there are three peaks for the asynchronous amplitude histogram of the distorted waveform without demodulation, as seen in Fig. 2.19.

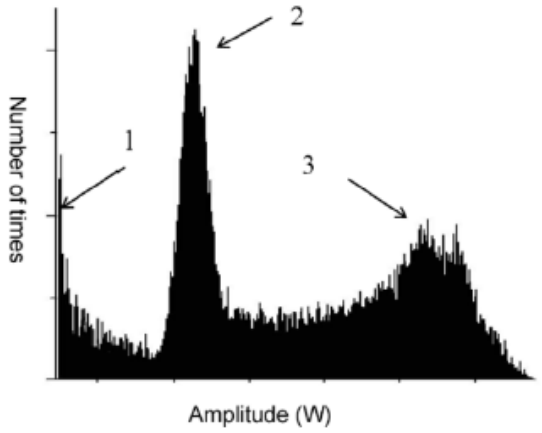

Fig. 2.19 Asynchronous amplitude histogram of RZ-DPSK signal after PM-AM conversion [58].

The chromatic dispersion can be determined from the dispersion factor, which is denoted as:

$$DF = \frac{\mu_3 - \mu_1}{\mu_2} \quad \text{(NRZ-DPSK)} \tag{2.20}$$

and

$$DF = \frac{\mu_2}{P_0} \quad \text{(RZ-DPSK)} \tag{2.21}$$

where μ is the mean of the Gaussian distribution for the corresponding peaks and P_0 is the average power of the DPSK signal.

This method can monitor the chromatic dispersion and OSNR simultaneously. However, it is only applicable to DPSK systems.

2.4.4 Nonlinear Effects Techniques

As an all optical approach, nonlinear effects techniques are appealing for CD monitoring. Using devices with nonlinear power transfer function, CD can be monitored by measuring the pulse width. However, as time-domain measurement techniques, they are more suitable for RZ signals. For NRZ systems, the monitoring sensitivity is quite low.

2.4.4.1 SPM induced spectral broadening method

An AM RZ signal will become spectrally broadened when propagating through a Kerr medium, such as a highly nonlinear fiber, due to the self-phase modulation (SPM). The spectral broadening can be used for measuring the pulse width of the distorted RZ signal and then monitoring the dispersion [60]. Fig. 2.20 illustrates the concept of this method.

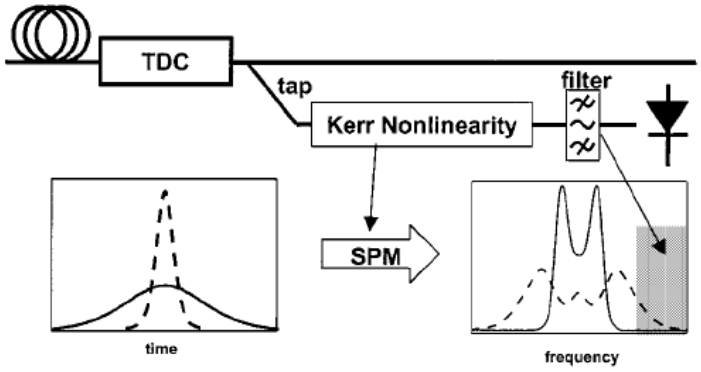

Fig. 2.20 Concept of the SPM induced spectral broadening method. Shaded part indicates monitor filter passband [60].

When the input pulse is dispersed by a tunable dispersion compensator (TDC), the corresponding peak power decreases, resulting in a decreased amount of spectral broadening. By adding a filter which passes the longer wavelength components of the spectrally broadened signal only, the spectral broadening may be measured, as shown in the shaded part of Fig. 2.20. Therefore, by detecting the filtered optical power, the residual dispersion can be determined.

2.4.4.2 FWM induced idler power method

With the fiber four wave mixing (FWM) induced idler power method, the accumulated dispersion can be monitored by measuring the power of the idler light which is generated by the fiber FWM effect [61]. Fig. 2.21 shows its experimental setup.

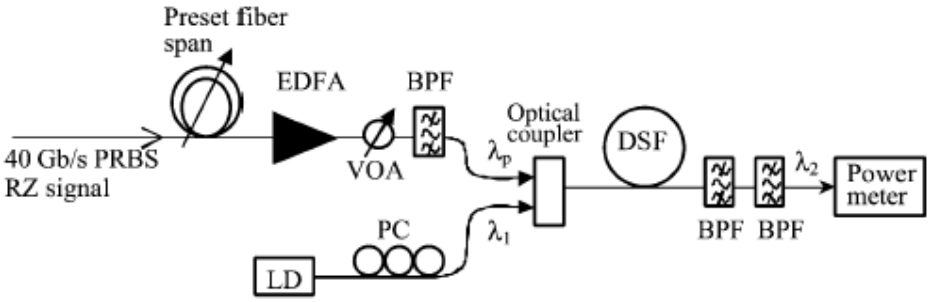

Fig. 2.21 Experimental setup for FWM induced idler power method [61].

As shown in the figure, after a length of dispersive fiber transmission, the input signal pulse stream with wavelength λ_p is boosted by an optical amplifier and used as the FWM pump in an optical fiber. A continuous wave (CW) signal with wavelength λ_1 from a tunable laser source is used as the probe signal. They are mixed by a 3-dB coupler and launched into a highly nonlinear fiber. A new pulsed signal (idler) at wavelength $\lambda_2 = 2\lambda_p - \lambda_1$ is generated at the output of the fiber through FWM. Due to the nonlinear relationship between the idler and pump amplitudes, the average power of the idler depends on the pulse width of the pump. Therefore, by measuring the average power of the idler, the pulse width and the residual dispersion of the input signal can be determined. However, this method is only suitable for RZ signal.

2.4.4.3 XPM generated optical tone power method

With this method, by measuring the cross-phase modulation (XPM) generated optical tone power in a highly nonlinear fiber, the CD effect on a high-speed RZ data signal is monitored [62]. Fig. 2.22 shows the conceptual illustration of this scheme.

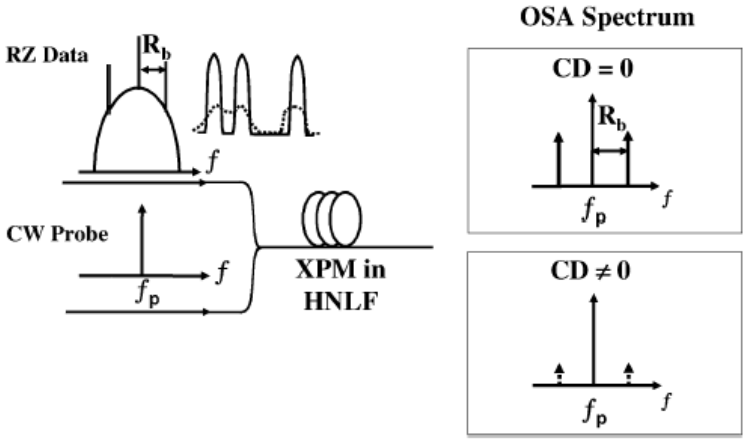

Fig. 2.22 Conceptual illustration of XPM generated optical tone power method [62].

Its system configuration is similar with the one using the fiber FWM induced idler power method. In the monitoring module, the data signal is combined with a CW probe, whose frequency is outside the signal bandwidth. Traveling through a piece of highly nonlinear fiber, the combined signals interact with each other, and generate a pair of optical tones around the probe at the frequency of $f_p \pm R_b$, as shown in Fig. 2.22. However, these two optical tones change with the CD value in the transmission link. As CD increases and distorts the data, these two optical tones fade with the CD value. Therefore, the optical tones at the frequency of $f_p \pm R_b$ are sensitive to CD and can be used for monitoring CD.

2.4.4.4 Two-photon absorption method

Nonlinear detection based on two-photon absorption (TPA) in detectors results in an electrical output signal that depends quadratic on the intensity of the incident light [63]. The TPA detector with quadratic intensity dependence will produce a signal that

is inversely proportional to the pulse width. Therefore, it is sensitive to the magnitude of the accumulated dispersion experienced by the pulses and will exhibit the qualitative dependence on the dispersion. It is another means to make time-domain measurements of optical pulses.

2.4.5 Comparison between Different CD Monitoring Techniques

Various CD monitoring techniques have been discussed above. Table 1 gives a comparison between different chromatic dispersion monitoring techniques. It shows the amplitude histogram techniques (including cross-point count, statistical moments of amplitude histogram, delay tap asynchronous sampling, and amplitude histogram with PM-AM conversion) have the capability for monitoring miscellaneous objectives as well as dispersion. As an all optical approach, nonlinear effects techniques (including SPM induced spectral broadening, FWM induced idler power, XPM generated optical tone power, and two-photon absorption) are appealing for CD monitoring in high bit-rate systems because no high frequency electronics is required. However, these two categories of CD monitoring techniques exhibit several disadvantages such as low sensitivity and accuracy, data format dependent, and highly vulnerable to other distortions such as noise and fiber nonlinearities. Compared with these two categories, phase shift techniques (including phase shift between spacing-fixed WDM signals, phase delay of DSB SCM, VSB clock phase-shift detection, and coherent detection) and RF power techniques (including regenerated clock power, PM-AM conversion, RF power fading, and subcarrier ratio) are normally based on mature RF techniques and applicable for today's high capacity WDM networks. They

have simple configuration and good monitoring capability. Between them, the implementation of RF power techniques is simpler because no high performance phase detectors and filters are required. However, there remain some challenging issues such as monitoring range, monitoring accuracy and implementation complexity that need to be addressed. This thesis aims to address these issues.

Techniques	Advantages	Disadvantages
Phase shift between spacing-fixed WDM signals [33]	Easy to implement No high performance phase detector is required	One additional wavelength is required Dispersion of individual channel cannot be monitored
Phase delay of DSB SCM [34, 35]	Good monitoring capability Data format independent	Additional subcarrier is required; Phase detector is required; The rejection of optical filters affects accuracy
VSB clock phase-shift detection [36, 37]	No modification at the transmitter	Clock recovery is required The rejection of optical filters affects the accuracy
Coherent detection [40]	No modification at the transmitter Mature RF filters replaces optical filters	Additional coherent tunable laser is required Clock signal is required
Regenerated clock power [42]	Simple configuration; No phase detector is required No modification at the transmitter and receiver	Data format dependent Constrained monitoring capability
PM-AM conversion [45, 46]	Good monitoring capability; Signal independent	Additional PM subcarrier and phase modulator are required
RF power fading [47]	Good monitoring capability Signal independent	Additional subcarrier is required Affected by optical loss and gain
Subcarrier ratio [35]	Data format independent Not affected by optical loss and gain	Two subcarriers are required Monitoring capability is not good enough
Cross-point count [53]	No modification at the transmitter Miscellaneous monitoring objectives	Low sensitivity and accuracy Susceptible to other distortions
Statistical moments of amplitude histogram [54]		
Delay tap asynchronous sampling [55]		
Amplitude histogram with PM-AM conversion [57-59]		Only for DPSK; Susceptible to other distortions
SPM induced spectral broadening [60]	No modification at the transmitter No high frequency electronics is required	Only for RZ Susceptible to other distortions Additional high power laser probe is required
FWM induced idler power [61]		
XPM generated optical tone power [62]		
Two-photon absorption [63]		Only for RZ; Susceptible to other distortions Special detector is required

Table 1 Comparison between different CD monitoring techniques.

2.5 Summary

Chromatic dispersion is one of the major limiting factors in today's high-bit-rate long haul WDM systems. It causes pulse broadening, signal energy overlapping and transmission error. The dispersion tolerance of optical communication systems decreases quadratic with the bit rate. Therefore, it is usually essential to compensate chromatic dispersion. DCF and chirped FBG are two main means for fixed dispersion compensation. However, CD may change with dynamic reconfigurations of the network and variations in environmental conditions. Nonlinear chirped FBG is an important tunable dispersion compensator. Moreover, it is essential to monitor the accumulated CD of individual optical channels to control the tunable dispersion compensator and ensure that the CD would not exceed the specified value and cause severe degradation of optical signals. Then two CD measurement methods and various CD monitoring techniques have been reviewed. The CD monitoring techniques can be roughly classified into four categories: phase shift technique, RF power technique, amplitude histogram technique, nonlinear effects technique. Among them, the RF power technique is most mature and simple and applicable for today's high capacity WDM networks with the well developed RF technologies. However, there remain some challenging issues for the existing CD monitoring techniques such as monitoring range, monitoring accuracy and implementation complexity that need to be addressed. This thesis aims to address these issues. Several enhanced approaches are proposed in the thesis. Theoretical, experimental and simulation means are employed to investigate the performance of the proposed approaches.

Chapter 3

Chromatic Dispersion Monitoring Using the RF Power Ratio with a Dispersion Offset

3.1 Introduction

Among the chromatic dispersion monitoring techniques reviewed in Chapter 2, the RF power fading method [47] is relatively simple and applicable for different modulation formats and bit rates, but the accuracy of the measured dispersion is influenced by the power loss or gain of the optical transmission line. The RF power ratio method in [35] can eliminate this influence. However, the monitoring range is quite small and the sensitivity is low. To address these problems, an improved CD monitoring method is considered, which is based on the RF power ratio technique reported in [35]. The main idea is to insert a dispersion offset before the photodetector within the monitoring module and then measure the power ratio of the two RF tones. It is experimentally demonstrated that this improved technique can effectively monitor

both positive and negative CD in 10-Gb/s WDM systems. The monitoring range can be extended to be greater than 1150 ps/nm and the sensitivity better than 0.064 dB/ps/nm, by selecting appropriate RF tones and suitable dispersion offsets. The investigations reveal that the modulation index should be larger than 10% but less than 20% so as to acquire a large monitoring range with a small power penalty (smaller than 1 dB). To further reduce the RF tones induced power penalty, an RF tone removal scheme is proposed. The CD monitoring errors caused by PMD and SPM are also examined. Experimental results show that the use of a dispersion offset can effectively reduce the PMD-induced monitoring errors.

The rest of this chapter is organized as follows. Section 2 describes the operational principle of the improved CD monitoring technique proposed in this chapter. In Section 3, experimental investigations of the proposed technique are presented. Section 4 discusses the effects of modulation index on the monitoring range and the power penalty. This section also presents an RF tone removal scheme to reduce the RF tone induced power penalty and examines the PMD and SPM caused CD monitoring errors. The summary is given in Section 5.

3.2 Operational Principle

When an RF modulated optical signal propagates along an optical link, the chromatic dispersion causes a phase difference between the upper and the lower sidebands [35, 47]. At the square-law photodetector, this will generate a destructive interference between the two sidebands, resulting in the RF power fading. The operational

principle of this technique and its application in chromatic dispersion monitoring will be analyzed in detail in this section.

3.2.1 Modulator Chirp and Alpha Parameter

The chirp of light is a characteristic of an intensity modulated light. It indicates the incidental phase shift to the intensity variation. For an externally modulated system, the chirp comes from the external modulator. Mach-Zehnder modulators (MZMs), which are widely used as intensity modulators in high capacity optical fiber communications, can be designed to work completely chirp-free. However, in an actual MZM, imbalanced optical amplitudes between two arms always make a small residual chirp [64]. To evaluate the chirp quantity of modulators, the Henry's alpha parameter α_H of modulators is defined as [65]

$$\alpha_H = 2I\frac{\delta\Phi}{\delta I} \tag{3.1}$$

where I and Φ are the instantaneous intensity and phase of the modulated light. Therefore, the instantaneous intensity induced phase variation can be represented as

$$\Phi(I) = \frac{\alpha_H}{2}\ln I \tag{3.2}$$

3.2.2 Intensity Modulated Signal Spectrum

For a laser whose linewidth is much less than the modulating frequency, the spectrum of the modulated signal depends solely on the laser's response to the modulating

signal and not on the intrinsic spectral width of the unmodulated source [66]. Considering a linear intensity modulated signal, the light intensity I can be expressed as:

$$I = I_0\left(1 + m\cos\omega_m t\right) \tag{3.3}$$

where I_0 is the input light intensity of the modulator, m is the modulation index which is defined as the ratio of the peak optical power variation (i.e., the difference between the maximum and average power) to the average optical power [67, 68], $\omega_m = 2\pi f_{\mathrm{RF}}$ is the modulating angular frequency of light intensity and f_{RF} is radio frequency (RF) for modulating the light.

The electric field of a light wave is written as

$$E = \sqrt{I}\exp\left[j\omega_0 t + \Phi\left(I\right)\right] \tag{3.4}$$

where ω_0 is the angular frequency of optical carrier signal.

Substituting Eqs. (3.2) and (3.3) into Eq. (3.4),

$$E = e^{j\omega_0 t}\left[I_0\left(1 + m\cos\omega_m t\right)\right]^{\frac{1+j\alpha_H}{2}} \tag{3.5}$$

Under the small signal condition ($m \ll 1$), expanding Eq. (3.5) in Taylor series at $m = 0$ and neglecting the higher order terms because they are very small, the electric field can be expressed as

$$\begin{aligned} E &= e^{j\omega_0 t} I_0^{\frac{1+j\alpha_H}{2}} + e^{j\omega_0 t}\frac{1+j\alpha_H}{2}\left[I_0\left(1 + m\cos\omega_m t\right)\right]^{\frac{-1+j\alpha_H}{2}}\Bigg|_{m=0} \cdot mI_0\cos\omega_m t + \cdots \\ &= e^{j\omega_0 t} I_0^{\frac{j\alpha_H}{2}}\left[\sqrt{I_0} + \sqrt{I_0}\,m\frac{1+j\alpha_H}{2}\cos\omega_m t + \cdots\right] \\ &= e^{j\left(\omega_0 t + \frac{1}{2}\alpha_H \ln I_0\right)}\left(\sqrt{I_0}\,m\frac{1+j\alpha_H}{4}e^{-j\omega_m t} + \sqrt{I_0} + \sqrt{I_0}\,m\frac{1+j\alpha_H}{4}e^{j\omega_m t} + \cdots\right) \end{aligned} \tag{3.6}$$

Eq. (3.6) shows that, an intensity modulated light can be approximated to a typical double sideband (DSB) signal separated by $2\omega_m$ with a small modulating level and a strong carrier.

$$E = e^{j\left(\omega_0 t + \frac{1}{2}\alpha_H \ln I_0\right)} \left\{ A_L \exp j\left(-\omega_m t + \tan^{-1}\alpha_H\right) + A_0 + A_U \exp j\left(\omega_m t + \tan^{-1}\alpha_H\right) \right\} \qquad (3.7)$$

where $A_0 = \sqrt{I_0}$, $A_L = A_U = \frac{1}{4} m \sqrt{I_0} \sqrt{1+\alpha_H^2}$ denote the amplitudes of the optical carrier, lower sideband (LSB) RF tone and upper sideband (USB) RF tone, respectively.

3.2.3 Chromatic Dispersion Induced Phase Shift

The chromatic dispersion induced phase shift of an intensity modulated light is analyzed here. Let $H(\omega)$ be the transfer function of the optical channel over which the light is transmitted. $H(\omega)$ can be expressed as:

$$H(\omega) = M(\omega) e^{j\theta(\omega)} \qquad (3.8)$$

where $M(\omega)$ is the magnitude weighting factor and $\theta(\omega)$ is the phase shift factor.

For an optical channel with single-mode fiber only, the magnitude weighting factor can be expressed as $M(\omega) = e^{-\alpha L/2}$, where α is the fiber power loss per unit length and L is the fiber length. However, for a practical optical channel includes loss and gain elements such as optical couplers and amplifiers, $M(\omega)$ is unknown. Because the modulation frequency is much smaller than the bandwidth of the optical channel, $M(\omega)$ can be treated as independent of ω and simplified as M.

For an optical fiber, the phase shift factor $\theta(\omega)$ can be expressed as:

$$\theta(\omega) = -\beta(\omega) \cdot L \tag{3.9}$$

where β is the propagation constant.

If a signal pulse contains a small spread of frequencies around a carrier frequency ω_0, the propagation constant $\beta(\omega)$ varies with frequency. Expanding $\beta(\omega)$ in a Taylor series and ignoring the 3rd and higher order terms, then $\theta(\omega)$ can be written as:

$$\theta(\omega) = -\beta_0 L - \beta_1(\omega - \omega_0)L - \frac{L}{2}\beta_2(\omega - \omega_0)^2 \tag{3.10}$$

Since the input optical signal is described by Eq. (3.7), the output electric field is given by

$$\begin{aligned} E &= Me^{j\left(\omega_0 t + \frac{1}{2}\alpha_H \ln I_0 - \beta_0 L\right)}\left[A_L e^{j\left(\tan^{-1}\alpha_H - \omega_m t + \beta_1 \omega_m L - \frac{L}{2}\beta_2 \omega_m^2\right)}\right. \\ &\quad \left. + A_0 + A_U e^{j\left(\tan^{-1}\alpha_H + \omega_m t - \beta_1 \omega_m L - \frac{L}{2}\beta_2 \omega_m^2\right)}\right] \\ &= \sqrt{I_0} Me^{j\left(\omega_0 t + \frac{1}{2}\alpha_H \ln I_0 - \beta_0 L\right)}\left[1 + \frac{m}{2}\sqrt{1+\alpha_H^2}\, e^{j\left(\tan^{-1}\alpha_H - \frac{L}{2}\beta_2 \omega_m^2\right)} \cos(\omega_m t - \beta_1 \omega_m L)\right] \end{aligned} \tag{3.11}$$

3.2.4 Detected Power of RF Tone

The optical signal received by a photodetector produces a photocurrent i_{out} proportional to the square of the electric field, which can be given as:

$$i_{out} = \rho I_0 M^2 \left[1 + m\sqrt{1+\alpha_H^2}\cos\left(\omega_m t - \beta_1 \omega_m L\right)\cos\left(\tan^{-1}\alpha_H - \frac{L}{2}\beta_2\omega_m^2 \right) + \frac{m^2}{4}\left(1+\alpha_H{}^2\right)\cos^2\left(\omega_m t - \beta_1\omega_m L\right) \right] \tag{3.12}$$

where ρ is the responsivity of the photodetector. The responsivity is defined as the ratio of the generated photocurrent to the incident light power. For commercial PIN photodetectors, it ranges from 0.8 to 0.9 A/W at the 1.55-μm wavelength.

Neglecting the direct current (DC) and the second order terms, the component at frequency f_{RF} of the output photocurrent can be expressed as:

$$i_{RF} = \rho I_0 M^2 m\sqrt{1+\alpha_H^2}\cos\left(\tan^{-1}\alpha_H - \frac{L}{2}\beta_2\omega_m^2 \right) \tag{3.13}$$

Therefore, the detected RF power at the modulation frequency f_{RF} of the signal can be represented as:

$$P = \rho^2 I_0^2 M^4 m^2 \left(1+\alpha_H^2\right)\cos^2\left(\tan^{-1}\alpha_H - \frac{L}{2}\beta_2\omega_m^2 \right) \tag{3.14}$$

where the load resistance of the photodetector is assumed as 1 ohm for normalization. Generally speaking, in a practical optical communication system, the values of ρ, I_0, and m are known and determined by the configuration of the transmitter and receiver. The magnitude weighting factor M is related to the properties of the transmission channel and varies with the loss or gain that the optical signal experiences.

Substituting $D = -2\pi c\beta_2/\lambda^2$ and $\omega_m = 2\pi f_{RF}$ into Eq.(3.14), the detected RF power P is written as:

$$P = \rho^2 I_0^2 M^4 m^2 \left(1+\alpha_H^2\right)\cos^2\left(\frac{\pi D L \lambda^2 f_{RF}^2}{c} + \tan^{-1}\alpha_H \right) \tag{3.15}$$

where λ is the carrier wavelength, c is the speed of light in vacuum and D is the dispersion coefficient. From Eq.(3.15), it is found that when an intensity modulated optical signal propagates along an optical channel, the accumulated dispersion causes a phase difference between the two sidebands. This would generate interference and result in that the power of the RF tone varies periodically as the square of cosine to an argument which depends on fiber dispersion coefficient, fiber length, chirp, optical carrier wavelength and modulation frequency. In a broad sense, the *DL* product is the accumulated dispersion induced by single-mode waveguides which include fibers and optical components. In the rest of the thesis, D_{acc}, instead of *DL,* is used to represent the accumulated dispersion (ps/nm) that is experienced by an optical signal. $P' = \left(1+\alpha_H^2\right)\cos^2\left(\pi D_{acc}\lambda^2 f_{RF}^2/c + \tan^{-1}\alpha_H\right)$ is defined as the normalized RF power, which is varied periodically with the accumulated dispersion and chirp. Fig. 3.1 plots the normalized RF power as a function of the accumulated dispersion at $\lambda = 1.55\mu m$ and $\alpha_H = 0$ for different RF frequencies.

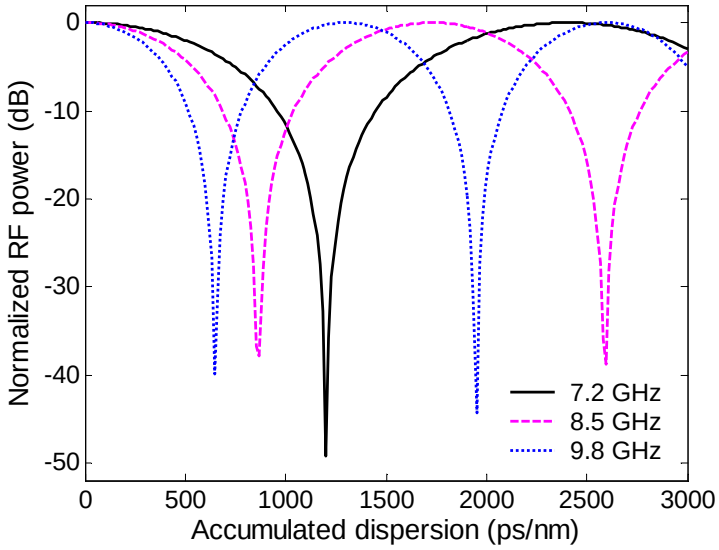

Fig. 3.1 The normalized RF power as a function of the accumulated dispersion at λ = 1.55 μm and $\alpha_H = 0$ for different RF frequencies.

As shown in Fig. 3.1, the dispersion induced phase difference between the two sidebands results in a periodical RF power variation at the photodetector. When the chirp and optical carrier wavelength are constant, the variation period decreases as the RF frequency increases. This effect can be utilized to monitor the residual chromatic dispersion of an optical channel. More specifically, if an RF signal is added as a pilot tone to the baseband data signal, the first monotonic power fading range of the RF tone can be used to monitor the amount of the accumulated dispersion of the data signal since they experience the same CD [47].

However, because the magnitude weighting factor M is an unknown constant whose value is influenced by the optical power loss or gain that the optical signal experiences, it is difficult to tell the exact RF power fading caused by the accumulated dispersion. Therefore, some technique is necessary to circumvent this ambiguous problem.

3.2.5 Power Ratio of Two RF Tones

If two RF tones at frequencies f_{RF1} and f_{RF2} ($f_{RF2} > f_{RF1}$) are added to the baseband data signal with the same modulation indices at the transmitter, the magnitude weighting factor M in Eq. (3.15) can be cancelled by taking the ratio of the RF power at f_{RF1} to that at f_{RF2}, since the two RF tones propagate through the same optical elements [35]. This eliminates the influence caused by the power loss or gain. Moreover, those factors with same values (m, ρ, I_0, and $1+\alpha_H^2$) can be cancelled too. Therefore, the

power ratio (R) of the two RF tones after being detected at the photodetector can be expressed as:

$$R = \frac{\cos^2\left(\pi D_{acc}\lambda^2 f_{RF1}^2/c + \tan^{-1}\alpha_H\right)}{\cos^2\left(\pi D_{acc}\lambda^2 f_{RF2}^2/c + \tan^{-1}\alpha_H\right)} \tag{3.16}$$

Fig. 3.2 shows the RF power ratio as a function of the accumulated dispersion at $\lambda = 1.55\mu m$ and $\alpha_H = 0$ for two different sets of the RF tones (f_{RF1} = 7.2 GHz and f_{RF2} = 8.5 GHz; f_{RF1} = 7.2 GHz and f_{RF2} = 9.8 GHz).

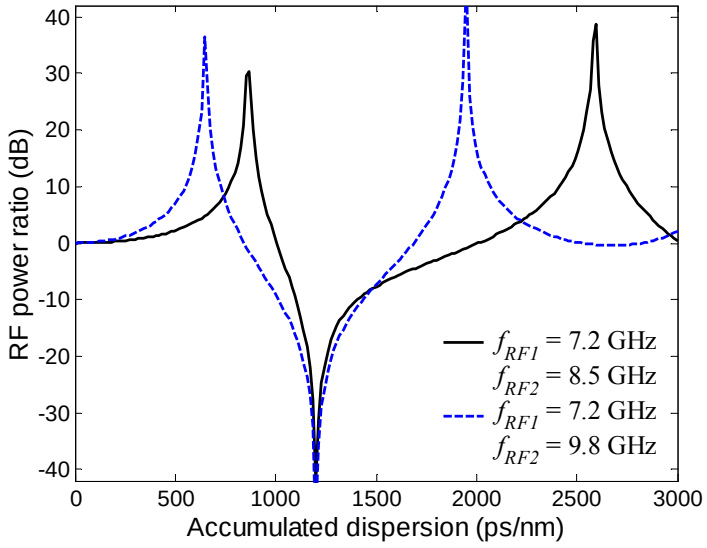

Fig. 3.2 The RF power ratio versus the accumulated dispersion at λ = 1.55 μm and α_H = 0 for two different sets of the RF tones (f_{RF1} = 7.2 GHz and f_{RF2} = 8.5 GHz; f_{RF1} = 7.2 GHz and f_{RF2} = 9.8 GHz).

It can be seen in Fig. 3.2 that the RF power ratio also varies with the accumulated CD. Compared with the normalized RF power shown in Fig. 3.1, the RF power ratio reaches its maximum when the RF power of f_{RF2} fades totally and reaches its minimum when the RF power of f_{RF1} equals zero. Because it is not affected by the loss or gain that the optical signal experiences, the RF power ratio is readily to be

used in CD monitoring. To avoid ambiguity in CD monitoring, the monitoring range has to be limited to the range of 0 to $c/2\lambda^2 f_{RF2}^2$ ($f_{RF1} < f_{RF2}$), within which the RF power ratio increases monotonically.

However, Fig. 3.2 also exposes the disadvantages of using the power ratio to monitor dispersion. Firstly, the monitoring range is limited to the range of 0 to $c/2\lambda^2 f_{RF2}^2$. Secondly, the monitoring sensitivity is relatively low since the RF power ratio curve is quite flat against the change of the accumulated CD for the most part of the region of 0 to $c/2\lambda^2 f_{RF2}^2$ (ps/nm), particularly in the vicinity of D_{acc} = 0 ps/nm where the sensitivity is considerably low. Here, the monitoring sensitivity is defined as the increase (or decrease) in the RF power ratio (in dB) for 1-ps/nm change of the accumulated CD. Considering the small CD tolerance of high-bit-rate WDM systems, this low sensitivity would limit the application of this method. Finally, only the positive value of the accumulated CD can be monitored and measured.

3.2.6 Power Ratio of Two RF Tones with a Dispersion Offset

To address the above-mentioned problems, it is proposed to insert a priori known dispersion offset D_{offset} such as a chirped fiber Bragg grating (FBG) or a length of dispersive fiber just before the photodetector of the CD monitoring module. It should be noted that the inserted dispersion offset is placed within the CD monitoring module, not in the path of the main optical signal (see Fig. 3.6 for more details). As such, the main data signal does not go through this dispersion offset and hence would not be affected by it, but only a small portion of the optical signal that is tapped and

coupled into the monitoring module passes through the dispersion offset. Therefore, the total CD experienced by an optical channel under monitoring is equal to the sum of the accumulated CD of the optical path and the added CD of the dispersion offset (i.e., $D_{total} = D_{acc} + D_{offset}$). The RF power ratio R in Eq. (3.16) can be changed to:

$$R = \frac{\cos^2\left[\pi\left(D_{acc} + D_{offset}\right)\lambda^2 f_{RF1}^2 / c + \tan^{-1}\alpha_H\right]}{\cos^2\left[\pi\left(D_{acc} + D_{offset}\right)\lambda^2 f_{RF2}^2 / c + \tan^{-1}\alpha_H\right]} \tag{3.17}$$

The RF power ratio versus the total dispersion for two different sets of the RF tones shown in Fig. 3.3 illustrates the difference between this RF power ratio method with a dispersion offset and the conventional one without a dispersion offset. With reference to Fig. 3.3, if the amount of the inserted dispersion offset is any value in the range of $c/2\lambda^2 f_{RF1}^2$ to $3c/2\lambda^2 f_{RF2}^2$, the original useful CD monitoring curves between 0 and $c/2\lambda^2 f_{RF2}^2$ (the dotted parts) can be shifted to the curves between $c/2\lambda^2 f_{RF1}^2$ and $3c/2\lambda^2 f_{RF2}^2$ (the solid parts). More specifically, the monitoring range is shifted from the range of (0 ps/nm to 850 ps/nm) to the range of (1200 ps/nm to 2600 ps/nm) for the case of f_{RF1} = 7.2 GHz and f_{RF2} = 8.5 GHz in Fig. 3.3(a), and from the range of (0 ps/nm to 650 ps/nm) to the range of (1200 ps/nm to 1950 ps/nm) for the case of f_{RF1} = 7.2 GHz and f_{RF2} = 9.8 GHz in Fig. 3.3(b). It should be noted that as compared to the original monitoring curve (without the dispersion offset), not only the shifted monitoring range (with the dispersion offset) becomes larger, but also it has a higher monitoring sensitivity (i.e., the RF power ratio changes more sharply with the increase/decrease in the accumulated CD). It is also observed in Fig. 3.3 that as the frequency difference ($f_{RF2} - f_{RF1}$) increases, the shifted monitoring range becomes smaller while the monitoring sensitivity is enhanced. Moreover, if the inserted

dispersion offset has a CD value in the middle of the region of $c/2\lambda^2 f_{RF1}^2$ to $3c/2\lambda^2 f_{RF2}^2$, both positive and negative CD can be monitored by measuring the RF power ratio.

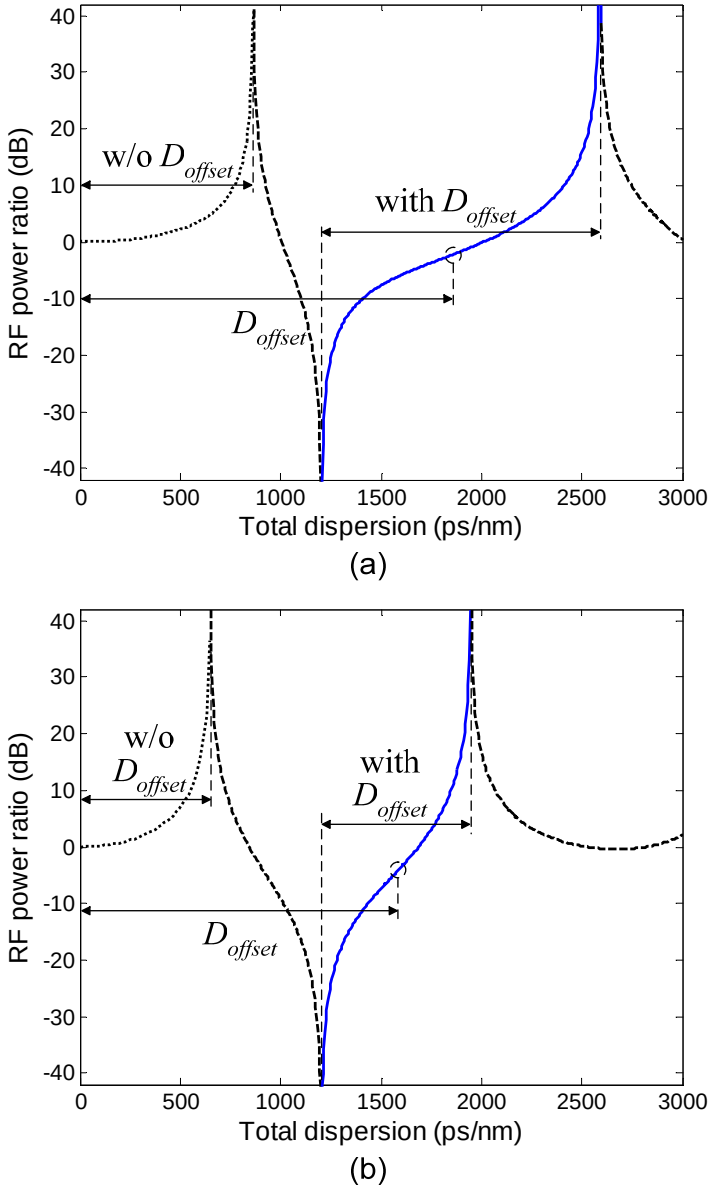

Fig. 3.3 The RF power ratio versus the total dispersion at λ = 1.55 μm and α_H = 0 for two different sets of RF frequencies;
(a) f_{RF1} = 7.2 GHz and f_{RF2} = 8.5 GHz; (b) f_{RF1} = 7.2 GHz and f_{RF2} = 9.8 GHz.

3.2.7 Frequency Selection Criteria for RF Tones

As seen in Fig. 3.3, a different RF frequencies set gives a different CD monitoring range and sensitivity. The CD monitoring range and the sensitivity are calculated and plotted in Fig. 3.4 and Fig. 3.5 against frequency difference between f_{RF1} and f_{RF2} for various values of f_{RF1}. Note that the sensitivity is calculated at the central point of the monitoring range because the RF power ratio curve is flattest at that point and hence the sensitivity at that point corresponds to the worst case (i.e., lowest) in the entire monitoring range.

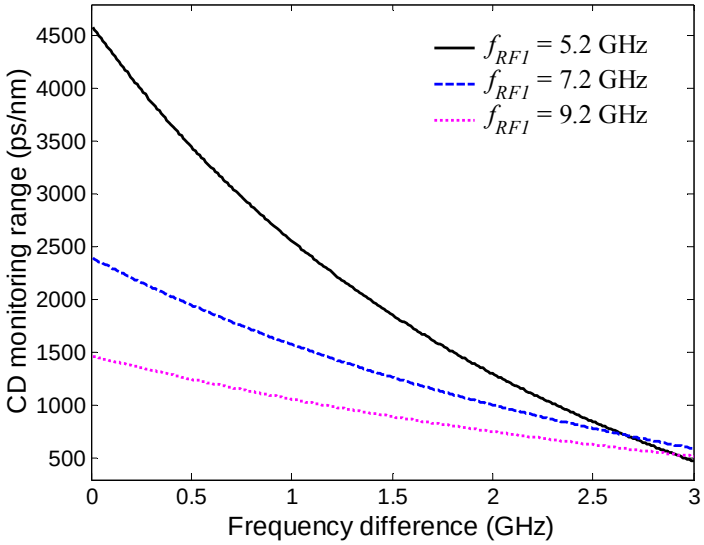

Fig. 3.4 CD monitoring range versus frequency difference ($f_{RF2} - f_{RF1}$) for various values of f_{RF1}.

Fig. 3.4 and Fig. 3.5 show that there is a trade-off between the CD monitoring range and sensitivity. As the frequency difference ($f_{RF2} - f_{RF1}$) increases, the monitoring range is reduced, but the monitoring sensitivity is enhanced. It is important to note that the monitoring sensitivity is mainly decided by the frequency difference whereas

both the frequency difference and the frequency f_{RF1} affect the monitoring range. Therefore, by selecting appropriate RF frequencies and dispersion offsets, the accumulated CD can be monitored with a good sensitivity for a large range.

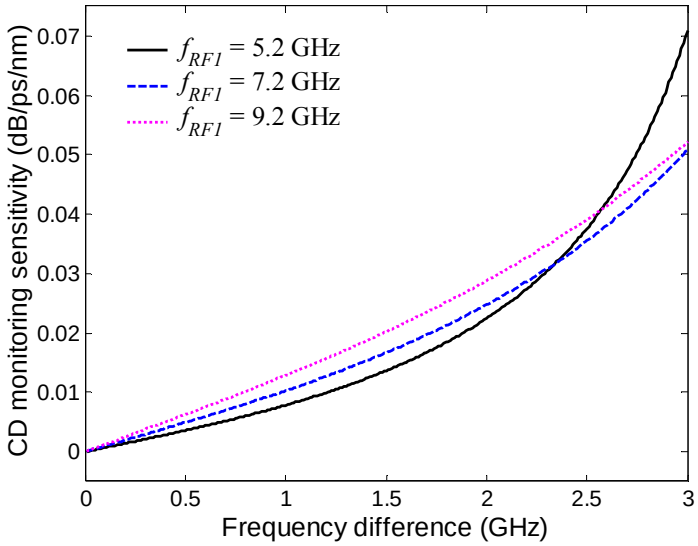

Fig. 3.5 CD monitoring sensitivity versus frequency difference ($f_{RF2} - f_{RF1}$) for various values of f_{RF1}.

There are two other considerations in selecting appropriate RF frequencies for the CD monitoring. One is the addition of RF tones should not induce significant power penalty for the data signal. The other is the cost of RF signal generators and RF power detectors should be as low as possible. Thereby, on the one hand, it is better to set the RF frequencies outside the optimum bandwidth of the low pass filter (LPF) of the data receiver so as to reduce the interference of RF tones to the data signal. On the other hand, it is preferable to use lower RF frequencies because RF signal generators and RF power detectors with lower frequency are cheaper and also the optical bandwidth will be more efficiently utilized (if DWDM systems are considered). Since the optimum bandwidth of the LPF of the receiver for detecting 10-Gb/s NRZ

data signals is approximately 7 GHz [69, 70], RF frequencies should be greater than 7 GHz but smaller than 10 GHz. Considering the compromised CD monitoring range and sensitivity, two different sets of RF frequencies are chosen in this study. The first set is f_{RF1} = 7.2 GHz and f_{RF2} = 8.5 GHz, for the larger CD monitoring range, and the second set is f_{RF1} = 7.2 GHz and f_{RF2} = 9.8 GHz, for the higher CD monitoring sensitivity. The detailed CD monitoring capability will be demonstrated in the next section.

3.3 Experimental Investigations

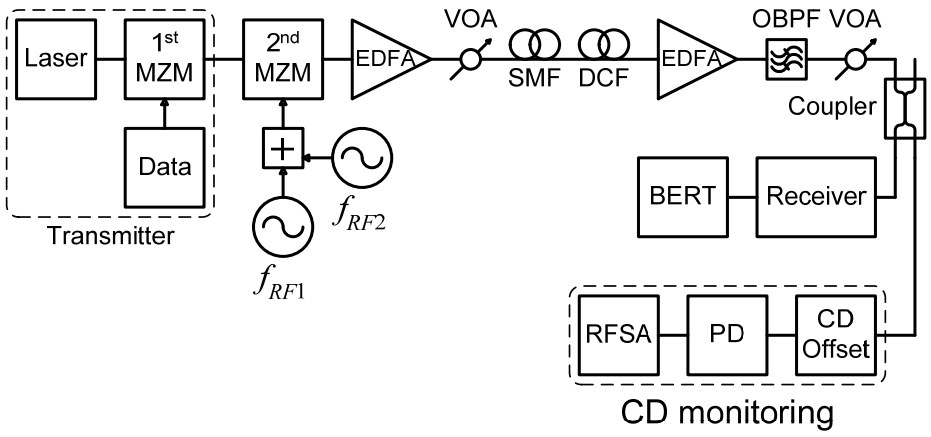

Fig. 3.6 Experimental setup for CD monitoring using the power ratio of two RF tones with an inserted dispersion offset.

Experiments have been carried out to verify this improved technique for monitoring the accumulated CD. Fig. 3.6 shows the experimental setup. The transmitter consists of a laser source which is modulated with 10-Gb/s Pseudo-random bit series (PRBS) data signal via a Mach-Zehnder modulator (MZM). A pulse pattern generator (PPG) (Anritsu MP1763C) is used as the PRBS data source. The data modulated light from

the transmitter is then modulated by two in-band RF tones (f_{RF1} and f_{RF2}) using another MZM with 10% modulation index. A synthesized high performance signal generator (Anritsu 68347C) works as one RF signal source. And a vector network analyzer (VNA) (Anritsu 37369C) acts as another RF signal source by simply operating at continuous wave (CW) mode. Although the light launched into the 2nd MZM is a data modulated light, the light power at the output of the 2nd MZM can be approximately expressed by Eq. (3.3) where its input light intensity is the average light intensity of data modulated light. Avanex PowerBit IM-10 intensity modulator is used here. Its insertion loss is 5 dB and the chirp parameter α_H is −0.2, which is measured using the method reported in [71]. Such a configuration can also be employed in a multichannel system where multiple data channels are first wavelength-division multiplexed and the combined WDM signal is then modulated by the two RF tones via the 2nd MZM. Note that the 2nd MZM is not necessary for a single channel system if these two RF tones are combined with the 10-Gb/s data signal before they are applied to an MZM. However, to suppress the generation of harmonics of the RF tones and intermodualtion products between the data signal and RF tones, it is better to use a 2nd MZM which allows the two RF tones to be imposed to the incident light linearly. The RF modulated light is then transmitted over different lengths of single mode fiber (SMF) and dispersion compensating fiber (DCF). Different combinations of SMF from 4 km to 60 km and DCF of 2.7 km are used to simulate different amounts of residual CD. To adjust the gain or attenuation and suppress the nonlinear effect of the optical link, erbium-doped fiber amplifiers (EDFAs) (5-dB noise figure and 1480-nm pump source) and variable optical attenuators (VOAs) are added in the optical channel. An optical band-pass filter (OBPF) is employed to remove the excess amplified spontaneous emission (ASE) noise. At the receiving side, the transmission

performance is measured by a bit-error-rate tester (BERT) (Anritsu MP1764C). A portion of the received light is tapped and coupled into the CD monitoring module which consists of a dispersion offset whose CD is pre-determined, a PIN photodetector (New Focus 1544-A), and an RF spectrum analyzer (RFSA) (Agilent E4407B) which works as RF power detectors. The RFSA bandwidth is set as small as 50 KHz, in order to decrease the RF power detection error induced by baseband data signal and ASE noise. The power ratio of two RF tones is measured from the received signals. In the experiment, two different sets of RF frequencies are used. The first set is f_{RF1} = 7.2 GHz and f_{RF2} = 8.5 GHz, and the second set is f_{RF1} = 7.2 GHz and f_{RF2} = 9.8 GHz. The inserted dispersion offset is set at 1680 ps/nm.

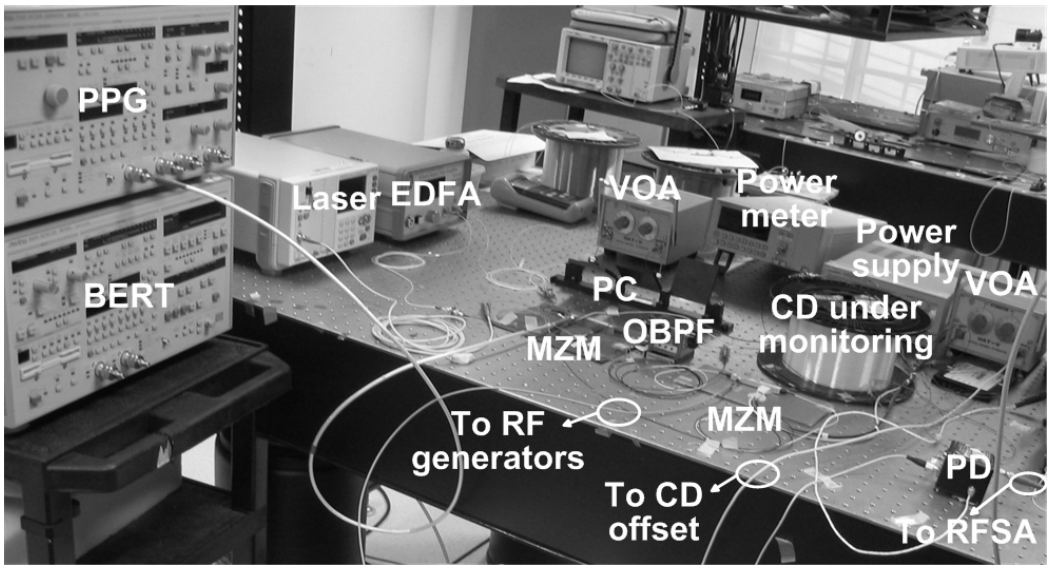

Fig. 3.7 Photograph of the proposed experimental setup.

Fig. 3.7 shows a photograph of the proposed experimental setup for further illustration. Note that in the experiment, the BERT and RFSA are connected to the photodetector alternately because of the photodetector quantity limitation. The RF power ratio is measured in a back to back system where the accumulated CD is 0 and

the RF power ratio should equal 1. However, for the photodetector used in the experiment, the measured RF power ratio is approximately 1 dB for the first set of RF frequencies, and 2.5 dB for the second set of RF frequencies. This difference is due to the photodetector resposne which is lower at higher frequency. Therefore, the normalization of the RF power ratio is required by measuring the RF power ratio in a back to back system first. Then the normailized RF power ratio with different accumulated CD values is acquired by changing the length of SMF and DCF.

Fig. 3.8 shows that both the theoretically calculated and experimentally measured normalized RF power ratio against the accumulated CD (which excludes the CD of 1680 ps/nm of the inserted dispersion offset) at λ = 1550 nm for two different sets of RF tones. The curves represent the theoretically calculated values, and the circular and triangular symbols are the experimental measurements. Note that, the theoretically calculated curves here are based on the experimentally measured chirp parameter of the 2nd MZM, $\alpha_H = -0.2$, not $\alpha_H = 0$ used in Fig. 3.3. As can be seen in the figure, the experimental results match very well with the theoretical ones, except for the places (the two ends of the curves) where one of the two RF powers is very low and cannot be measured accurately.

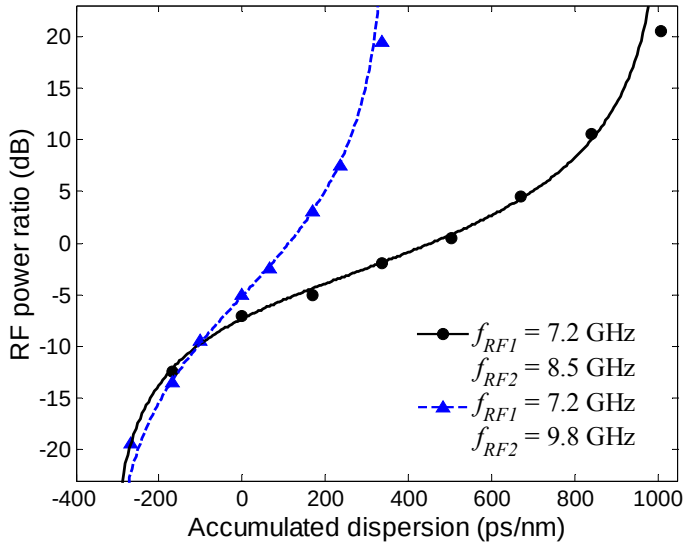

Fig. 3.8 The RF power ratio versus accumulated dispersion (λ = 1550 nm and D_{offset} = 1680 ps/nm).

Fig. 3.9 shows the spectrum of the combined data signal and RF tones for such a place (D_{offset} = 1680 ps/nm, D_{acc} = –270 ps/nm), where the RF power of f_{RF1} (7.2 GHz) is very low (hiding in the data signal and noise spectrum) and hence cannot be measured accurately. Note that the high spike at frequency 10 GHz is the regenerated clock frequency of the NRZ data signal [42]. It is also verified in the experiment that the RF power ratio remains constant when the RF power is changed by varying the gain or attenuation of the optical link. This reconfirms that the fluctuation of the received optical power will not affect the CD monitoring results using the RF power ratio method.

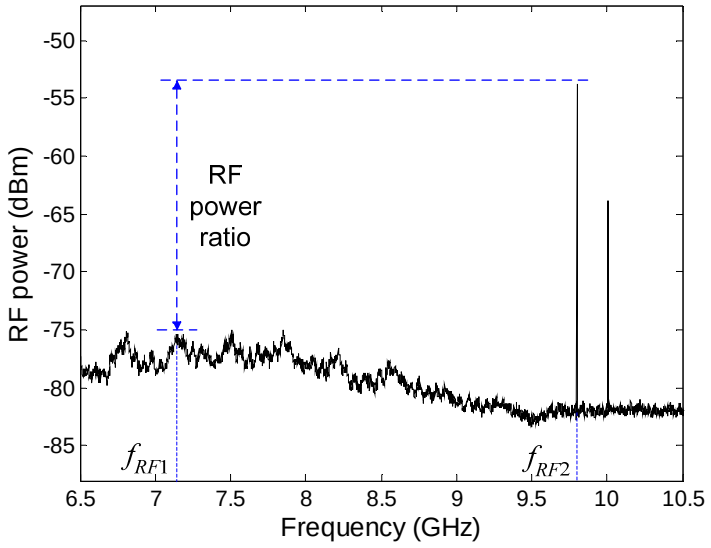

Fig. 3.9 RF spectrum of the combined signal.

As shown in Fig. 3.8, the monitoring range with small monitoring error is approximately from –200 ps/nm to +950 ps/nm for the 1st case of f_{RF1} = 7.2 GHz and f_{RF2} = 8.5 GHz. In this case, the RF power ratio varies from –15 dB to +20 dB. The lowest sensitivity is 0.014 dB/ps/nm (at the middle of the curve), and the average sensitivity is 0.03 dB/ps/nm for the entire monitoring range. It is worth noting that if the value of the dispersion offset is set at 1480 ps/nm, the monitoring range would be in the region of 0 to 1150 ps/nm. For the 2nd case of f_{RF1} = 7.2 GHz and f_{RF2} = 9.8 GHz, the monitoring range is smaller but the sensitivity is much higher. For this case, the monitoring range with small monitoring error is approximately from −200 ps/nm to +350 ps/nm, the lowest sensitivity is 0.04 dB/ps/nm and the average sensitivity is 0.064 dB/ps/nm. In this case, if the value of dispersion offset is set at 1480 ps/nm, the monitoring range would be from 0 to 550 ps/nm.

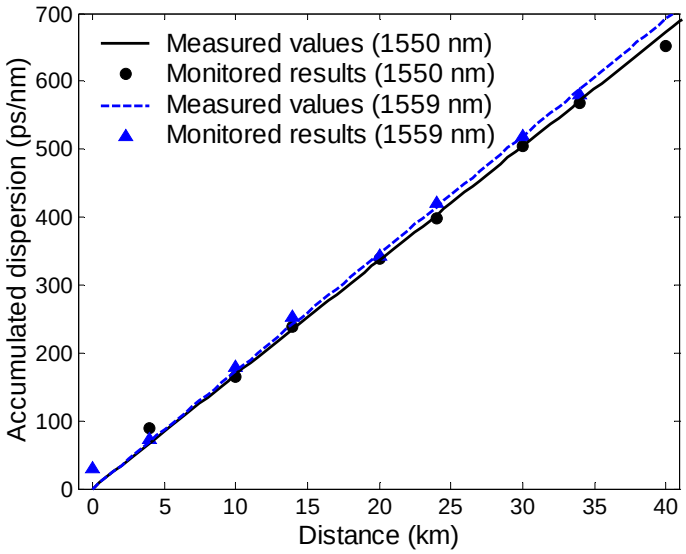

Fig. 3.10 Measured and monitored dispersion values at different lengths of SMF in a WDM system with two different wavelengths.

An experiment is also conducted where two WDM channels at 1550 nm and 1559 nm are first multiplexed and then modulated with two RF tones (7.2 GHz and 9.8 GHz). The dispersion offset used in this experiment is a length of 80-km SMF. Then the accumulated CD of different lengths of SMF is monitored for each wavelength. Fig. 3.10 shows the monitored accumulated CD value versus the length of SMF for the two different wavelengths. For the purpose of comparison, Fig. 3.10 also shows the actually measured CD for each of the two wavelengths, using Agilent 86038A optical dispersion analyzer. The actually measured CD values of the used SMF are 16.8 ps/nm/km and 17.3 ps/nm/km at wavelengths of 1550 nm and 1559 nm, respectively. As shown in Fig. 3.10 the monitored accumulated CD values using the proposed method agree very well with the actually measured CD values for various fiber lengths. The difference at around 0 km and 40 km is because one of the two received RF powers is quite low as explained previously.

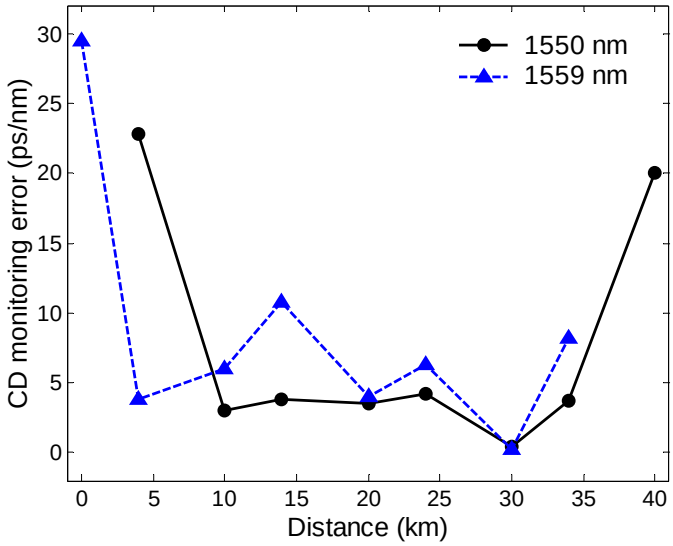

Fig. 3.11 CD monitoring errors between the monitored and measured dispersion value in a WDM system with two different wavelengths.

Fig. 3.11 shows the CD monitoring error against the fiber length for two different wavelengths. Here the monitoring error is defined as the absolute value of the difference between the monitored CD value using the proposed RF power ratio method and the actually measured value using Agilent 86038A optical dispersion analyzer. In Fig. 3.11, the circle and triangular symbols represent the CD monitoring errors for wavelengths of 1550 nm and 1559 nm, respectively. As shown in Fig. 3.11, the CD monitoring error is within 10 ps/nm for the most part of the monitoring range, but it increases to 20 – 30 ps/nm towards two edges of the monitoring range. These results have reconfirmed that the improved CD monitoring technique can be used to monitor the accumulated CD for WDM systems, and the monitoring error is acceptable within the monitoring range.

3.4 Discussions

3.4.1 Effects of Modulation Index

As illustrated in Fig. 3.9, the RF signal may be hidden behind the noise and spectrum components of the data signal. Under such a situation, the RF power cannot be measured accurately, resulting in higher monitoring errors. Hence, the effective monitoring range may be smaller than the theoretical one shown in the Fig. 3.4. The carrier-to-noise ratio (CNR) of the RF tone is defined as the ratio of the power of the RF tone to the total power of the data signal and the noise that pass through the RF filter of the RF power detector [72, 73]. According to Eq. (3.15), the CNR of the RF tone is given by:

$$CNR = \frac{\rho^2 I_0^2 M^4 m^2 R\left(1+\alpha_H^2\right)\cos^2\left(\frac{\pi D_{acc}\lambda^2 f_{RF}^2}{c}+\tan^{-1}\alpha_H\right)}{P_{Data}+P_{Noise}} \qquad (3.18)$$

where P_{Data} and P_{Noise} are the power of the data signal and the noise that pass through the RF filter, respectively.

In the experiment (m = 10%, λ = 1550 nm, D_{offset} = 1680 ps/nm, and the bandwidth of RF filters is 50 KHz), the CNRs of the RF tones were measured at 10dB, 19 dB, and 22 dB at 7.2 GHz, 8.5 GHz, and 9.8 GHz respectively when the CD under monitoring was fully compensated in the optical link (D_{acc} = 0 ps/nm). The measured CNR is high at higher frequency, due to the decreased level of data spectrum with frequency. When the CD under monitoring changes, the RF power changes with CD according to Eq. (3.15). The power of the data signal and noise also changes with CD but to a

smaller extent. Therefore, the CNRs of the RF tones will change with the CD under monitoring. When the CNR approaches to 0 dB, the RF power is greatly affected by the data signal and noise, which leads to the monitoring error. The experimental study has shown that a good accuracy can be obtained if the CNR is greater than 1 dB. Moreover, the narrow RF filter bandwidth is helpful for getting a high CNR. In the experiment, the bandwidth of RF filter is set as narrow as 50 KHz. The increase in the modulation index will increase the RF power and hence increase the CNRs of the RF tones. Therefore, a higher modulation index is desirable for getting a wider CD monitoring range. According to the Eq. (3.18), the CNR increases by 6 dB if the modulation index is doubled and other conditions remain unchanged. The experiment results have revealed that the monitoring range increases rapidly with the modulation index (m) when m is smaller than 10%. After the modulation index m reaches 20%, further increase in m would only increase the monitoring range slightly for a given set of RF frequencies, since the theoretical maximum monitoring range is ultimately determined by the two RF frequencies used (see Fig. 3.4). Furthermore, the larger modulation index m would saturate the limiting amplifier at the receiver, and limit the maximum RF power that can be measured. As will be seen later, a larger modulation index will cause a higher power penalty to the data signal.

Next, the power penalty of the baseband data signal caused by the two RF tones is investigated. As described in the section 3.3, the CD monitoring method using the RF power ratio requires the addition of two RF tones to the baseband data signal at the transmitting side. Since these two RF tones are within the frequency band of the baseband data signal, they will cause system impairment and result in the increase in bit-error-rate (BER). It is expected that a higher input RF power (i.e. higher

modulation index) will cause larger impairment to the data signal. Therefore, there is a trade-off between the CD monitoring range and the power penalty of the data signal. To evaluate this system impairment, the BER performance of a 10-Gb/s data signal with various RF modulation indices is measured for a 20-km SMF transmission.

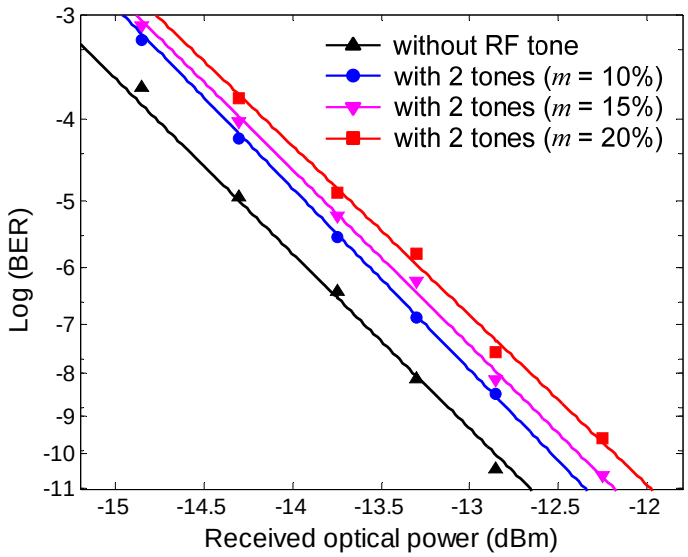

Fig. 3.12 BER versus received optical power without RF tones and with two RF tones for different RF modulation indices.

Fig. 3.12 shows the BER versus the received optical power for various RF modulation indices, where the two RF tones are 7.2 GHz and 8.5 GHz. For the comparison purpose, the figure also shows the case when the two RF tones are not applied to the 2nd MZM. As shown in Fig. 3.12, the power penalty at BER = 10^{-9} is increased as the modulation index (m) increases. More specifically, the power penalty is about 0.4 dB for m = 10%, and is increased to 0.7 dB and 0.9 dB as m increases to 15% and 20%, respectively. The power penalty with the two RF tones of 7.2 GHz and 9.8 GHz is also investigated. No obvious difference was observed. Therefore, the power penalty caused by the two RF tones can be made small enough (within 1 dB) and acceptable

for practical WDM systems if the modulation index is made smaller than 20%. Considering both the monitoring range and the power penalty, it can be concluded that the optimum modulation index should be set in the range of 10% to 20%.

3.4.2 RF Tone Removal Scheme

As described above, a larger modulation index will cause a higher power penalty to the data signal. To reduce the system impairment induced by the addition of two RF tones, one way is to reduce the input RF power. However, the reduction in the modulation index results in smaller CD monitoring range because of inaccuracy in measuring the low RF power. Some techniques using optical amplifier gain saturation effect [74, 75] or an acousto-optic attenuator [76] were reported to suppress pilot tones. But these methods can only remove the pilot tones with low frequencies. The inverting and re-modulating method in [77] can be used, but an extra intensity modulator is needed.

In order to ensure a large CD monitoring range with low system impairment, an RF tone removal scheme using RF notch filters is proposed here. Two RF notch filters whose center frequencies match with the two RF tones are inserted after the photodetector in the main data path to suppress the two RF tones. Practically, only one notch filter with frequency matching f_{RF1} should be enough for the case of f_{RF1} = 7.2 GHz and f_{RF2} = 9.8 GHz, because 9.8-GHz tone will be mostly removed by the filter of 10-GHz receiver. Due to the lack of the required RF notch filters, simulation is employed to examine the effectiveness of inserting two RF notch filters for RF tone

removal. A commercial simulation tool, VPItransmissionMaker [78] is used to study the BER performance. The system configuration for the simulation is similar to that for the experiment described in Fig. 3.6 (20-km SMF transmission of 10-Gb/s data). Fig. 3.13 depicts the transfer function of RF notch filters at 7.2 GHz, 8.5GHz and 9.8 GHz used in the simulations. The insertion loss is set to 1.7 dB. The 3-dB and 20-dB bandwidth are set to 180 and 60 MHz respectively. These specifications are set to match with some commercially available YIG RF notch filters [79].

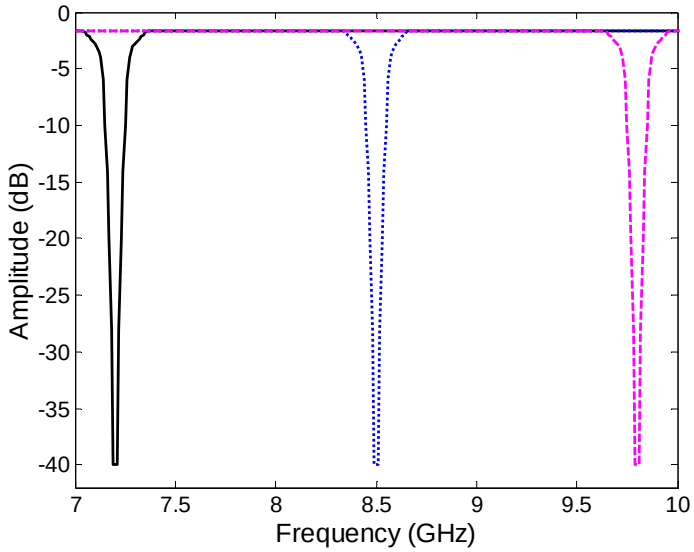

Fig. 3.13 Transfer function of RF notch filters at 7.2 GHz, 8.5 GHz and 9.8 GHz.

I next show how much BER performance is improved when two RF notch filters are used to suppress the two RF tones. Fig. 3.14 compares the BER curves with and without two additional RF notch filters at the corresponding frequencies of tones (7.2 and 8.5 GHz). For comparing the power penalty at BER=10^{-9}, the simulated BER result without the RF tone is plotted in the same figure. As shown in Fig. 3.14, the simulated power penalty is about 4 dB with the two RF tones. When the RF notch filters are introduced to suppress these RF tones, the decrease of the power penalty

due to the RF tone removal scheme is more than 2 dB. The BER performance is also examined by changing the parameter of RF notch filters such as the insertion loss between 1 dB to 2 dB, 3-dB bandwidth between 80 MHz to 200 MHz, 20-dB bandwidth between 40 MHz to 80 MHz, and the maximum rejection between 15 dB to 50 dB. The power penalty with the RF tones at 7.2 GHz and 9.8 GHz is also investigated. No obvious difference is observed. This may come from the fact that the importance of the high frequency components of NRZ data is reduced. Therefore, the use of RF notch filters can effectively reduce the impairment induced by the two RF tones.

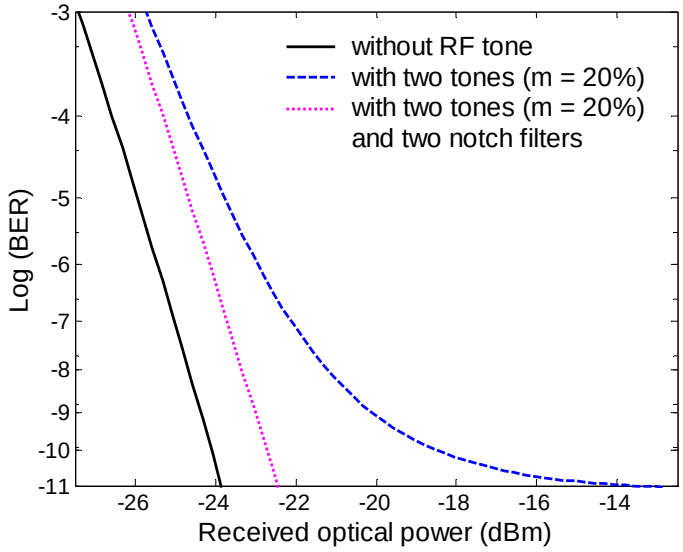

Fig. 3.14 BER versus received optical power with and without the two RF notch filters at 7.2 and 8.5 GHz.

It is worth to note that, compared with the experimental results of the BER performance in Section 3.4.1, the simulated power penalty is much larger when the RF tone removal scheme is not employed. For instance, with two 20% RF tones, the experimental power penalty is only 0.9 dB whereas the simulated one is 4 dB. The reason is that the limiting amplifier used in the experiment can shape the data pulse

and suppress the impairment coming from the RF tones, while such a component is not available in the simulation software (VPItransmissionMaker, version 4.0). However, the proposed RF tone removal scheme can further suppress the impairment induced by the two RF tones and make it be small enough and acceptable for practical WDM systems even at high modulation index.

3.4.3 CD Monitoring Error Induced by PMD and SPM

In a practical optical transmission system, the polarization mode dispersion (PMD) of the light induces a differential group delay (DGD) between two principal states of polarization (PSPs) and may reduce the detected RF power. Considering the effect of PMD, Eq. (3.17) is modified as [46]:

$$R = \frac{\left[1-4\gamma\left(1-\gamma\right)\sin^2\left(\pi f_{RF1}\Delta\tau\right)\right]}{\left[1-4\gamma\left(1-\gamma\right)\sin^2\left(\pi f_{RF2}\Delta\tau\right)\right]}\cdot\frac{\cos^2\left[\pi\left(D_{acc}+D_{offset}\right)\lambda^2 f_{RF1}^2/c+\tan^{-1}\alpha_H\right]}{\cos^2\left[\pi\left(D_{acc}+D_{offset}\right)\lambda^2 f_{RF2}^2/c+\tan^{-1}\alpha_H\right]} \quad (3.19)$$

where γ is the power splitting ratio between the two PSPs and $\Delta\tau$ is the DGD. The detailed derivation of Eq. (3.19) will be presented in the next chapter.

Eq. (3.19) shows that the DGD (1st order PMD) also affects the normalized RF power ratio. This means that the presence of PMD will induce the CD monitoring error if the DGD value is unknown. Let X_1 be the calculated CD without considering the DGD influence (i.e., using Eq. (3.17)) and X_2 be the calculated CD with considering the DGD influence (i.e., using Eq. (3.19)). The PMD-induced CD monitoring error is defined as $|\boldsymbol{X}_1-\boldsymbol{X}_2|$, i.e., the difference between X_1 and X_2. The curves of Fig. 3.15(a) and Fig. 3.15(b) show the calculated PMD-induced CD monitoring error against the

DGD without and with a dispersion offset (D_{offset} = 1680 ps/nm), respectively, when γ = 0.5, λ = 1550 nm, f_{RF1} = 7.2 GHz and f_{RF2} = 8.5 GHz. The PMD-induced CD monitoring error with a dispersion offset of 1680 ps/nm has also been experimentally measured using a PMD emulator. The experimental results are depicted as circular, triangular and rectangular symbols in Fig. 3.15(b). The results agree with the calculated values very well.

Both of Fig. 3.15(a) and Fig. 3.15(b) illustrate that the CD monitoring error increases with the DGD. Comparing Fig. 3.15(a) and Fig. 3.15(b), the monitoring error with a dispersion offset of 1680 ps/nm is greatly reduced as compared to that without the dispersion offset, especially when the CD under monitoring is small. This can be explained as follows. When a dispersion offset of 1680 ps/nm is inserted before the photodetector of the monitoring module, the monitoring range is shifted to the region of $c/2\lambda^2 f_{RF1}^2$ to $3c/2\lambda^2 f_{RF2}^2$ (ps/nm) (refer to Fig. 3.3), where a small change of CD would cause a relatively larger RF power ratio change. As a result, the increase in the DGD would cause a relatively smaller RF power ratio change as compared to the change caused by the CD, hence the CD monitoring error due to the DGD can be effectively reduced with the insertion of a dispersion offset. As shown in Fig. 3.15(b), the CD monitoring error with the dispersion offset of 1680 ps/nm is smaller than 25 ps/nm when the DGD is smaller than 20 ps. Similar results are also observed for f_{RF1} = 7.2 GHz and f_{RF2} = 9.8 GHz.

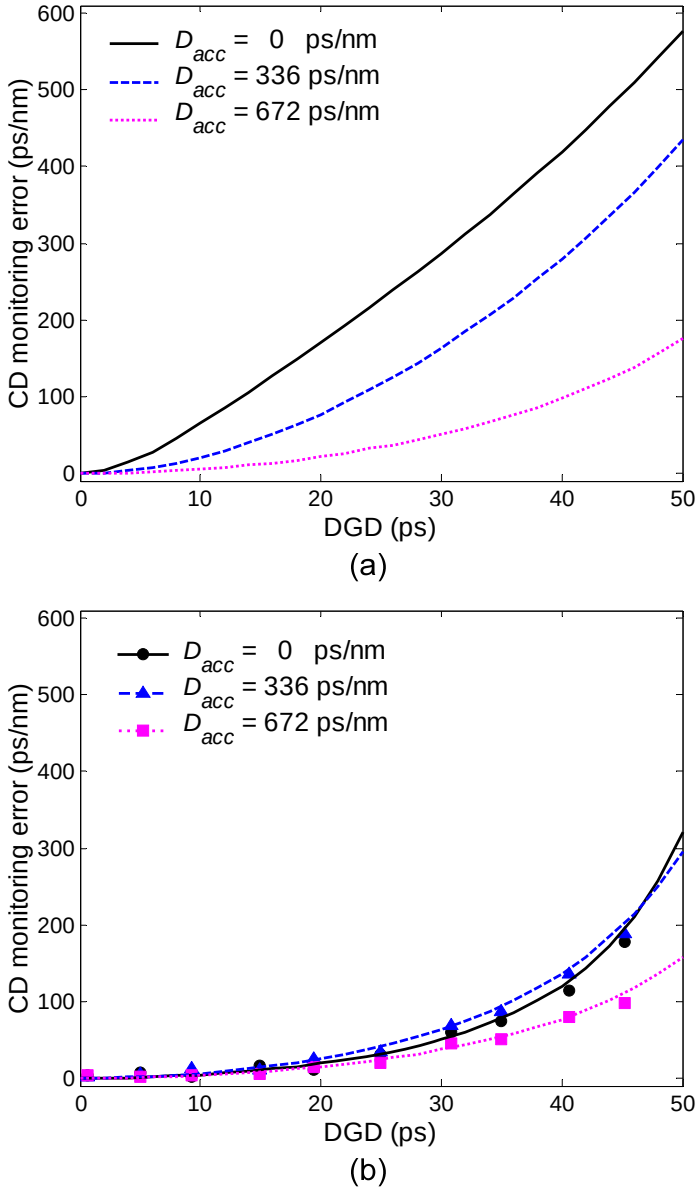

Fig. 3.15 Theoretical (curves) and experimental (symbols) PMD-induced CD monitoring errors for different CD values;
(a) without a dispersion offset; (b) with a dispersion offset (D_{offset} = 1680 ps/nm).

The detected power of RF tones may also be affected by the self-phase modulation (SPM) [46]. To investigate the SPM-induced CD monitoring errors, an experiment has been carried out to measure the normalized RF power ratio with different launched optical power by adjusting a VOA. The fiber length under test is 100 km

and two sets of RF frequencies are used. Fig. 3.16 shows the SPM-induced CD monitoring error versus the launched optical power. The results have indicated that the SPM may significantly increase the CD monitoring error if the launched optical power is greater than +6 dBm.

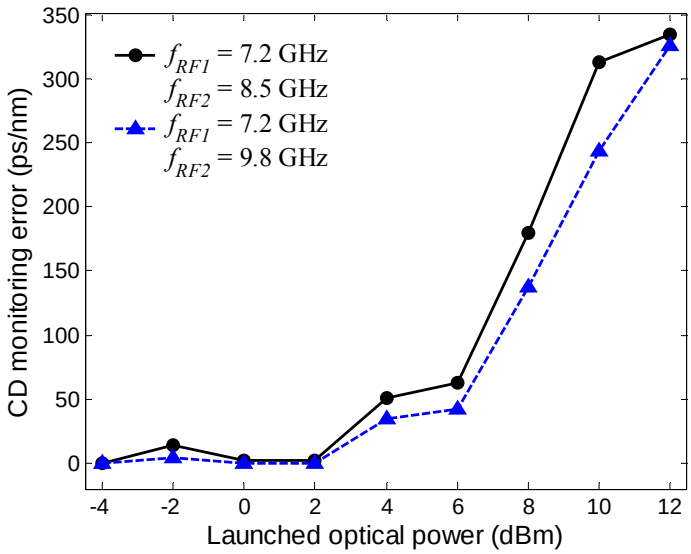

Fig. 3.16 The SPM-induced CD monitoring errors versus launched optical power for two different sets of RF frequencies (λ = 1550 nm).

3.5 Summary

In this chapter, an improved CD monitoring technique using the power ratio of two RF tones with an inserted dispersion offset has been presented and investigated. Two RF tones are added at the transmitter and a dispersion offset is inserted just before the photodetector within the monitoring module for CD monitoring purpose. By simply tracking the power ratio of two RF tones, this improved technique can monitor both the positive and negative accumulated CD caused by optical fibers and other optical

components in WDM systems. The operational principle of the RF power fading technique has been analyzed thoroughly in Section 3.2. Then, experiments have been conducted in a two-channel WDM system to demonstrate the monitoring capability of the improved method. The experiment results have shown that the monitoring range can be greater than 1150 ps/nm and the sensitivity can be as high as 0.064 dB/ps/nm by selecting appropriate dispersion offsets and suitable RF frequencies. While the high RF power may induce high power penalty for baseband data, the low RF power cannot be measured accurately, resulting in high monitoring errors and reduced monitoring range. The investigations on the effects of the modulation index have revealed that the modulation index should be greater than 10% but less than 20% to acquire a larger monitoring range with a small power penalty (smaller than 1 dB). Simulation results show that by adding two RF notch filters at the frequencies of RF tones before the baseband data receiver, I can make the impairment induced by the two RF tones be sufficiently small and acceptable for practical WDM systems even at high modulation index. The monitoring errors induced by PMD and SPM have also been investigated. The investigations have shown that the use of a dispersion offset can effectively reduce the PMD-induced monitoring error, and the SPM may significantly affect the monitoring accuracy if the launched optical power is greater than +6 dBm.

Chapter 4

Chromatic Dispersion Monitoring Error and Its Suppression Using DSB/SSB Power Ratio Detection

4.1 Introduction

For the RF power based chromatic dispersion monitoring techniques, the RF power is not only affected by the chromatic dispersion, but also fluctuated with other optical impairments, such as polarization mode dispersion (PMD), self-phase modulation (SPM), cross-phase modulation (XPM), chirp, etc. These impairments will lead to chromatic dispersion monitoring errors. In this chapter, the CD monitoring errors induced by those optical impairments are investigated. The study shows that the presence of some impairments induces significant CD monitoring errors. To tackle this problem, a new CD monitoring technique is proposed to suppress the influence

caused by these impairments. In the proposed CD monitoring scheme, one RF tone is added at the transmitter. The light is split into two branches in the monitoring module. An FBG filter which can remove one sideband is inserted before the photodetector of one branch. By taking the ratio of the RF power at the DSB and SSB branches, the monitoring error induced by PMD, SPM, and XPM effect is eliminated or suppressed. Furthermore, if another RF tone is added at the transmitter and an a priori known dispersion offset is inserted before the 50:50 coupler in the monitoring module, the monitoring error induced by the small chirp fluctuation can be suppressed. The operational principle is analyzed and the experimental and simulation investigations are presented. Experimental results show that this technique can accurately monitor the accumulated CD without being affected by the PMD and small chirp fluctuation. SPM and XPM induced CD monitoring errors can also be suppressed by this technique. Finally, the influence comes from other impairments such as stimulated Brillouin scattering (SBS), stimulated Raman scattering (SRS) and cross gain modulation (XGM) are also discussed in this chapter.

This chapter is organized as follows. Section 2 investigates the PMD induced CD monitoring errors and propose an optically sideband filtering and DSB/SSB RF power ratio detection method to eliminate it. In Section 3, the optically sideband filtering and DSB/SSB RF power ratio detection method is explored for suppressing the SPM and XPM induced CD monitoring errors. The influence arising from the small chirp fluctuation and its suppression are presented in Section 4. Section 5 discusses the effects of other optical impairments for RF power based CD monitoring methods.

4.2 PMD Induced CD Monitoring Error and Its Suppression

Polarization mode dispersion (PMD) is an important limiting factor in high capacity WDM networks. It may lead to monitoring errors for the RF tone based CD monitoring techniques. As discussed in Section 3.4.3, for the CD monitoring technique using the DSB/SSB RF power ratio, adding a dispersion offset can reduce the monitoring error as compared to that without the dispersion offset. However, when the differential group delay (DGD) is large, it may cause high CD monitoring errors even for the CD monitoring technique using the DSB/SSB RF power ratio with a dispersion offset. In Section 4.2.1, an expression for the power fading of an RF signal is derived by considering not only CD and chirp parameter, but also PMD. To tackle this issue, an optically sideband filtering and DSB/SSB RF power ratio detection method is proposed in Section 4.2.2. Both the operational principle and experimental results show that this technique can eliminate the PMD effect in the CD monitoring. Finally, in Section 4.2.3, by deriving a general expression for the DSB/SSB RF power ratio, the impact of non-ideal filtering is discussed.

4.2.1 CD and PMD Induced RF Power Fading

As discussed in Section 3.2.2, when an RF signal (f_{RF}) is intensity modulated to a light, the electric field of an RF modulated light wave can be written as:

$$E = e^{j\left(\omega_0 t + \frac{1}{2}\alpha_H \ln I_0\right)} \left\{ A_L \exp j\left(-\omega_m t + \tan^{-1}\alpha_H\right) + A_C + A_U \exp j\left(\omega_m t + \tan^{-1}\alpha_H\right)\right\} \qquad (4.1)$$

where I_0 is the input light intensity to the modulator; ω_0 is the angular frequency of the optical carrier; $\omega_m = 2\pi f_{RF}$ is the angular frequency of the modulation frequency; α_H is the Henry's alpha parameter of the modulator; and

$$A_C = \sqrt{I_0}\ , A_L = A_U = \frac{1}{4} m \sqrt{I_0}\sqrt{1+\alpha_H^2} \tag{4.2}$$

where m is the modulation index.

When such a signal light with two sidebands is launched into a length of fiber whose PMD is not negligible, the output electric field does not obey Eq. (3.11). In the absence of higher order PMD, considering the CD effect and the first order PMD effect, i.e., differential group delay (DGD), the output electric field can be expressed by [80-83]:

$$\begin{aligned} E = Me^{j\left(\frac{1}{2}\alpha_H \ln I_0 - \beta_0 L\right)} \Bigg[& A_C \left(\cos\theta e^{j\omega_0 t}\vec{x} + \sin\theta e^{j\omega_0 (t-\Delta\tau)}\vec{y}\right) \\ & + A_L e^{j\left(\tan^{-1}\alpha_H + \beta_1\omega_m L - \frac{L}{2}\beta_2\omega_m^2\right)} \left(\cos\theta e^{j(\omega_0-\omega_m)t}\vec{x} + \sin\theta e^{j(\omega_0-\omega_m)(t-\Delta\tau)}\vec{y}\right) \\ & + A_U e^{j\left(\tan^{-1}\alpha_H - \beta_1\omega_m L - \frac{L}{2}\beta_2\omega_m^2\right)} \left(\cos\theta e^{j(\omega_0+\omega_m)t}\vec{x} + \sin\theta e^{j(\omega_0+\omega_m)(t-\Delta\tau)}\vec{y}\right) \Bigg] \end{aligned} \tag{4.3}$$

where $\vec{x}$ and $\vec{y}$ represent the two unit vectors of the two principal states of polarization (PSPs), θ is the angle between the linear polarized field vectors and the x-axes of the two PSPs, and $\Delta\tau$ is the DGD between the two PSPs.

Since $\left|\vec{x}\right|^2 = \left|\vec{y}\right|^2 = 1$, and $\vec{x}\cdot\vec{y}^{*} = \vec{x}^{*}\cdot\vec{y} = 0$, the output light intensity can be written as:

$$
\begin{aligned}
|E|^2 = M^2 \Big[& A_L^2 + A_C^2 + A_U^2 \\
& + A_C A_L e^{-j\left(\beta_1\omega_m L - \frac{L}{2}\beta_2\omega_m^2 + \tan^{-1}\alpha_H\right)} \left(\cos^2\theta e^{j\omega_m t} + \sin^2\theta e^{j\omega_m(t-\Delta\tau)}\right) \\
& + A_C A_L e^{j\left(\beta_1\omega_m L - \frac{L}{2}\beta_2\omega_m^2 + \tan^{-1}\alpha_H\right)} \left(\cos^2\theta e^{-j\omega_m t} + \sin^2\theta e^{-j\omega_m(t-\Delta\tau)}\right) \\
& + A_C A_U e^{j\left(\beta_1\omega_m L + \frac{L}{2}\beta_2\omega_m^2 - \tan^{-1}\alpha_H\right)} \left(\cos^2\theta e^{-j\omega_m t} + \sin^2\theta e^{-j\omega_m(t-\Delta\tau)}\right) \\
& + A_C A_U e^{-j\left(\beta_1\omega_m L + \frac{L}{2}\beta_2\omega_m^2 - \tan^{-1}\alpha_H\right)} \left(\cos^2\theta e^{j\omega_m t} + \sin^2\theta e^{j\omega_m(t-\Delta\tau)}\right) \\
& + A_L A_U e^{j2\beta_1\omega_m L} \left(\cos^2\theta e^{-j2\omega_m t} + \sin^2\theta e^{-j2\omega_m(t-\Delta\tau)}\right) \\
& + A_L A_U e^{-j2\beta_1\omega_m L} \left(\cos^2\theta e^{j2\omega_m t} + \sin^2\theta e^{j2\omega_m(t-\Delta\tau)}\right) \Big]
\end{aligned}
\tag{4.4}
$$

Using the Euler formula, Eq. (4.4) can be re-written as:

$$
\begin{aligned}
|E|^2 = M^2 \Big\{ & A_L^2 + A_C^2 + A_U^2 \\
& + 2A_C A_L \cos^2\theta \cos\left(\omega_m t - \beta_1\omega_m L + \frac{L}{2}\beta_2\omega_m^2 - \tan^{-1}\alpha_H\right) \\
& + 2A_C A_L \sin^2\theta \cos\left(\omega_m(t-\Delta\tau) - \beta_1\omega_m L + \frac{L}{2}\beta_2\omega_m^2 - \tan^{-1}\alpha_H\right) \\
& + 2A_C A_U \cos^2\theta \cos\left(\omega_m t - \beta_1\omega_m L - \frac{L}{2}\beta_2\omega_m^2 + \tan^{-1}\alpha_H\right) \\
& + 2A_C A_U \sin^2\theta \cos\left(\omega_m(t-\Delta\tau) - \beta_1\omega_m L - \frac{L}{2}\beta_2\omega_m^2 + \tan^{-1}\alpha_H\right) \\
& + 2A_U A_L \left[\cos^2\theta \cos 2\left(\omega_m t - \beta_1\omega_m L\right) + \sin^2\theta \cos 2\left(\omega_m(t-\Delta\tau) - \beta_1\omega_m L\right)\right] \Big\}
\end{aligned}
\tag{4.5}
$$

After the essential triangular transform, Eq. (4.5) is changed to:

$$
\begin{aligned}
|E|^2 = {} & M^2\left(A_C^2 + A_U^2 + A_L^2\right) + 2M^2\sqrt{1 - 4\cos^2\theta\sin^2\theta\sin^2\left(\pi f_{RF}\Delta\tau\right)}\cdot \\
& \Big[A_C A_L \cos\left(\omega_m t - \tan^{-1}\alpha - \beta_1\omega_m L + \frac{L}{2}\beta_2\omega_m^2 - \tan^{-1}\varphi\right) \\
& + A_C A_U \cos\left(\omega_m t + \tan^{-1}\alpha - \beta_1\omega_m L - \frac{L}{2}\beta_2\omega_m^2 - \tan^{-1}\varphi\right) \\
& + A_U A_L \cos\left(2\omega_m t - 2\beta_1\omega_m L - \tan^{-1}\frac{\sin^2\theta\sin\left(2\omega_m\Delta\tau\right)}{\cos^2\theta + \sin^2\theta\cos\left(2\omega_m\Delta\tau\right)}\right) \Big]
\end{aligned}
\tag{4.6}
$$

where $\varphi = \dfrac{\sin^2\theta \sin(\omega_m \Delta\tau)}{\cos^2\theta + \sin^2\theta \cos(\omega_m \Delta\tau)}$.

Neglecting the DC and the second order terms, the component at frequency f_{RF} of the output photocurrent is approximately given as:

$$i_{out} = 2\rho A_C \sqrt{1-4\cos^2\theta \sin^2\theta \sin^2(\pi f_{RF}\Delta\tau)} \cdot \sqrt{(A_L - A_U)^2 + 4A_L A_U \cos^2\phi} \cdot \cos\left[\omega_m t - \beta_1 \omega_m L - \tan^{-1}\varphi + \tan^{-1}\left(\frac{(A_L - A_U)}{(A_L + A_U)}\tan\phi\right)\right] \tag{4.7}$$

where $\phi = \pi\lambda^2 D_{acc} f_{RF}^2 / c + \tan^{-1}\alpha_H$.

Therefore, the detected RF power at the modulation frequency f_{RF} of the signal can be expressed as:

$$P = 4\rho^2 M^4 A_C^2 \left[1-4\cos^2\theta \sin^2\theta \sin^2(\pi f_{RF}\Delta\tau)\right] \cdot \left[(A_L - A_U)^2 + 4A_L A_U \cos^2\left(\frac{\pi\lambda^2 D_{acc} f_{RF}^2}{c} + \tan^{-1}\alpha_H\right)\right] \tag{4.8}$$

Because $|E_x|^2 = \cos^2\theta \cdot |E|^2$ and $|E_y|^2 = \sin^2\theta \cdot |E|^2$, Eq. (4.8) can be rewritten as:

$$P = 4\rho^2 M^4 A_C^2 \left[1-4\gamma(1-\gamma)\sin^2(\pi f_{RF}\Delta\tau)\right] \cdot \left[(A_L - A_U)^2 + 4A_L A_U \cos^2\left(\frac{\pi\lambda^2 D_{acc} f_{RF}^2}{c} + \tan^{-1}\alpha_H\right)\right] \tag{4.9}$$

where γ is the power splitting ratio between the two PSPs.

Substituting Eq. (4.2) into Eq. (4.9), the detected RF power of the double sideband (DSB) signal can be written as:

$$P = \rho^2 m^2 I_0^2 M^4 \left[1 - 4\gamma(1-\gamma)\sin^2(\pi f_{RF}\Delta\tau)\right] \cdot \left(1+\alpha_H^2\right)\cos^2\left(\frac{\pi\lambda^2 D_{acc} f_{RF}^2}{c} + \tan^{-1}\alpha_H\right) \tag{4.10}$$

From this equation, I can readily acquire Eq. (3.19) as stated in the last chapter.

According to Eq. (4.10), the normalized RF power is plotted against the accumulated CD with various values of DGD as shown in Fig. 4.1, when $\alpha_H = 0$, $\gamma = 0.5$, $f_{RF} = 9$ GHz, and $\lambda = 1558$ nm. Here, the normalized RF power is defined as the ratio of the calculated RF power under different CD and DGD to the same reference RF power which does not experience any CD and DGD. Fig. 4.1 indicates that not only CD, but also DGD (first order PMD) may considerably influence the RF power. As the value of DGD increases, the measured RF power decreases, leading to CD monitoring error. As shown in Fig. 4.1, when the total CD is 300 ps/nm, the CD monitoring error can be as high as 400 ps/nm with the presence of a DGD of 50 ps.

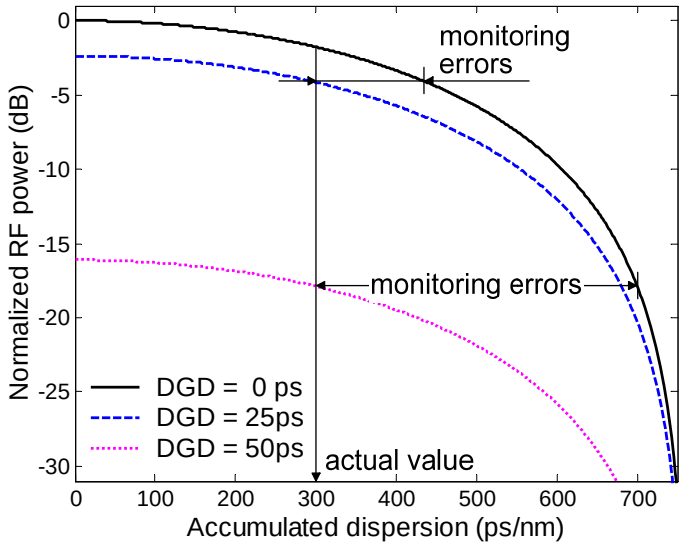

Fig. 4.1 The normalized RF power versus accumulated chromatic dispersion with different DGD values.

4.2.2 Optically Sideband Filtering and DSB/SSB RF Power Ratio Detection for Suppressing PMD Induced CD Monitoring Error

4.2.2.1 System configuration and experimental setup

Equation (4.10) indicates that not only CD, but also DGD (first order PMD) may considerably influence the RF power. Because DGD varies randomly with environmental conditions such as temperature, it may lead to monitoring errors for the CD monitoring techniques using RF power. As discussed in Section 3.4.3, for the CD monitoring technique using the RF power ratio of two tones, adding a dispersion offset can reduce the monitoring error as compared to that without the dispersion offset. However, when the DGD is large, it causes high CD monitoring error even for the CD monitoring technique using the RF power ratio of two tones with a dispersion offset.

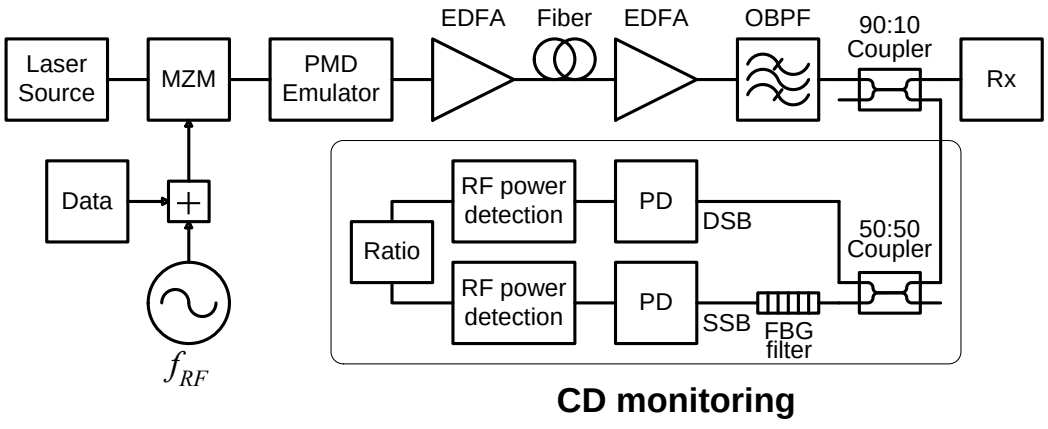

Fig. 4.2 System configuration and experimental setup of the proposed CD monitoring scheme for suppressing PMD induced CD monitoring error.

To tackle this issue, an optically sideband filtering and DSB/SSB RF power ratio detection method is proposed, which can eliminate the PMD effect in the CD monitoring. Fig. 4.2 illustrates the system configuration and experimental setup of the proposed CD monitoring scheme. An RF tone is combined with a data signal and then modulated to a light at 1558 nm using a Mach-Zehnder modulator (MZM) to generate an NRZ data with a double sideband (DSB) RF tone. The chirp of the MZM can be measured using the method reported in [71]. The light is coupled into a PMD emulator which has a tunable differential group delay (DGD) and can achieve equal power in two PSPs, i.e., $\gamma = 0.5$. The light propagates along different lengths of SMF to emulate various amounts of residual CD. Two EDFAs (5-dB noise figure and 1480-nm pump source) are used to compensate for the loss induced by fiber and other components. An optical bandpass filter (OBPF) is used to remove the excess amplified spontaneous emission (ASE) noise. At the monitoring point, the light is split into two branches by a 50:50 coupler. An FBG filter which can reject one sideband (either the upper or lower sideband) is inserted just before the photodetector (PD) of one branch in order to obtain single sideband (SSB) signal. Note that the sideband filtering is only in the monitoring module, and hence would not affect the baseband data signal. The light of each branch is fed into a PD followed by RF power detection. In the experiment, the RF power detection is achieved by an RFSA. The RFSA bandwidth is set as small as 50 KHz, in order to decrease the RF power detection error induced by baseband data signal and ASE noise. The residual CD can be monitored by measuring the DSB/SSB RF power ratio between two branches.

It is important to note that the proposed configuration is applicable to WDM systems where multiple wavelengths can be firstly combined and then modulated by the RF

tone via another shared MZM. At the monitoring point, the multiwavelength sideband filtering can be obtained by an FBG array tandem device [84] or other tunable periodical optical filters such as arrayed waveguide grating (AWG) [85] and Mach-Zehnder interferometer (MZI) [86] with a free spectral range (FSR) equal to the channel spacing.

4.2.2.2 Operational principle

When the light passes through the FBG sideband filter whose phase response is frequency independent, replacing the A_C, A_L and A_U in Eq. (4.9) by H_CA_C, H_LA_L and H_UA_U, the detected RF power at the modulation frequency f_{RF} of the signal can be expressed as:

$$P = 4\rho^2 M^4 H_C^2 A_C^2 \left[1-4\gamma(1-\gamma)\sin^2(\pi f_{RF}\Delta\tau)\right] \cdot\left[\left(H_L A_L - H_U A_U\right)^2 + 4H_L A_L H_U A_U \cos^2\left(\frac{\pi\lambda^2 D_{acc} f_{RF}^2}{c} + \tan^{-1}\alpha_H\right)\right] \quad (4.11)$$

where H_C, H_L and H_U are the electrical field magnitude transfer function of the optical filter at the frequencies of the optical carrier, the lower side band (LSB) RF tone and the upper side band (USB) RF tone, respectively.

Here, it is assumed that the LSB RF tone is removed completely by the FBG sideband filter, i.e., $H_L = 0$. Substituting Eq. (4.2) into Eq. (4.11), the detected RF power of the single sideband (SSB) signal can be written as:

$$\begin{aligned} P &= 4\rho^2 M^4 H_C^2 H_U^2 A_C^2 A_U^2 \left[1-4\gamma(1-\gamma)\sin^2(\pi f_{RF}\Delta\tau)\right] \\ &= \frac{1}{4} m^2 M^4 I_0^2 \left(1+\alpha_H^2\right)\rho^2 H_C^2 H_U^2 \left[1-4\gamma(1-\gamma)\sin^2(\pi f_{RF}\Delta\tau)\right] \end{aligned} \quad (4.12)$$

This equation indicates that CD does not affect the power of an SSB RF tone.

Therefore, by taking the ratio of the RF power without the FBG sideband filter (DSB) to that with the FBG sideband filter (SSB), the power variation related term M, PMD-related term $1-4\gamma(1-\gamma)\sin^2(\pi f_{RF}\Delta\tau)$ and other equal terms are cancelled. The DSB/SSB RF power ratio is then given by:

$$R = \frac{4\cos^2\left(\pi\lambda^2 D_{acc} f_{RF}^2 / c + \tan^{-1}\alpha_H\right)}{H_C^2 H_U^2} \tag{4.13}$$

In a practical system, the LSB tone may not be completely removed. However, normally only a small residual of the LSB tone exists and the detected DSB/SSB RF power ratio can be approximately given by Eq. (4.13). The detailed discussion will be given in the next section. Note that H_C and H_U are fixed and can be easily measured. Therefore, CD can be monitored by measuring this DSB/SSB RF power ratio without the influence of PMD.

4.2.2.3 Experimental results

Fig. 4.3 shows the measured optical spectra of the FBG filter profile, the optical signal at the DSB branch and the optical signal at the SSB branch. Here, in order to make the RF tone appear in the spectra clearly, the NRZ data is not modulated to the light. As can be seen in the figure, with the sideband filtering FBG, the low sideband is successfully removed. The sideband filtering ratio η can be as low as more than –20dB where it is defined as the magnitude transfer function ratio of the LSB tone to the USB tone (H_L/H_U). In this condition, the LSB tone can be regarded as completely

removed and the detected DSB/SSB RF power ratio can be approximately given by Eq. (4.13). The detailed discussion will be given in the next section.

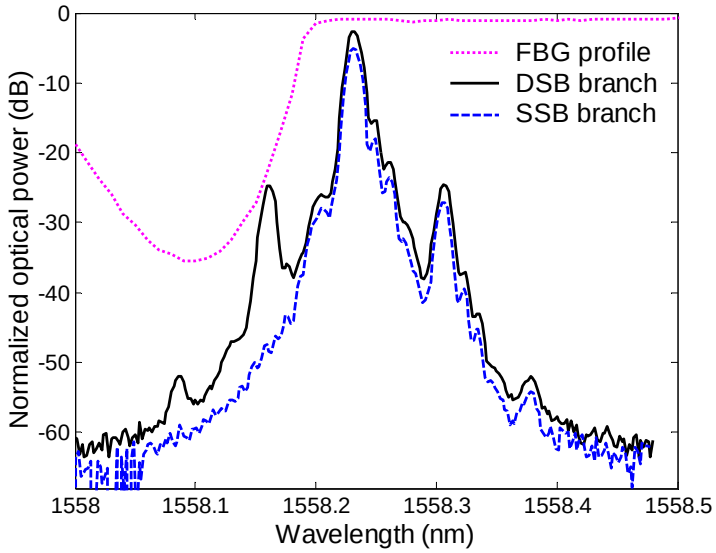

Fig. 4.3 Optical spectra of the FBG filter profile, the signal at DSB branch and the signal at SSB branch where LSB is removed by the FBG filter.

Fig. 4.4 shows the experimentally measured RF power at the DSB branch against the accumulated CD with various values of DGD for $\alpha_H = 0.2$, $\gamma = 0.5$, $f_{RF} = 9$ GHz, and $\lambda = 1558$ nm. Different CD amounts are emulated by different lengths of SMF. The lengths of SMF used are 0 km, 10 km, 13 km, 20 km, 23 km, 30 km, and 33 km. The curves represent the theoretical calculations for comparison, which match with the experimental results very well. The CD monitoring error induced by the ASE noise is very small. Note that, the theoretically calculated curves here are based on the experimentally measured chirp parameter of $\alpha_H = 0.2$, not $\alpha_H = 0$ used in Fig. 4.1. Here, the received optical power is kept constant so that the measured RF power is not affected by the optical power variation (due to optical loss or gain). Similar to Fig. 4.1, Fig. 4.4 demonstrates that as the value of DGD increases, the measured RF power

decreases, which causes CD monitoring error. As shown in Fig. 4.4, when the total CD is 220 ps/nm, the CD monitoring error can be as high as 330 ps/nm with the presence of a DGD of 45 ps.

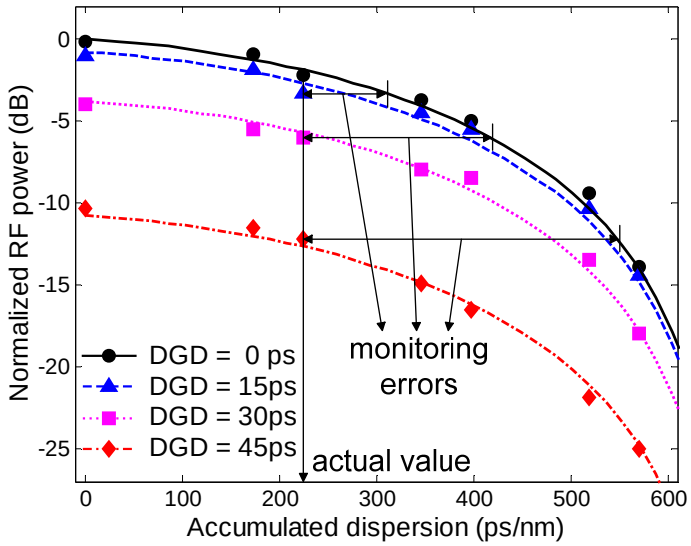

Fig. 4.4 The normalized RF power versus accumulated chromatic dispersion with different DGD values.

The theoretical (curve) and experimental (symbols) results of the DSB/SSB RF power ratio are shown in Fig. 4.5. As can be seen in the figure, the experimental results match quite well with the theoretical calculations for various values of DGD. The ratio is 11.2 dB when CD is zero because the sideband filtering and the insertion loss of FBG make the detected RF power of the SSB signal smaller than that of the DSB signal. This ratio decreases with the increase of CD since the DSB RF power fades with both PMD and CD but the SSB RF power experiences fading from PMD only. Therefore, the DSB/SSB RF power ratio is not affected by PMD, i.e., the CD monitoring error due to PMD is eliminated as shown in Fig. 4.5. It should be noted that the RF power measured at the SSB branch could also be used for PMD

monitoring simultaneously as reported in [87]. In [88], a simultaneous CD and PMD monitoring technique is presented by inserting a polarization scrambler before the fiber transmission. Keeping scrambling the polarization of the input signal, CD can be monitored by the maximum RF power, and PMD can be measured by the difference between maximum and minimum RF power. Compared with the technique in [88], the proposed optically sideband filtering scheme is cost-efficient and has higher processing speed. It is because in [88], a polarization scrambler is required at the transmitter side to keep the PMD effect on the output RF power varying periodically, and the maximum and minimum RF power has to be measured after full periodical polarization scrambling.

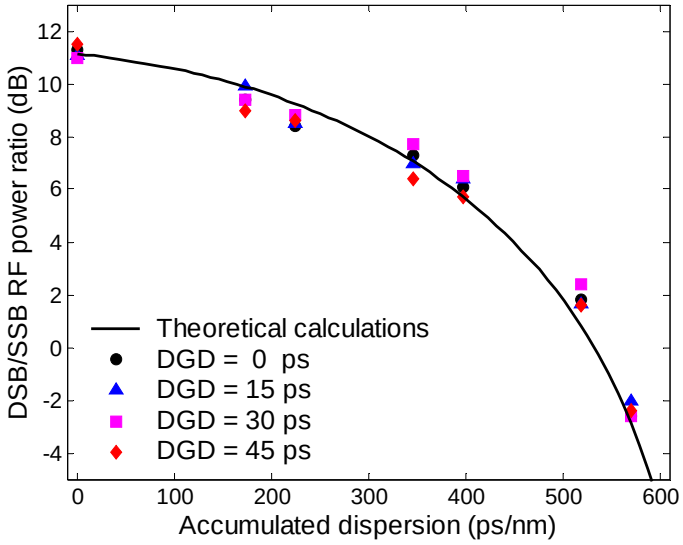

Fig. 4.5 The DSB/SSB RF power ratio versus accumulated chromatic dispersion with different DGD values.

Fig. 4.6 shows the CD monitoring error versus the DGD with and without PMD cancellation, when the total residual CD is 400 ps/nm. As shown in Fig. 4.6, the CD monitoring error induced by PMD is greatly suppressed by the PMD cancellation using the optical sideband filtering and the DSB/SSB RF power ratio detection, even

when the DGD is as large as 45 ps. It is also important to note that the received optical power do not have to be kept constant when measuring CD, since the method takes the DSB/SSB RF power ratio of the two branches, which cancels the received power variation caused by loss or gain along the optical path, which is similar to that proposed in Chapter 3.

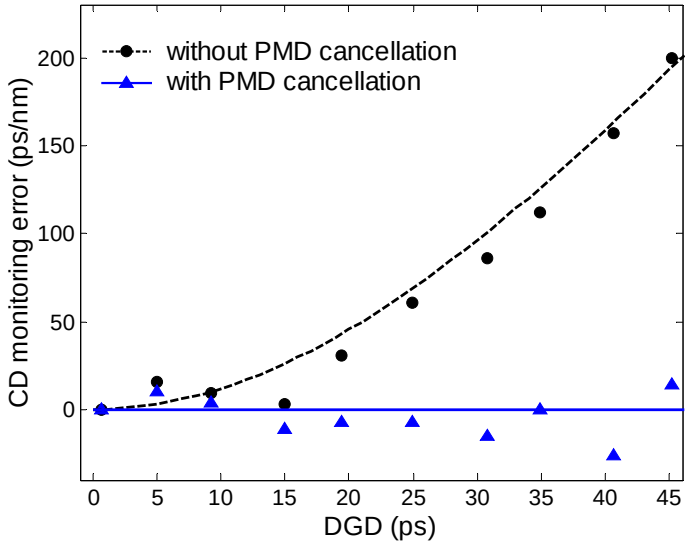

Fig. 4.6 CD monitoring error versus DGD without and with PMD cancellation.

4.2.3 Impact of Non-ideal Filtering

In Section 4.2.2, it is assumed that the LSB RF tone is removed completely by the FBG sideband filter, i.e., $H_L = 0$. However, in a practical system, the center frequency (i.e. Bragg wavelength) of the FBG filter used for removing the LSB or the carrier frequency of the optical signal may drift around the desired value. In such situation, the magnitude transfer function of the optical filter H may change. As long as the frequency drift is small, the variations of H_C and H_U are normally small because the

carrier and the USB tone are in the passband of the FBG filter (as shown in Fig. 4.3). Next, the situation where the LSB tone cannot be removed completely is considered. According to Eq. (4.2) and Eq. (4.11), the detected RF power can be written as:

$$P = \frac{1}{4} m^2 M^4 I_0^2 \left(1+\alpha_H^2\right) \rho^2 H_C^2 H_U^2 \left[1-4\gamma\left(1-\gamma\right)\sin^2\left(\pi f_{RF}\Delta\tau\right)\right] \cdot\left[\left(1-\eta\right)^2 + 4\eta\cos^2\left(\frac{\pi\lambda^2 D_{acc} f_{RF}^2}{c} + \tan^{-1}\alpha_H\right)\right] \tag{4.14}$$

where η is defined as the sidebands filtering ratio and given by $\eta = H_L / H_U$.

Then the ratio of the RF power with DSB to that with the incomplete LSB filtering can be written as:

$$R = \frac{4\cos^2\left(\pi\lambda^2 D_{acc} f_{RF}^2 / c + \tan^{-1}\alpha_H\right)}{H_C^2 H_U^2 \left[\left(1-\eta\right)^2 + 4\eta\cos^2\left(\pi\lambda^2 D_{acc} f_{RF}^2 / c + \tan^{-1}\alpha_H\right)\right]} \tag{4.15}$$

when $\eta = 0$, Eq. (4.15) simplifies to Eq. (4.13).

Eq. (4.15) gives a general expression for the DSB/SSB RF power ratio, which is indispensable for discussing the impact of non-ideal filtering. The CD monitoring errors induced by the incomplete LSB filtering are calculated according to Eq. (4.15) and plotted in Fig. 4.7 against the sidebands filtering ratio η when $\alpha_H = 0.2$, $f_{RF} = 9$ GHz, and $\lambda = 1558$ nm for two different accumulated CD values (200 and 400 ps/nm).

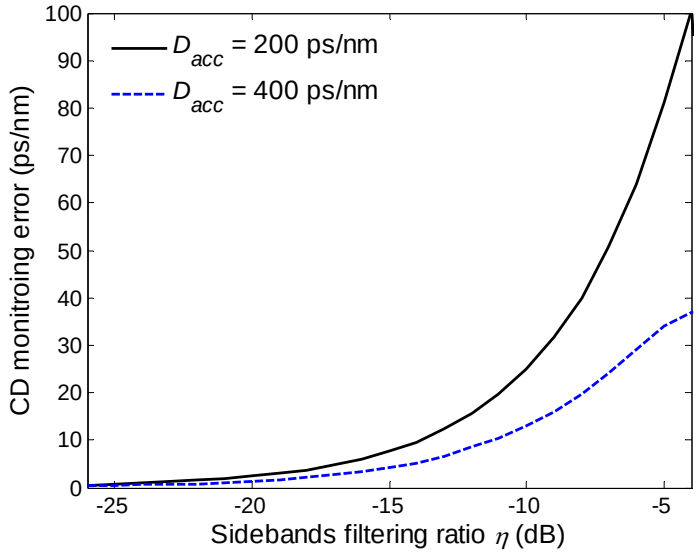

Fig. 4.7 The CD monitoring errors induced by the incomplete LSB filtering versus the sidebands filtering ratio for two different accumulated CD values.

As can be seen in Fig. 4.7, for D_{acc} = 200 ps/nm and D_{acc} = 400 ps/nm, the CD monitoring errors induced by the incomplete LSB filtering are less than 10 and 5 ps/nm, respectively, when the sidebands filtering ratio η is smaller than –15 dB, and are negligible if the sidebands filtering ratio η is less than –20 dB. If the sidebands filtering ratio η is greater than –10 dB, the CD monitoring errors become considerably large. The incomplete LSB filtering induced error for D_{acc} = 200 ps/nm is larger than the one for D_{acc} = 400 ps/nm, because the monitoring curve is steeper and has higher monitoring sensitivity when D_{acc} = 400 ps/nm, as shown in Fig. 4.5. This error can be eliminated using an athermally packaged FBG filter. Presently, numerous commercial FBGs with athermal packaging offer very small thermal drift (smaller than 0.5 pm/°C) [89]. And the wavelength drifts of temperature stabilized DFB laser sources are normally very small [90]. Considering the small thermal drift of state-of-the-art components, this required sidebands filtering ratio is easy to achieve using athermal FBG filters with very high signal rejection (> 25 dB) and sufficient

bandwidth [84]. Therefore the monitoring error induced by the drift of the filter and signal can be very small.

4.3 CD Monitoring Error Induced by Kerr Effect and Its Suppression

Silica fiber behaves nonlinearly at high input optical intensity and its refractive index changes with the intensity. This is known as Kerr effect [2, 18]. It leads to the phenomena of self phase modulation (SPM), cross phase modulation (XPM) and four wave mixing (FWM). For an RF tone based CD monitoring technique, SPM and XPM may induce phase modulation to the RF tone, leading to RF power variation and CD monitoring errors [91]. The scheme of optically sideband filtering and DSB/SSB RF power ratio detection for suppressing PMD induced CD monitoring error is also expected to reduce the influence of SPM and XPM when the launched optical power is not extremely high. The simulation investigations are carried out for verifying its feasibility in this section.

4.3.1 Self Phase Modulation

In optical communication systems, Kerr effect creates SPM that converts power fluctuations in propagating wave to spurious phase fluctuations in the same wavelength signal. This SPM effect may also influence CD monitoring and induce monitoring error [46, 91-93]. Since this scheme measures the ratio of the RF power

with DSB to that with SSB, the impact of SPM is also expected to be partially cancelled. To demonstrate the effectiveness, I resort to a commercially-available numerical simulation tool, VPItransmissionMaker [78]. A single wavelength 10-Gb/s system with 9-GHz RF tone for CD monitoring is simulated according to the setup in Fig. 4.2 except a variable optical attenuator (VOA) is inserted before the fiber for controlling the launched optical power. The transmission link is a 100-km standard SMF with full dispersion compensation. The RF frequency is 9 GHz in the simulation. The chirp of the MZM is zero. The fiber nonlinear refractive index is set at 2.6×10^{-20} m^2/W, which is the typical value for the standard SMF [2]. The effective core areas are 80×10^{-12} m^2 and 25×10^{-12} m^2 for the standard SMF and DCF, respectively. The simulated normalized RF power (lower curve) and DSB/SSB RF power ratio (upper curve) with different values of input optical power are shown in Fig. 4.8.

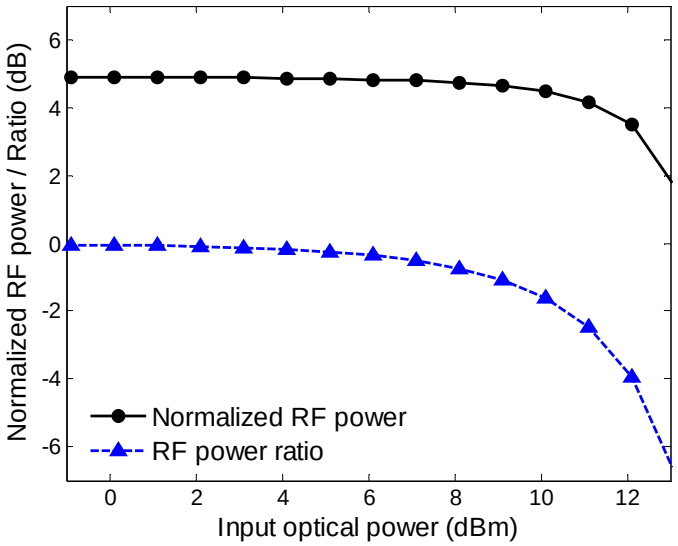

Fig. 4.8 SPM effect on the RF tone based CD monitoring technique.
(upper: DSB/SSB RF power ratio versus input optical power; lower: the normalized RF power at DSB branch versus input optical power.)

Fig. 4.8 shows that the normalized RF power (lower curve) is reduced as the input optical power is increased. When the launched optical power is larger than +6dBm, the fading of the normalized RF power becomes very obvious and the impact of SPM cannot be neglected. Fig. 4.8 also shows that DSB/SSB RF power ratio (upper curve) between two branches versus the input optical power. Because it is a single wavelength system, the XPM effect does not exist and only the SPM effect needs to be considered. As can be seen in the figure, in comparison with the curve of the normalized RF power, the DSB/SSB RF power ratio curve is relatively flat when the input optical power increases up to +9 dBm. The reason is that both the RF powers at the DSB branch and at the SSB branch are affected by the SPM effect and decrease with the increasing input optical power. Nevertheless, if the input optical power is very high, for example, larger than +9 dBm as shown in Fig. 4.8, the RF power at DSB branch fades with a faster pace. In this case, the DSB/SSB RF power ratio will decrease with the input optical power dramatically.

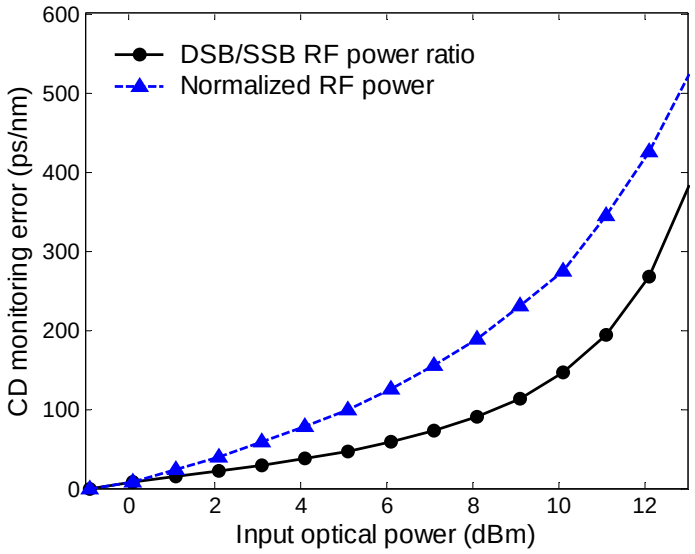

Fig. 4.9 SPM induced CD monitoring error versus input optical power without and with DSB/SSB RF power ratio detection.

The decreased normalized RF power or DSB/SSB RF power ratio may induce CD monitoring error for the RF tone based CD monitoring techniques. Fig. 4.9 compares the CD monitoring errors induced by the SPM effect using the conventional RF power method and the optically sideband filtering and DSB/SSB RF power ratio detection method proposed in this thesis. As shown in Fig. 4.9, the SPM induced CD monitoring error is as high as 120 ps/nm for the conventional RF power method, when the launched optical power is +6 dBm. When the launched optical power is larger than +6 dBm, the CD monitoring error increase dramatically. If the optically sideband filtering and DSB/SSB RF power ratio detection method is used, the CD monitoring error induced by SPM effect is considerably suppressed to around 55 ps/nm. The rapid increase in the CD monitoring only occurs when the input optical power is higher than +9 dBm. Simulation results have demonstrated that the proposed optically sideband filtering and DSB/SSB RF power ratio detection method can suppress the CD monitoring error induced by the SPM effect when the accumulated CD is around zero.

4.3.2 Cross Phase Modulation

In WDM systems, in addition to the SPM effect, another important Kerr effect is cross phase modulation (XPM). It converts intensity fluctuations from one channel to phase fluctuations in other co-propagating channels. It may induce RF power variation, leading to CD monitoring errors [91]. The use of the proposed optical sideband filtering and DSB/SSB RF power ratio detection scheme can also cancel the XPM

induced CD monitoring error partially. VPI TransmissionMaker [78] is used in this work to carry out simulation in order to verify the effectiveness. The system configuration is shown in Fig. 4.10. Two wavelengths with 50-GHz channel spacing are employed in the simulation. A 9-GHz RF tone is modulated via a zero-chirp MZM to the channel at λ_1 = 1558.2 nm for CD monitoring. The other channel at λ_2 = 1558.6 nm, which is amplified by an EDFA and followed by a VOA, is multiplexed with λ_1 by a multiplexer (MUX). The input optical power at λ_1 is as low as –9 dBm, so that the SPM effect is negligible here. Tuning the EDFA and VOA, the input optical power at λ_2 is varied. Thus, the XPM effect arising from channel λ_2 would give different impact to the channel λ_1 when the input optical power of λ_2 is changed. After a 100-km standard SMF transmission with full dispersion compensation, channel λ_1 with the RF tone is demultiplexed from channel λ_2, and the XPM effect on the RF tone of channel λ_1 is evaluated.

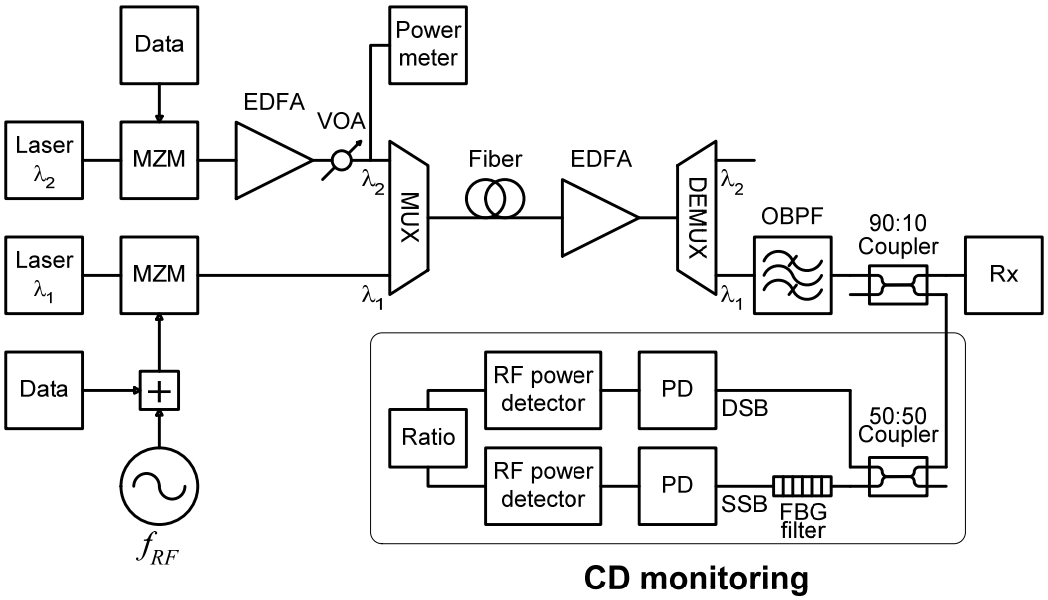

Fig. 4.10 Simulation configuration of the performance evaluation for suppressing XPM induced CD monitoring error.

Fig. 4.11 shows the simulated normalized RF power (lower curve) and DSB/SSB RF power ratio (upper curve) against the input optical power at channel λ_2. As shown in the figure, the normalized RF power decreases quickly as the launched optical power at channel λ_2 increases. In contrast, the DSB/SSB RF power ratio between two branches remains almost unchanged when the input power is varied in the range of 0 to 6 dBm, and decreases very slowly when the input power is changed from 6 dBm to 13 dBm, then increases as the launch power is greater than 13 dBm. This is because both of the RF powers at the DSB and SSB branches are affected by the XPM effect, and they both decrease in the almost same pace as the launched optical power increases from 0 to 6 dBm. However, when the input optical power is increased from 6 dBm to 13 dBm, the RF powers at two branches change with slightly different paces and consequently the DSB/SSB RF power ratio decreases slowly, as shown in Fig. 4.11. When the input optical power is greater than 13 dBm, the RF power ratio is increased instead of being reduced.

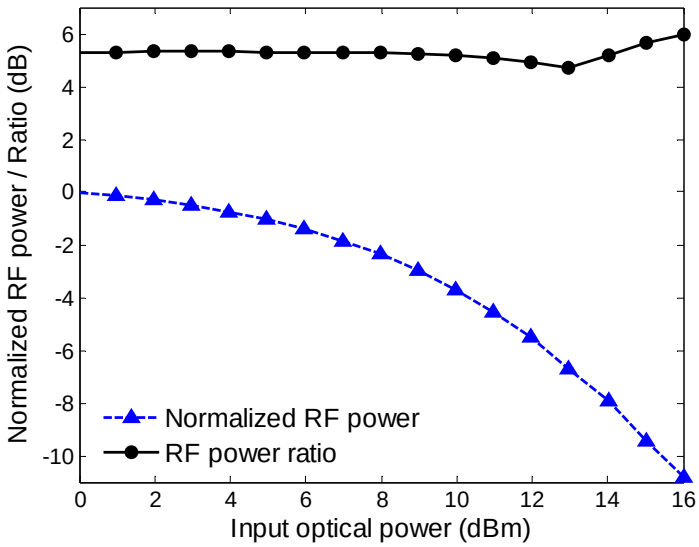

Fig. 4.11 XPM effect on the RF tone based CD monitoring technique.
(upper: the DSB/SSB RF power ratio versus input optical power at λ_2; lower: the normalized RF power at DSB branch versus input optical power at λ_2.)

As shown in Fig. 4.11, when the input optical power of another channel is changed, both the normalized RF power and DSB/SSB RF power ratio does not remain constant due to the XPM effect, which may induce CD monitoring error. Fig. 4.12 shows the CD monitoring errors induced by the XPM effect using the conventional RF power method and the proposed optically sideband filtering and DSB/SSB RF power ratio detection method, when λ_1 = 1558.2 nm, λ_2 = 1558.6 nm, $\alpha_H = 0$, f_{RF} = 9 GHz, with 100-km standard SMF transmission and full dispersion compensation. As can be seen in Fig. 4.12, using the conventional RF power method, the XPM induced CD monitoring error increases dramatically with the increase of the input optical power. For example, the CD monitoring error is as high as 280 ps/nm when the launched input optical power at channel λ_2 is +6 dBm. However, if the optically sideband filtering and DSB/SSB RF power ratio detection method is used, the CD monitoring error arising from the XPM effect is considerably suppressed. No obvious CD monitoring error can be observed when the launched optical power at channel λ_2 is less than +6 dBm. Even if the input optical power is as high as +13 dBm, the CD monitoring error is only about 180 ps/nm. Hence, when the input optical power is lower than 13 dBm, the proposed DSB/SSB RF power ratio detection method also considerably suppresses the CD monitoring error induced by the XPM effect when the accumulated CD is around zero. It is noted that when the input optical power is larger than 13 dBm, the RF power ratio is increased rather than being reduced. In this situation, the monitoring error cannot be determined. It is also noted that while the proposed method can suppress the XPM induced CD monitoring error, it does not change the XPM effect itself. Fiber nonlinearity still exists and causes significant degradation to the transmitted data when the input optical power is high.

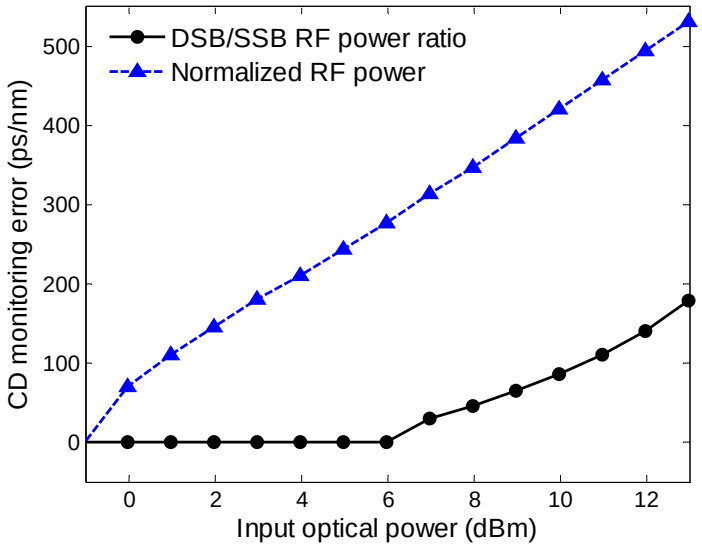

Fig. 4.12 XPM induced CD monitoring error versus input optical power at λ_2 without and with DSB/SSB RF power ratio detection.

4.4 Chirp Effect in CD Monitoring and Its Suppression

Next, how chirp may affect CD monitoring is examined. As described before, Eqs. (4.10) and (4.13) indicate that the chirp can influence the RF power as well as the DSB/SSB RF power ratio. Although both chirp and CD cause the detected RF power fading, they have different originations. Chirp arises from the transmitter (initial condition), while CD arises from the transmission line (propagation). So they have different impact on signal performance at the receiver side, as well as RF power and DSB/SSB RF power ratio used for CD monitoring, as shown in Eqs. (4.10) and (4.13).

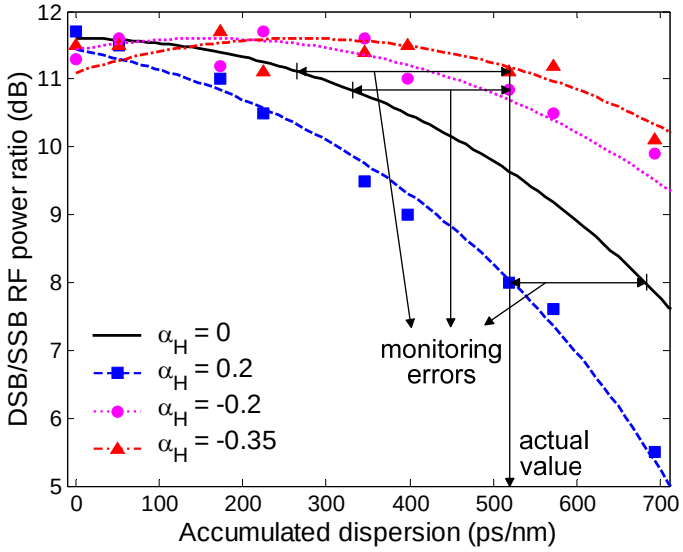

Fig. 4.13 The theoretical (curves) and experimental (symbols) DSB/SSB RF power ratio versus the accumulated CD with different chirp values when f_{RF} = 7 GHz.

Although the modulator with small negative chirp may induce smaller dispersion penalty for certain transmission distance, the zero-chirp modulator is still widely used in the practical communication systems. However, considering a practical MZM where an optical light is intensity modulated, the imbalanced optical amplitudes between the two arms of the MZM make the chirp (Henry's alpha parameter α_H) slightly deviate from zero [94, 95]. In a CD monitoring system, the chirp α_H needs to be pre-measured to determine its influence. However, the chirp may fluctuate with the bias point shift due to temperature variation and aging [96]. For an x-cut $LiNbO_3$ MZM, it has been shown that the chirp α_H tested using the method in [71] fluctuates with the bias voltage. The chirp α_H can be really low, and normally varies within ±0.4 near the quadrature bias point [97]. However, even such a small chirp may induce a large CD monitoring error which has been observed in the experiments. Fig. 4.13 shows the DSB/SSB RF power ratio versus the accumulated CD for various small

chirps of an x-cut $LiNbO_3$ MZM. As shown in Fig. 4.13, the CD monitoring error induced by $\alpha_H = -0.35$ can be as high as –250 ps/nm for $D_{acc} = 520$ ps/nm and $f_{RF} = 7$ GHz.

To suppress the CD monitoring error caused by chirp fluctuation, an improved CD monitoring scheme is proposed here as shown in Fig. 4.14. Compared with the system setup shown in Fig. 4.2, two RF tones are modulated to the light and an a priori known CD offset D_{offset} such as a chirped FBG or a length of dispersive fiber are inserted before the 50:50 coupler. To reduce the power penalty from the added tones and make good use of the RF generators and power detectors, the two tones can be time division multiplexed [98].

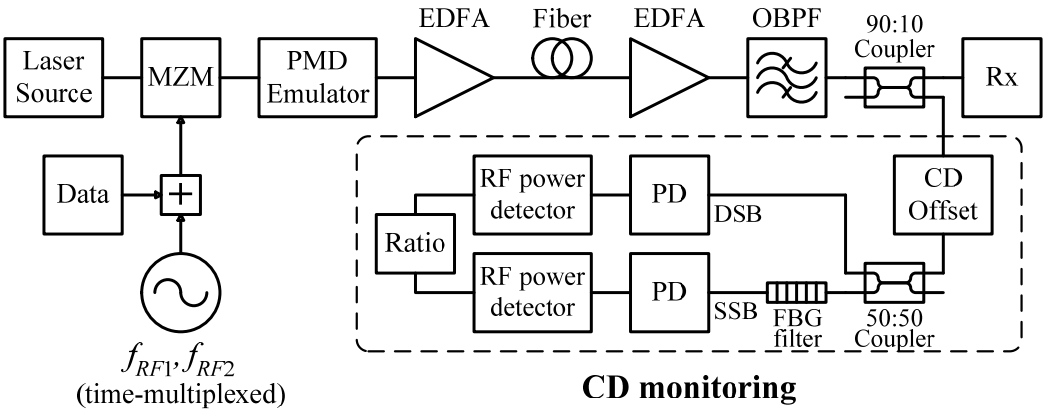

Fig. 4.14 System configuration and experimental setup of the proposed CD monitoring scheme for suppressing chirp effect.

If $K = RH_C^2 H_U^2/4$ is defined as the normalized DSB/SSB RF power ratio, according to Eq. (4.13), the normalized DSB/SSB RF power ratios at f_{RF1} and f_{RF2} ($f_{RF1} < f_{RF2}$) can be written as:

$$K_1 = \cos^2\left(\pi D_{total}\lambda^2 f_{RF1}^2/c + \tan^{-1}\alpha_H\right) \tag{4.16}$$

$$K_2 = \cos^2\left(\pi D_{total}\lambda^2 f_{RF2}^2/c + \tan^{-1}\alpha_H\right) \tag{4.17}$$

where D_{total} is the total CD induced by the fiber and other optical components, including the accumulated CD under monitoring D_{acc} and the CD offset D_{offset} within the CD monitoring module.

When the argument is between 0 and $\pi/2$, K_1 changes monotonically, and Eq. (4.16) can be changed to:

$$\tan^{-1}\alpha_H = \cos^{-1}\sqrt{K_1} - \pi D_{total}\lambda^2 f_{RF1}^2/c \tag{4.18}$$

Substituting (4.18) into (4.17), the relationship between the total CD and the two normalized DSB/SSB RF power ratios irrelevant to the alpha parameter can be written as:

$$K_2 = \cos^2\left[\pi D_{total}\lambda^2\left(f_{RF2}^2 - f_{RF1}^2\right)/c + \cos^{-1}\sqrt{K_1}\right] \tag{4.19}$$

Hence, by measuring these two normalized DSB/SSB RF power ratios K_1 and K_2, CD can be monitored without the influence of small chirp fluctuation. Note that $\tan^{-1}\alpha_H$ normally ranges between $\pm\pi/8$ because the chirp α_H fluctuates less than ±0.4, so that $\pi/8 \le \pi D_{total}\lambda^2 {f_{RF1}}^2/c \le 3\pi/8$ can ensure the argument of Eq. (4.16) is between 0 and $\pi/2$. According to Eq. (4.16), the CD monitoring is limited in the range of $c/(8\lambda^2{f_{RF1}}^2)$ to $3c/(8\lambda^2{f_{RF1}}^2)$. To shift the CD monitoring from the range of $c/(8\lambda^2{f_{RF1}}^2)$ to $3c/(8\lambda^2{f_{RF1}}^2)$ to the range of 0 to $c/(4\lambda^2{f_{RF1}}^2)$, a dispersion offset whose value is $c/(8\lambda^2{f_{RF1}}^2)$ is inserted within the monitoring module. For instance, when the two RF tones are f_{RF1} = 7 GHz and f_{RF2} = 9.9 GHz, the CD offset should be 315 ps/nm and the CD between 0 to 630 ps/nm can be monitored without the influence of chirp fluctuation. Being different from the case shown in Fig. 3.5, the CD monitoring

sensitivity here depends on $f_{RF2}^2 - f_{RF1}^2$, as shown in Eq. (4.19). In order to achieve a higher monitoring sensitivity, higher f_{RF2} and lower f_{RF1} are desired. However, as discussed in Section 3.2.7, the RF frequency used should be greater than 7 GHz but smaller than 10 GHz. To avoid the interference with the data clock tone, 7-GHz and 9.9-GHz RF tones are chosen here. Note that, only a small fraction of the optical signal is tapped into the monitoring module and passes through the dispersion offset, and the main data signal does not go through the dispersion offset and hence would not be affected by it. Furthermore, if the CD offset has a value in the middle of the range of $c/(8\lambda^2 f_{RF1}{}^2)$ to $3c/(8\lambda^2 f_{RF1}{}^2)$, this technique can also give the sign of CD. Fig. 4.15 shows the CD monitoring error versus the chirp α_H with and without the chirp suppression, when D_{offset} is 315 ps/nm and D_{acc} is 205 ps/nm. As shown in Fig. 4.15, the CD monitoring error induced by chirp fluctuation is considerably suppressed.

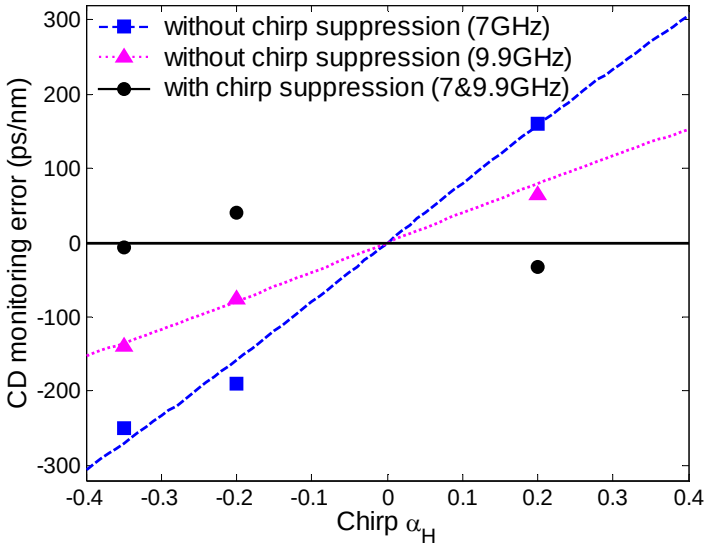

Fig. 4.15 Measured CD monitoring error versus chirp α_H with and without chirp suppression.

4.5 Impacts from Other Optical Impairments

For the RF tone based CD monitoring technique, some other optical impairments, including stimulated Brillouin scattering (SBS), stimulated Raman scattering (SRS) and cross gain modulation (XGM), may also induce RF power variation and CD monitoring error. The impacts arising from these impairments will be discussed in this section.

When a light travels in single-mode fiber, the incident photon may interact with the molecule vibration of the fiber material and cause the inelastic scattering [2]. At high power levels, the inelastic scattering becomes dominant, including SBS and SRS.

SBS arises when a light generates acoustic vibrations in silica glass and then the light scatters from the acoustic waves induced material refractive index variation. Scattered light goes backward and obtains gain from forward propagating signals resulting in reduction of signal power. If the launch power is sufficiently high, the optical carrier may generate a 10.9-GHz downshifted component for the backward propagating light, which is close to the RF tone used for CD monitoring. However, since the optical carrier is modulated with 10-Gb/s baseband data, its linewidth is significantly increased, leading to increased SBS threshold [99]. Consequently, if the signal launch power is within the conventional margin, the effect of SBS is expected to be negligible, and was not observed in the experiment.

SRS arises when a light scatters by the silica molecules. When a photon is incident on a molecule, this molecule can absorb some energy from photon. Photon is then

scattered and has lower energy. This process generates scattered light with wavelength longer than that of incident light. Because no acoustic wave is involved, SRS can occur in both directions. Previous theoretical and experimental results show that SRS can induce ghost tones for WDM systems with RF tones [100-102]. Here, ghost tone means the SRS induced crosstalk from other channels. It is problematic for the RF tone based monitoring techniques. Fortunately, because of the chromatic dispersion, there is walkoff between the RF tones with different channels. When the RF frequencies are higher than 400 MHz, the walkoff becomes obvious and greatly suppresses the SRS induced ghost tones [101]. For the RF tone used in the CD monitoring application, the RF frequency is normally several GHz. Therefore, SRS effect to the proposed RF tone based CD monitoring technique is also negligible.

XGM comes from the gain saturation of optical amplifiers in a multi-wavelength system. XGM is serious in semiconductor optical amplifiers (SOAs) and can be employed for the application of wavelength conversion for multigigabit data streams because the carrier lifetime of a SOA is typically a few 100 ps [89]. However, the typical gain recovery time of an EDFA is between 110 – 340 μs [89]. Therefore, XGM only affects the RF tones whose frequencies are smaller than 1 MHz in WDM systems with EDFAs, which has already been verified by theoretical and experimental investigations in [100] and [103]. In the scheme without employing SOA, the RF tones are several GHz and hence would not be affected by the cross gain modulation.

4.6 Summary

For the RF power based chromatic dispersion monitoring techniques, the RF power is not only affected by the chromatic dispersion, but also fluctuated with other optical impairments, such as PMD, SPM, XPM, chirp, etc. All these impairments will lead to chromatic dispersion monitoring errors. In this chapter, the CD monitoring errors induced by those optical impairments have been investigated. The study has shown that the presence of some impairments induces significant CD monitoring errors. To tackle this problem, a new CD monitoring technique has been proposed to suppress the influence caused by these impairments. In the proposed CD monitoring scheme, one RF tone is added at the transmitter. The light is split into two branches in the monitoring module. A FBG filter which can remove one sideband is inserted before the photodetector of one branch. By taking the ratio of the RF power at the DSB and SSB branches, the monitoring error induced by PMD, SPM, and XPM effect is eliminated or suppressed. Furthermore, it has been shown in this work that the monitoring error induced by a small chirp fluctuation in the modulator can be suppressed if another time-multiplexed RF tone is added at the transmitter and an a priori known dispersion offset is inserted before the 50:50 coupler in the monitoring module. The operational principle is analyzed and the experimental and simulation investigations are presented. Experimental results have shown that this technique can accurately monitor the accumulated CD without being affected by the PMD and small chirp fluctuation. SPM and XPM induced CD monitoring errors can also be suppressed by this technique when the accumulated CD is around zero. Finally, the influence arising from other impairments such as SBS, SRS and XGM are discussed. In intensity modulated baseband optical transmission systems with high frequency RF

tones and EDFAs, the impacts from these effects to CD monitoring are very small and negligible.

Chapter 5

Chromatic Dispersion Monitoring for DPSK Systems

5.1 Introduction

Differential phase-shift keying (DPSK) and its variant such as RZ-DPSK and π/2-DPSK have attracted significant attention in long-haul high-bit-rate WDM systems recently [104-107]. DPSK has 3-dB lower requirement in optical signal-to-noise ratio (OSNR) and better resilience to fiber XPM than non-return-to-zero on-off-keying (NRZ-OOK). Moreover, DPSK experiences the suppressed degradation induced by SPM + dispersion combination and XPM + dispersion combination [108]. However, as in NRZ-OOK systems, CD remains as an important factor limiting transmission distance of DPSK systems. It may change with dynamic network reconfigurations and variations in environmental conditions such as temperature [17]. As a result, it is also essential to monitor the residual CD for DPSK systems. Although the CD

monitoring is intensively investigated in OOK systems, including those RF tone techniques [35, 47, 109, 110], little work has been done on CD monitoring for DPSK systems. Pan et al. recently reported a CD monitoring technique for DPSK signals, based on the power detection of the regenerated clock tone [111]. This method is quite simple. However, because the monitoring sensitivity and range depend on the frequency of the clock tone, the monitoring capability is greatly limited by the data bit-rate.

In this chapter, a new CD monitoring technique with enhanced monitoring capability and a more cost-effective DPSK transmitter configuration are presented. The proposed CD monitoring method is based on the power detection of the clock tone as well as a radio frequency (RF) tone. By utilizing the RF tone with different frequencies, flexible CD monitoring sensitivity and large range can be acquired. Experimental and simulation results show that the technique can significantly improve the CD monitoring capability compared with the one using the clock tone power only, especially the monitoring range. The RF tone induced power penalty to DPSK signal is also investigated. The impact of RF frequency on the power penalty shows that by simply selecting the RF frequency close to half of the DPSK data-rate frequency, the RF tone induced power penalty to DPSK signal can be significantly suppressed without any additional RF filter. Moreover, a new design of transmitter configuration is proposed which can generate an RF tone together with DPSK signal using only a single dual electrode Mach-Zehnder modulator (DE-MZM). This transmitter configuration is further explored for an optical label switching (OLS) system with DPSK payload and subcarrier multiplexed (SCM) label. Simulation results demonstrate the feasibility of the new optical labelling scheme. The SCM label which

is intensity modulated to a DPSK optical signal can also be exploited for CD monitoring. Simulation results show that by detecting the RF power of both the clock tone and the SCM label, the CD monitoring range is greatly improved compared with the one using the clock tone power only.

The chapter is organized as follows. In Section 2, the CD monitoring technique using the power detection of the clock tone as well as an RF tone is investigated. Then a new transmitter configuration using only a single DE-MZM is presented in Section 3. In Section 4, the OLS system with a new SCM labelling scheme and the CD monitoring technique using the clock tone and SCM label power detection is investigated. The chapter is summarized in Section 5.

5.2 CD Monitoring Using RF and Clock Tone for DPSK System

5.2.1 System Configuration

When a light carrying a phase modulated DPSK signal and an intensity modulated RF tone travels along a dispersive optical channel, CD causes phase modulation to amplitude modulation (PM-to-AM) conversion for the DPSK signal and a phase difference between the two sidebands of the RF tone. This results in the regeneration of the clock tone and the power fading of the RF tone after the photo detection [47,

111]. CD monitoring can be realized by detecting the RF power of the clock and RF tones.

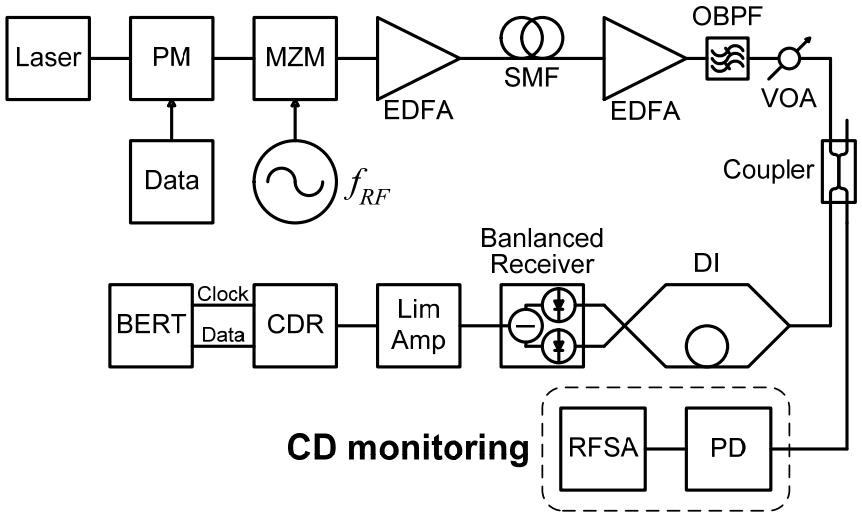

Fig. 5.1 System configuration of the proposed CD monitoring scheme

Fig. 5.1 illustrates the system configuration of the newly proposed CD monitoring scheme for DPSK systems. Pseudo-random bit series (PRBS) data are phase modulated onto a continuous wave laser with a phase modulator (PM) to generate the DPSK signal. Then the signal light is modulated by an RF tone at f_{RF} using a zero-chirp Mach-Zehnder modulator (MZM). The light propagates along a length of single mode fiber (SMF). The length of SMF is varied to emulate different amounts of residual CD. Two erbium-doped fiber amplifiers (EDFAs) (5-dB noise figure and 1480-nm pump source) are used to compensate the attenuation induced by fiber and other components. An optical band pass filter (OBPF) is used to remove the excess amplified spontaneous emission (ASE) noise. At the receiver side, the DPSK signal is demodulated with a Mach-Zehnder one bit delay interferometer (DI) and then detected with a balanced receiver followed by a limiting amplifier and a clock data recovery device (CDR). By adjusting the variable optical attenuator (VOA), the

transmission performance is measured by a bit-error-rate tester (BERT). For monitoring purpose, a small portion of light is tapped out before the DI and coupled into the CD monitoring module which consists of a photodetector and an RF spectrum analyzer (RFSA). The residual CD is monitored by measuring the RF power of the clock tone and an RF tone. Here, the received optical power is kept constant so that the measured RF power is not affected by the optical power variation. In a practical implementation, the RFSA can be replaced by narrow-band band-pass filters and RF power detectors at the corresponding frequencies.

5.2.2 Experimental and Simulation Results

To verify the monitoring capability of the proposed scheme, the simulation is carried out by commercial software (VPItransmissionMaker) for both 10.7-Gb/s and 43-Gb/s DPSK systems. Experiment is also conducted for a 10.7-Gb/s DPSK system. The laser wavelength is set at 1552.5 nm. RF tones at 5 GHz and 20 GHz are used in 10.7-Gb/s and 43-Gb/s DPSK systems, respectively. The modulation index (m) of the RF tones is set at 30% for both 10.7-Gb/s and 43-Gb/s DPSK systems. Fig. 5.2 plots the simulated and measured normalized RF power of the clock and RF tones against the accumulated CD for 10.7-Gb/s and 43-Gb/s DPSK systems. As seen in Fig. 5.2(a), the experiment results (symbols) match very well with the simulation results (curves), except for the places where the simulated clock tone power is very low. At these places, the tone may be hidden behind the PM-to-AM converted spectrum components of the DPSK signal and noise. Under such a situation, the tone power

cannot be measured accurately, resulting in higher monitoring errors and narrower CD monitoring range, as discussed in Chapter 3.

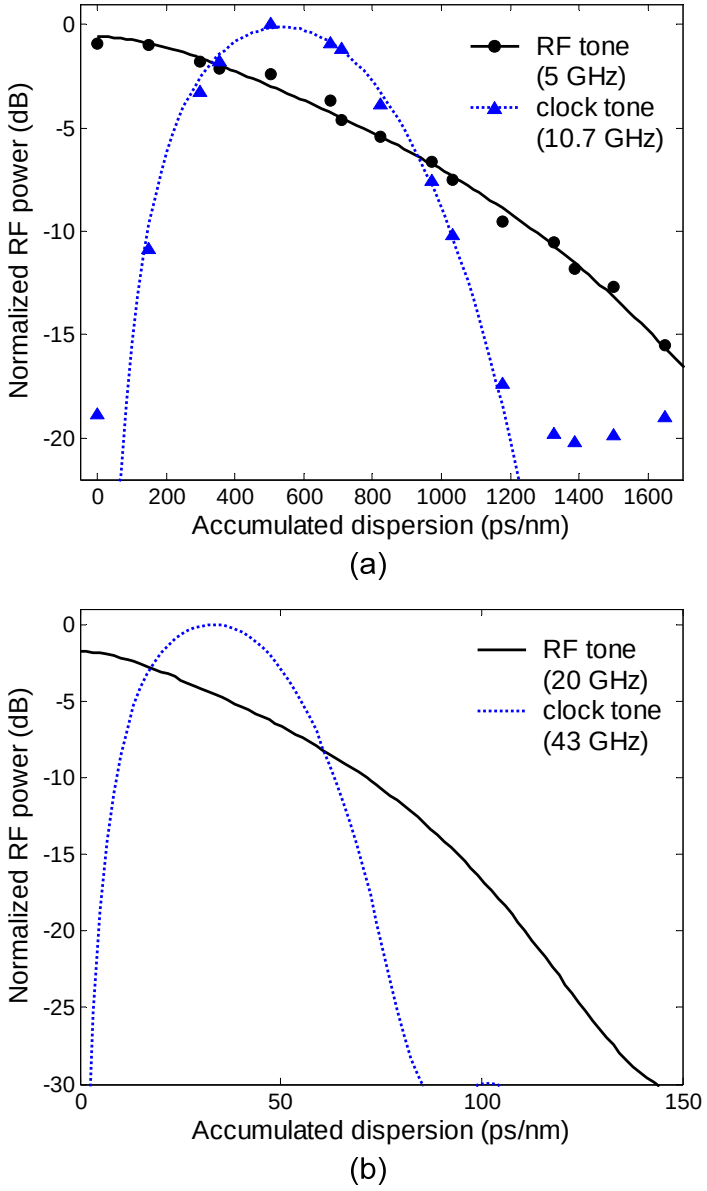

Fig. 5.2 Normalized RF power versus accumulated chromatic dispersion for (a) 10.7-Gb/s DPSK system; (b) 43-Gb/s DPSK system.

The results have also shown that the regenerated clock tone is very sensitive to CD, but the monitoring range is quite narrow, especially for the 43-Gb/s system in Fig.

5.2(b) (only several tens ps/nm). An RF tone with lower frequency has a larger CD monitoring range. In Fig. 5.2(a), the 5-GHz RF tone fades with CD while the 10.7-GHz clock tone increases firstly and then decreases. By referring to the RF tone power, the monotonically decreasing region of the clock power can be distinguished from its monotonically increasing region. By detecting the RF power of the two tones, CD can be monitored with the high sensitivity of the clock tone in a more than doubled range for the 10.7-Gb/s DPSK system. Similarly, for a 43-Gb/s DPSK system as shown in Fig. 5.2(b), by tracking the RF power at 20 GHz, it can achieve 150-ps/nm monitoring range. In such a high bit rate system, it is imperative to make sure that the residual CD is as small as several tens ps/nm. Combining with the 43-GHz clock tone with 1-dB/(ps/nm) monitoring sensitivity, the accumulated CD can be monitored accurately and hence compensated fully with a tunable CD compensator. Therefore, as compared with the technique using the regenerated clock tone alone [111], by using a faded RF tone together with the regenerated clock tone, the monitoring range can be significantly improved without compromising the monitoring sensitivity.

5.2.3 RF Tone Induced Penalty and Its Suppression

As described in Section 5.2.1, the proposed method requires an additional RF tone to the DPSK signal at the transmitter side. An RF frequency lower than the clock frequency is preferred to increase the CD monitoring range. An RF tone within the data bandwidth of the DPSK signal also decreases the cost of the RF tone generator/detector and improves spectral efficiency. However, like the case in OOK

systems, the RF tone may induce impairment to the DPSK data signal and result in power penalty. To evaluate this impairment, the BER performance of a 10.7-Gb/s DPSK signal with RF tones is experimentally measured using both the balanced and single-ended receivers after transmission of an 80-km standard SMF with full CD compensation. With reference to the receiver sensitivity of DPSK data without RF tone at BER of 10^{-9}, the RF tone induced power penalty to DPSK data is plotted against the RF frequency in Fig. 5.3 for different modulation indices (30% and 45%) and different detection methods (balanced and single-ended detections). The solid curve with circular symbols represents the balanced detected power penalty with 30% modulation index; the dashed curve with triangular symbols represents the balanced detected power penalty with 45% modulation index; and the dotted curve with rectangular symbols represents the single-ended detected power penalty with 30% modulation index.

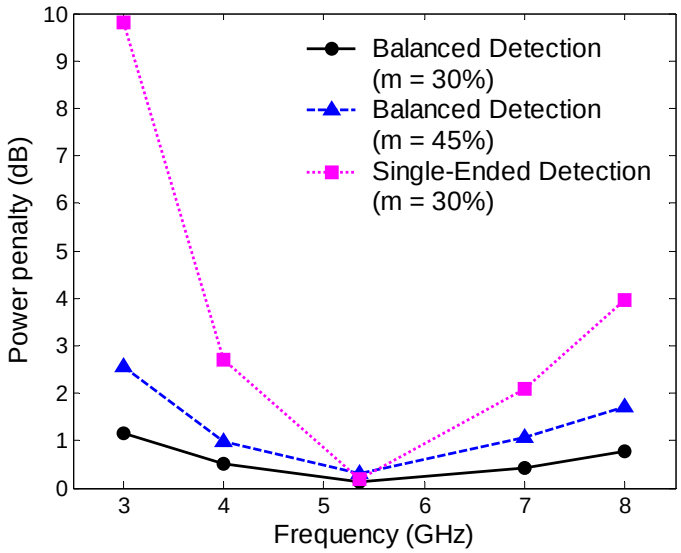

Fig. 5.3 Measured RF tone induced power penalty versus RF frequency at 30% and 45% modulation indices with different detection methods.

The comparison between the solid curve and the dashed curve in Fig. 5.3 shows that, as expected, a lower RF tone modulation index causes a smaller power penalty. Note that similar conclusion has been experimentally obtained in [112] where low frequency (about 300 MHz) pilot tones were used for identifying channels with different wavelengths. Fig. 5.3 also reveals that, the power penalty with balanced detection is smaller than the one with single-ended detection. The reason is that the balanced receiver can partially cancel the power fluctuations of its two input ports.

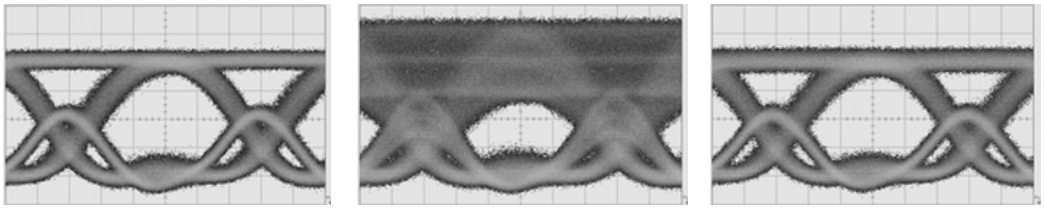

Fig. 5.4 Measured eye diagrams at the destructive port of the DI;
(a) eye diagram without RF tone; (b) eye diagram with 2.5-GHz RF tone (m = 30%);
(c) eye diagram with 5.35-GHz RF tone (m = 30%).

It is also important to note that, for both balanced and single-ended detection methods, the power penalty also changes with the frequency of the RF tone. As shown in Fig. 5.3, the lowest penalty for DPSK systems occurs when the RF tone's frequency is half of the DPSK data rate frequency (i.e., f_{RF} = 5.35 GHz). Fig. 5.3 also shows that the power penalty induced by the 5.35-GHz RF tone is smaller than 0.5 dB for all three cases. The power penalty induced by the RF tone increases with the difference between the RF tone frequency and the half of the DSPK data rate frequency. The eye diagrams have also been measured at the destructive port of the DI. Fig. 5.4(a) shows the eye diagram without RF tone. Fig. 5.4(b) and Fig. 5.4(c) show the eye diagrams with 2.5-GHz and 5.35-GHz RF tones at 30% modulation index, measured

at the destructive port of the DI. No obvious difference can be observed between the eye diagrams in Fig. 5.4(a) and Fig. 5.4(c). As can be seen in Fig. 5.4(b), the eye diagram is severely distorted by 2.5-GHz RF tone.

This can be easily understood by the attribution of the delay interferometer (DI) used in the DPSK demodulation. The DI is constructed by connecting two 3-dB fiber couplers in series [2]. There is one bit delay between its two arms. Thus, the DI not only demodulates DPSK payload back to intensity modulated data, but also induces a phase difference between the sinusoidal fluctuated optical powers of the two arms. When the frequency of RF tone equals half of the DSPK data rate frequency, the signal with one bit delay is out of phase with the original signal. As a result, the amplitude fluctuation induced by the RF tone is cancelled at the DI output and the resulted power penalty is greatly suppressed. As the difference between the RF frequency and half of the DSPK data rate frequency increases, the suppression of amplitude fluctuation becomes less effective and the power penalty induced by RF tone becomes larger. Consequently, unlike OOK systems where notch filters are required for suppressing the power penalty induced by RF tones, as discussed in Chapter 3, by simply selecting the RF frequency close to half of the DPSK data rate frequency, the RF tone induced power penalty can be considerably suppressed. Note that, in the CD monitoring system presented in Section 5.2.2, in order to keep their second order harmonics away from the clock tones, the RF tones with frequencies slightly deviated from half of the corresponding DPSK data rate frequencies were used, which were 5 GHz and 20 GHz for 10.7-Gb/s and 43-Gb/s systems, respectively.

More specifically, the above observations can be explained by the following equations. For an RF tone modulated DPSK signal, the electrical field of $E(t)$ can be expressed as:

$$E(t)=\sqrt{2P_0\left[1-m\sin\left(2\pi f_{RF}t\right)\right]}\cdot\exp\left\{j\left[\omega_c t+\theta(t)\right]\right\} \tag{5.1}$$

where P_0 is the average optical power at the interferometer input, m is the modulation index of the RF tone, f_{RF} is the frequency of the RF tone, ω_c is the optical carrier angular frequency, and $\theta(t)$ is the modulating phase. Then the electrical fields at the output of the constructive and destructive arms of the DI can be written in the following matrix expression [113]:

$$\begin{bmatrix}E_{con}(t)\\E_{de}(t)\end{bmatrix}=\begin{bmatrix}1-\varepsilon & \varepsilon e^{j\pi}\\ \sqrt{\varepsilon(1-\varepsilon)}e^{j\pi/2} & \sqrt{\varepsilon(1-\varepsilon)}e^{j\pi/2}\end{bmatrix}\begin{bmatrix}E(t-\tau)\\E(t)\end{bmatrix} \tag{5.2}$$

where ε is the power coupling ratio of the directional coupler and τ is the differential delay between the two arms. For an ideal DI with one bit delay, ε equals 0.5 and τ is the inverse of the bit-rate of the DPSK data signal B. Thus, Eq. (5.2) can be simplified as:

$$E_{con}(t)=\frac{1}{2}\left[E(t-\tau)-E(t)\right] \tag{5.3}$$

$$E_{de}(t)=\frac{j}{2}\left[E(t-\tau)+E(t)\right] \tag{5.4}$$

Subsitituing Eq. (5.1) into Eqs. (5.3) and (5.4), the output light intensity at the output of two arms can be obtained as:

$$\left|E_{con}(t)\right|^2=\frac{P_0}{2}\left\{2-m(X+Y)+2\cos\left[\theta(t)-\theta(t-\tau)\right]\sqrt{1-m(X+Y)+m^2XY}\right\} \tag{5.5}$$

$$\left|E_{de}(t)\right|^2=\frac{P_0}{2}\left\{2-m(X+Y)-2\cos\left[\theta(t)-\theta(t-\tau)\right]\sqrt{1-m(X+Y)+m^2XY}\right\} \tag{5.6}$$

where $X = \sin(2\pi f_{RF} t)$ and $Y = \sin[2\pi f_{RF}(t-\tau)]$.

For the receiver using the balanced detection, the received signal is proportional to

$$|E_{con}(t)|^2 - |E_{de}(t)|^2 = 2P_0 \cos[\theta(t) - \theta(t-\tau)]\sqrt{1 - m(X+Y) + m^2 XY} \quad (5.7)$$

Comparing Eqs. (5.5) and (5.6) with Eq. (5.7), the RF tone related factor $m(X+Y)$ of the $\theta(t)$ irrelevant terms is canceled at the output of the balanced receiver. Hence, the power penalty with balanced detection is smaller than the one with single-ended detection. However, the $m(X+Y)$ still exists in the $\theta(t)$ relevant root square term and leads to power penalty after data demodulation.

When the modulation index m is a small value, because $|X| \le 1$, and $|Y| \le 1$, the factor $m^2 XY$ is much smaller than $m(X+Y)$ and can be neglected. In order to reduce the power penalty induced by the added RF tone, the factor $m(X+Y)$ should be reduced. There are two approaches to reduce it. One is to reduce m. Therefore, the RF tone with lower modulation index may induce smaller impact on the received data signal. The other way is to reduce the value of $X+Y$. The sum of $X+Y$ can be rewritten as:

$$X + Y = \sin(2\pi f_{RF} t) + \sin[2\pi f_{RF}(t-\tau)] = 2\sin\left[2\pi f_{RF}\left(t - \frac{\tau}{2}\right)\right]\cos(\pi f_{RF}\tau) \quad (5.8)$$

The factor $\cos(\pi f_{RF}\tau)$ increases with the difference between the RF tone frequency and half of the DSPK data rate frequency. When the frequency of the RF tone equals half of the DSPK data rate frequency, i.e., $f_{RF} = 1/2\tau$, Eq. (5.8) becomes zero. Consequently, the lowest penalty for DPSK systems occurs when the RF tone's

frequency is half of the DPSK data rate frequency, and the power penalty induced by the RF tone increases with the difference between the RF tone frequency and half of the DSPK data rate frequency. Note that when the modulation index is large, the RF tone induced power penalty cannot be cancelled completely by choosing the RF frequency equals half of the DSPK data rate because the factor m^2XY cannot be neglected in this condition.

5.3 Transmitter Configuration for Simultaneous DPSK and RF Tone Generation

In OOK systems, the RF tone can be simply combined with the baseband data using an electrical combiner and then the combined signal is used to modulate an optical CW wave via an optical amplitude (intensity) modulator such as an optical MZM. However, in DPSK systems, to produce a phase modulated DPSK signal together with an amplitude modulated RF tone, two external modulators are normally required: one optical phase modulator for generating the DPSK data, and another optical amplitude modulator for adding the RF tone. Therefore this scheme suffers from relatively high cost. Dual electrode Mach-Zehnder modulator (DE-MZM) has been extensively demonstrated for generating some advanced modulation formats [114, 115]. In this section, a new DE-MZM configuration is presented for generating a DPSK signal and an RF tone simultaneously. The detailed transmitter configuration, operational principle and simulation results will be described below.

5.3.1 Transmitter Configuration

Fig. 5.5 shows the transmitter configuration for simultaneous DPSK and RF tone generation using a single DE-MZM. Both a data signal and an RF tone signal (f_{RF}) are first divided into two equal branches. The respective data and RF tone signal of the upper branch are combined by a combiner. The RF tone signal of the lower branch is delayed by $1/(2f_{RF})$ via a delay line and then combined with the data signal of the lower branch. The two combined signals are used to drive the upper and lower arms of the DE-MZM separately. Unlike the operation condition of the DE-MZM in [114], the proposed DE-MZM is biased at the quadrature, i.e., the bias voltages of the upper and lower arms are set at $V_\pi/4$ and $-V_\pi/4$, respectively, where V_π is the switching voltage of the DE-MZM for π phase shift. It is noted that the scheme in [114] requires the RF frequency to be half of the DPSK signal data rate and to be synchronized with the DPSK data. With the newly proposed scheme, the RF frequency is not limited to half of the DPSK data rate, and no synchronization between them is required.

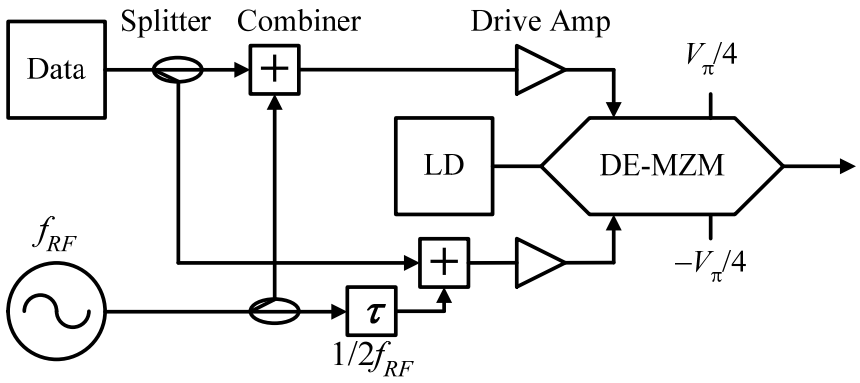

Fig. 5.5 Transmitter configuration for simultaneous generation of DPSK signal and RF tone using a single DE-MZM.

5.3.2 Operational Principle

Theoretical analysis shows that the output signal of the DE-MZM $E_{\text{out}}(t)$ can be written as [94, 114]

$$E_{out}(t) = \frac{E_{in}/2}{10^{\alpha/20}}\left[\exp\left(j\varphi_{upper}(t)\right) + \exp\left(j\varphi_{lower}(t)\right)\right] \tag{5.9}$$

where E_{in} is the optical field amplitude of input signal, α is the modulator insertion loss in dB, and the phase terms $\varphi_{\text{upper}}(t)$ and $\varphi_{\text{lower}}(t)$ are given by

$$\varphi_{upper}(t) = \frac{\pi}{V_\pi}\left[D(t) + V_{RF}\sin\left(2\pi f_{RF}t\right) + \frac{V_\pi}{4}\right] \tag{5.10}$$

$$\varphi_{lower}(t) = \frac{\pi}{V_\pi}\left[D(t) - V_{RF}\sin\left(2\pi f_{RF}t\right) - \frac{V_\pi}{4}\right] \tag{5.11}$$

where V_π is the switching voltage of the DE-MZM, $D(t)$ is the data signal being 0 and V_π, and $V_{RF}\cdot\sin(2\pi f_{RF}t)$ represents the RF tone signal.

Substituting (5.10) and (5.11) into (5.9),

$$E_{out}(t) = \frac{E_{in}}{10^{\alpha/20}}\exp\left(j\frac{\pi}{V_\pi}D(t)\right)\cos\left(\frac{\pi}{4} + \frac{\pi V_{RF}}{V_\pi}\sin\left(2\pi f_{RF}t\right)\right) \tag{5.12}$$

Using the Jacobi-Anger identity to expand the output power of the DE-MZM into Fourier series and neglecting the high order terms, the approximate output power can be written as,

$$P_{out}(t) = \frac{|E_{in}|^2}{2\cdot 10^{\alpha/10}}\left[1 - 2J_1\left(\frac{2\pi V_{RF}}{V_\pi}\right)\sin\left(2\pi f_{RF}t\right)\right] \tag{5.13}$$

where $J_1(x)$ is the first-kind Bessel function of order 1.

Eq. (5.12) shows that the DE-MZM encodes the data with the binary phase modulation. Eq. (5.13) indicates that the RF tone signal at f_{RF} is sinusoidally intensity modulated to the output power and $m = 2J_1(2\pi V_{RF}/V_\pi)$ is the modulation index of the RF tone.

5.3.3 Simulation Results

Due to the lack of DE-MZM, the numerical simulation software VPItransmissionMaker is employed to verify the feasibility of the proposed transmitter configuration. Fig. 5.6 shows the simulated RF spectra using the proposed transmitter configuration and the direct detection when the output light experiences 0- and 68-ps/nm accumulated CD. Here, the DPSK signal is 43 Gb/s and the RF tone is 20 GHz with 30% modulation index. Fig. 5.6(a) depicts that without using an additional amplitude modulator, the RF tone is modulated to the DPSK data. No DPSK signal spectrum is seen in the RF spectrum since the envelop detection removes the phase information. The CD of 68 ps/nm induces the fading of the RF tone (20 GHz) and the regenerated clock tone (43 GHz), as shown in Fig. 5.6(b). Further simulation results demonstrate that the power variation at both the RF tone and the clock tone for different CD values using the proposed DE-MZM configuration are the same as the one using the conventional two cascaded modulators. Therefore, it is verified that the RF tone generated by the proposed technique can be employed in CD monitoring. By varying the phase of the RF tone signal, it is observed that the synchronization between the RF tone and the DPSK data does not affect the RF power of the generated RF tone signal. Note that another spike at 23 GHz in Fig. 5.6(b) is

the beating signal between the RF tone and clock tone. This also occurs in the RF spectrum using the two cascaded modulators.

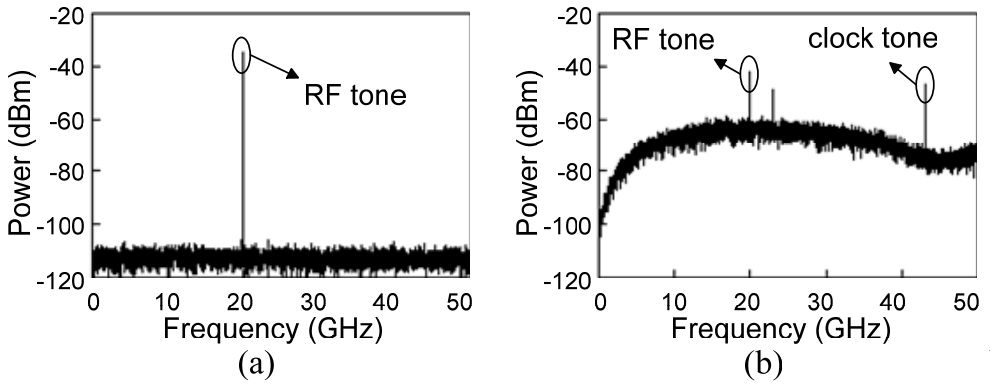

Fig. 5.6 Simulated RF spectra of the 43-Gb/s DPSK with a 20-GHz RF tone; (a) without CD; (b) with 68-ps/nm CD.

5.4 CD Monitoring for DPSK/SCM OLS System

5.4.1 DPSK/SCM OLS System Using a Single DE-MZM

Optical label switching (OLS) is a promising technique to switch and route optical packets over high-bit-rate WDM networks [116]. Optical labelling schemes for DPSK payload have attracted significant attention recently because of its 3-dB lower OSNR requirement and better resilience to XPM compared with OOK formats [117-121]. Several techniques have been reported to implement it, including orthogonal modulation [117, 118] and subcarrier multiplexing (SCM) [119-121] techniques. For the orthogonal modulation based labelling technique, an orthogonal modulation

format, normally amplitude shift keying (ASK), is applied to the label information for DPSK payload. For the SCM labelling technique, the label signal is imposed into a subcarrier tone. These labelling schemes are also termed as DPSK/ASK and DPSK/SCM labelling. However, both techniques require two external modulators: one for generating DPSK payload and the other for labelling. Peng et al. have recently demonstrated a novel labelling method by simulation for return-to-zero (RZ) DPSK payload [122] and carrier-suppressed return-to-zero (CSRZ) DPSK payload [123] using a single dual electrode Mach-Zehnder modulator (DE-MZM). Nevertheless, the synchronization between the payload and the half payload bit-rate clock is required for curving the payload into pulses with the label signal. Moreover, as an orthogonal modulation based labelling method, it requires an additional label erasure for payload detection [117, 118, 122, 123]. In this section, the proposed DE-MZM transmitter configuration described in Section 5.3 is applied to an in-band SCM based labelling technique for DPSK payload and demonstrate its feasibility by simulation. This technique is more cost-effective as compared with the conventional methods using two modulators. Moreover, the subcarrier frequency is not limited to half of the DPSK payload data rate, and no synchronization between them is required.

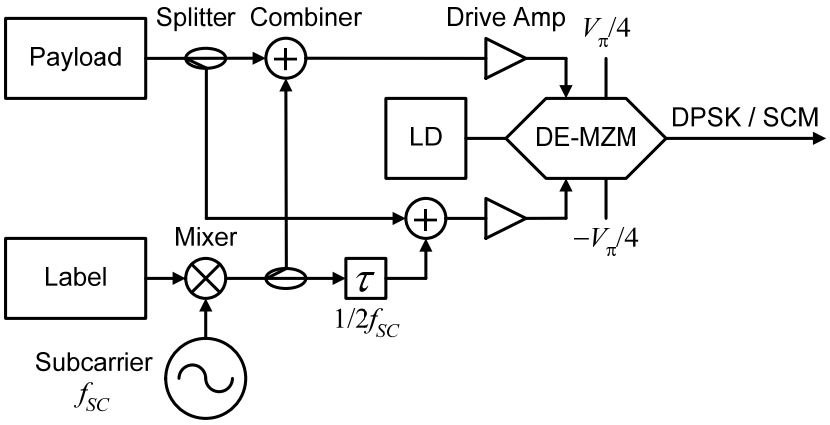

Fig. 5.7 Transmitter configuration for simultaneous DPSK payload and SCM label generation using a single DE-MZM

Fig. 5.7 shows the new optical SCM labelling scheme for DPSK payload using a single DE-MZM. The transmitter configuration is similar with the one in Fig. 5.5 except that the label signal is first modulated to the subcarrier (f_{SC}) using a mixer, resulting in an SCM label. Thus, Eqs. (5.12) and (5.13) can be rewritten as

$$E_{out}(t) = \frac{E_{in}}{10^{\alpha/20}} e^{j\frac{\pi}{V_\pi}P(t)} \cos\left(\frac{\pi}{4} + \frac{\pi}{V_\pi} V_{SC} \sin(2\pi f_{SC} t) L(t)\right) \tag{5.14}$$

$$P_{out}(t) = \frac{|E_{in}|^2}{2 \cdot 10^{\alpha/10}} \left[1 - 2J_1\left(\frac{2\pi V_{SC} L(t)}{V_\pi}\right) \sin(2\pi f_{SC} t)\right] \tag{5.15}$$

where $V_{SC}\cdot\sin(2\pi f_{SC}t)$ represents the subcarrier signal, $P(t) = [0, V_\pi]$ is the payload data levels, and $L(t) = [0, 1]$ is the label information. Eq. (5.14) shows that the DE-MZM encodes the payload with the binary phase modulation and Eq. (5.15) indicates that the label signal is intensity modulated to the output power with the subcarrier frequency f_{SC}.

To verify the feasibility of the new SCM labelling scheme, simulations are conducted using the commercial software - VPItransmissionMaker. Fig. 5.8 shows the simulated RF spectrum of the combined 40-Gb/s DPSK payload and 622-Mb/s SCM label with 30% modulation index at the transmitter output when f_{SC} = 15 GHz. Here, the modulation index is defined as the ratio of the peak optical power variation (i.e., the difference between the maximum and average power) to the average optical power [67]. When the label information is 1, m equals $2J_1(2\pi V_{SC}/V_\pi)$, as Eq. (5.15) indicates. Fig. 5.8 depicts that the label signal as well as the subcarrier tone are intensity modulated to the DPSK payload with only one DE-MZM. By varying the phase of

the subcarrier signal, it is observed that the synchronization between the subcarrier label and the DPSK payload does not affect the spectrum of the output signal.

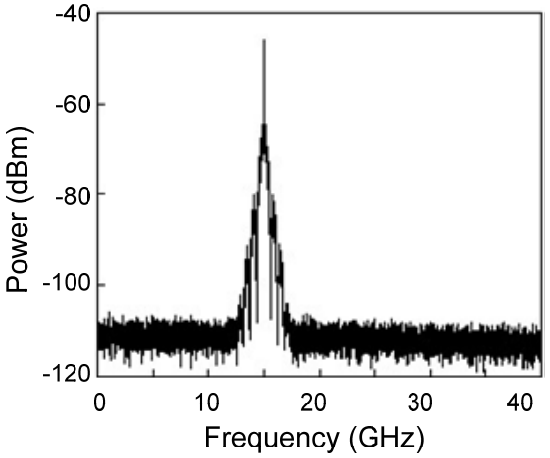

Fig. 5.8 Simulated RF spectrum of the 40-Gb/s DPSK with 622-Mb/s subcarrier label at f_{SC} = 15 GHz.

For evaluating the OLS system performance and examining the mutual interference between the DPSK payload and the SCM label, the OLS system simulations have been carried out, according to the setup in Fig. 5.9. The modulated light propagates along a transmission link consisting of 80-km nonzero dispersion shifted fiber (NZDSF) with full dispersion compensation, an EDFA and an OBPF with a bandwidth of 1.3 nm is used to remove the excess ASE noise, as shown in Fig. 5.9. The output light is divided into two branches for payload and label detection. Adjusting the VOA, the BER is evaluated as a function of received optical power for both payload and label.

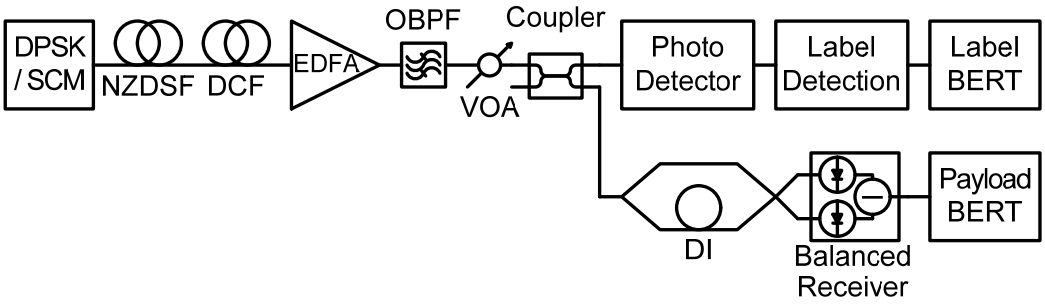

Fig. 5.9 Schematic for BER performance evaluation of the proposed labelling scheme.

Fig. 5.10 plots the simulated BER curves for two different subcarrier frequencies (15 and 20 GHz). For comparison, the BER curves are simulated and plotted for the conventional SCM labelling scheme that use two modulators, one for generating DPSK payload and the other for labelling [119]. No difference is observed between the two schemes in Fig. 5.10. Moreover, the label signals exhibit almost the same BER performance for different subcarrier frequencies, whereas the BER of the DPSK payload changes with the subcarrier frequency.

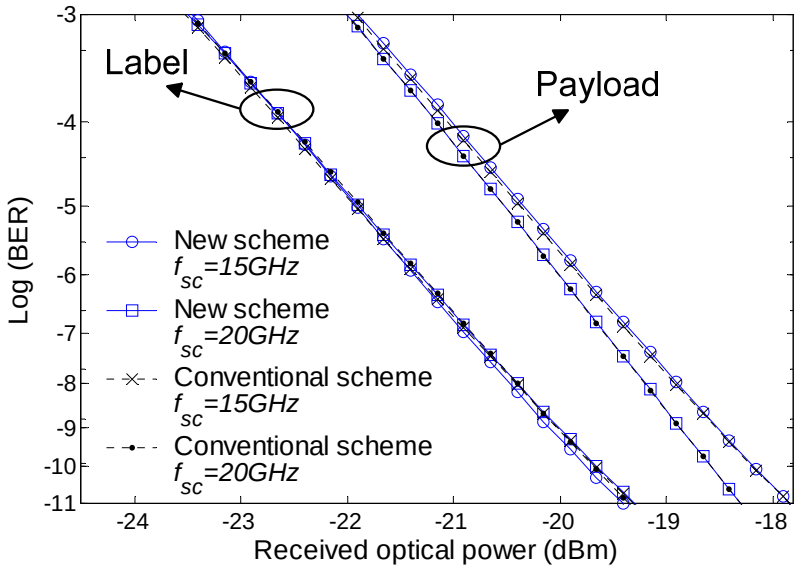

Fig. 5.10 BER performance comparison between two labelling schemes.

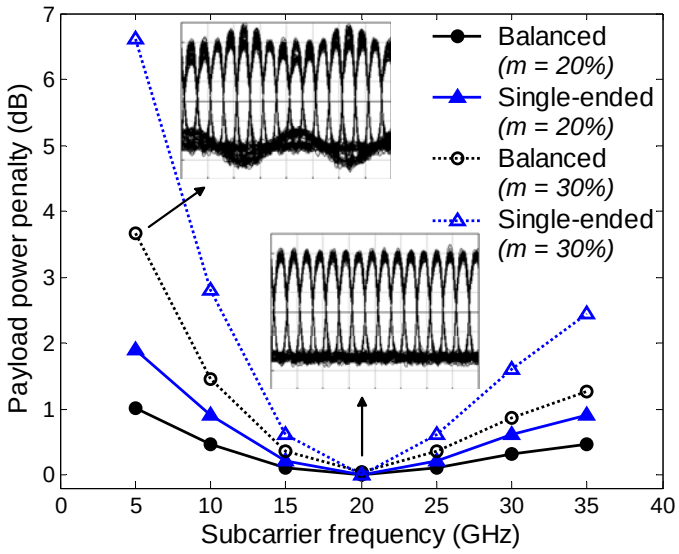

Fig. 5.11 SCM label induced DPSK payload penalty versus subcarrier frequency. Insets show the balanced-detected eye diagrams (50 ps/div) for 30% modulation index with different subcarriers (upper: f_{SC} = 5 GHz; lower: f_{SC} = 20 GHz).

Due to the same reason for the RF tone induced DPSK penalty, as given in Section 5.2.3, the lowest penalty of the DPSK payload occurs when the subcarrier frequency is half of the payload bit-rate (i.e. f_{SC} = 20 GHz) and the penalty increases with the difference between the subcarrier frequency and 20 GHz. It has also been mathematically analyzed and experimentally demonstrated in [120] for the balanced detection. The simulation results further show that, for the single-ended detection methods, the lowest penalty occurs with half of the payload bit-rate subcarrier frequency (i.e., f_{SC} = 20 GHz) as well. The power penalty of the DPSK payload induced by the subcarrier label at f_{SC} = 20 GHz is smaller than 0.1 dB for both modulation indices of 20% and 30% and no obvious degradation can be observed from the eye diagram in the lower inset of Fig. 5.11. Moreover, the penalty increases with the difference between the subcarrier frequency and 20 GHz. The upper inset of Fig. 5.11 shows the eye diagram which has strong amplitude fluctuation with the

subcarrier label at f_{SC} = 5 GHz. Fig. 5.11 also shows that, as expected, a lower subcarrier modulation index induces smaller power penalty.

On the other hand, a lower subcarrier modulation index results in poorer BER performance for the SCM label. This can be explained as follows. As a small signal modulation, the SCM label signal is intensity modulated to the light with a small extinction ratio. At the receiver, the SCM label is detected by direct detection. A lower subcarrier modulation index leads to a smaller extinction ratio, and hence results in poorer BER performance for the SCM label. This has been verified via simulation as shown in Fig. 5.12, which plots the simulated BER of SCM label signal against the received optical power for 20-GHz subcarrier with two different modulation indices (20% and 30%). The sensitivity of the label receiver at 30% modulation index is around 3 dB better than the one at 20% modulation index. By turning off the DPSK data input, the label transmission performance without the impact from the DPSK payload is also simulated and plotted it in Fig. 5.12. Comparing the label BERs with and without the DPSK payload, it is observed that the DPSK payload does not affect the label performance greatly because the DPSK signal does not change the optical signal intensity at the transmitter side. As shown in Fig. 5.12, the DPSK induced label penalty is only 0.1 dB for 30% modulation index, and this is increased to around 0.6 dB for 20% modulation index. This can be explained from the fact that the fiber dispersion and optical filtering induce phase modulation to amplitude modulation (PM-to-AM) conversion. Even with the full dispersion compensation, there will still be the PM-to-AM conversion due to fiber nonlinear effects, while the conversion is smaller compared with the case of no dispersion compensation. Such a small intensity fluctuation does not affect the performance of

the SCM label obviously with a relatively high modulation index, but its impact is still observable for the SCM label with low modulation index. When the modulation index is small (≤ 20%), the extinction ratio of the detected label is also small and hence the small intensity fluctuation due to the PM-to-AM conversion plays a more important role.

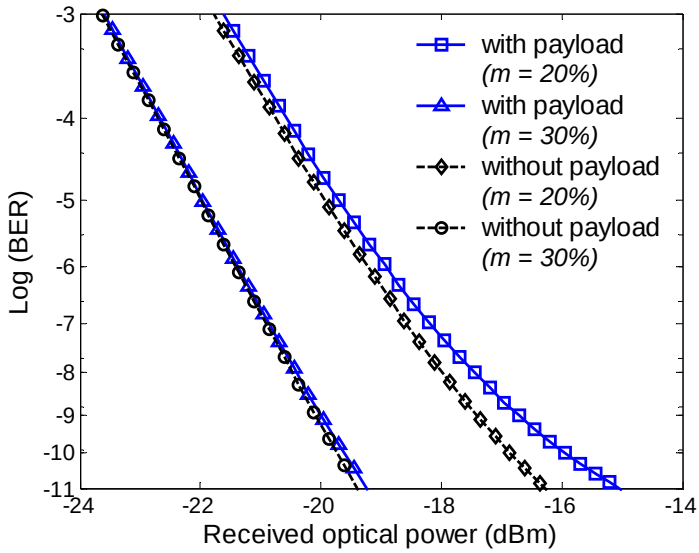

Fig. 5.12 Label BER versus received optical power under different conditions.

5.4.2 CD Monitoring Using SCM Label and Clock Tone for DPSK/SCM OLS System

Besides those benefits as described in [119-121], it is to be shown here that in-band SCM labelling offers another advantage, i.e., it can be applied to chromatic dispersion (CD) monitoring. In this section, the SCM label generated by the proposed labelling scheme is applied to CD monitoring for DPSK/SCM OLS systems. Similar to the CD monitoring technique discussed in Section 5.2, by detecting the RF power of both the

clock tone and the SCM label, the CD monitoring range can be greatly improved compared with the one using the clock tone power only [111].

Simulations have been carried out for assessing the capability of this CD monitoring technique. The configuration is similar to the one in Fig. 5.9 except that for monitoring purpose, a portion of signal is tapped out after the photodetector of the label detection branch. The extracted signal is split into two identical branches and each is then coupled into a 3-MHz band-pass Bessel filter and an RF power detector for measuring the RF power at the clock and subcarrier frequencies, respectively. Fig. 5.13 plots the normalized RF power of the clock tone and SCM label against the accumulated CD for 40-Gb/s DPSK system. Here, a 622-Mb/s SCM label (m = 30%) with different subcarrier frequencies (15 and 20 GHz) is used. The measured RF power varies (fades) with the accumulated CD. The normalized RF power is defined as the ratio of the measured RF power to the measured maximum RF power.

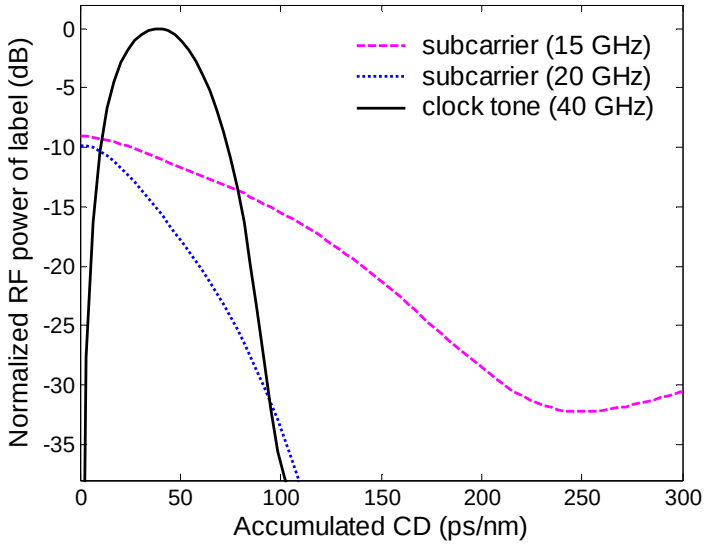

Fig. 5.13 Normalized RF power of label signal versus accumulated chromatic dispersion.

As seen in Fig. 5.13, the RF power of both the clock tone and SCM label changes with CD because of the PM-to-AM conversion for the DPSK signal [111] and the phase difference between two sidebands of the subcarrier [35]. The RF power of the clock tone is very sensitive to CD, but its monotonic increasing or decreasing range is quite narrow (about 50 ps/nm). Thus, the CD monitoring range using the clock power is very small. In contrast, the RF power of the in-band SCM label fades slowly with CD. As shown in Fig. 5.13, the monotonic decreasing ranges of the SCM label power with 20-GHz and 15-GHz subcarriers are approximately 110 ps/nm and 240 ps/nm, respectively. Therefore, using the RF power of SCM label with lower subcarrier frequency, the CD monitoring range can be enlarged. Moreover, its monitoring range is adjustable with the subcarrier frequency. By utilizing the SCM label power as a coarse CD measurement of an automatic CD compensator, I can monitor and compensate the CD as large as few hundreds ps/nm for 40-Gb/s DPSK systems. The coarse CD monitoring and compensation makes the residual CD fall in the range of several tens ps/nm first. Then the CD can be monitored accurately by detecting the clock tone power with high sensitivity at around 0.8 dB/(ps/nm). Hence, the proposed technique has a significantly improved monitoring capability as compared with the technique using the clock power alone [111].

5.5 Summary

A CD monitoring technique with enhanced monitoring capability and cost-effective transmitter configuration for DPSK systems is presented. This CD monitoring

method is based on the power detection of the clock tone as well as an added RF tone. By utilizing the RF tone with different frequencies, flexible CD monitoring sensitivity and large range can be acquired. Experimental and simulation results have shown that the technique can significantly improve the CD monitoring capability compared with the one using the clock tone power only, especially the monitoring range. The RF tone induced power penalty to DPSK signal is also investigated. The impact of RF frequency on the power penalty shows that by simply selecting the RF frequency close to half of the DPSK data-rate frequency, the RF tone induced power penalty to DPSK signal can be significantly suppressed without any additional RF filter. The RF tone cannot be simply added to the baseband data by a simple combiner in DPSK systems as it can be done so in OOK systems. Therefore, a new transmitter configuration using a single DE-MZM for simultaneous DPSK signal and RF tone generation is proposed.

This transmitter configuration is further explored for an OLS system with DPSK payload and SCM label. It has been shown in this work that the SCM label which is intensity modulated to the optical DPSK signal can be exploited for CD monitoring as well. Due to the lack of DE-MZM, simulations have been carried out to examine the CD monitoring range using the SCM label and also studied the BER performance for both DPSK payload and SCM label signals. Simulation results have demonstrated the feasibility of the new optical labelling scheme. When the subcarrier frequency close to half of the DPSK payload data-rate frequency (f_{SC} = 20 GHz), the power penalty of the DPSK payload induced by the SCM label is smaller than 0.1 dB without an additional label eraser. For the performance of the SCM label with a relatively high modulation index, DPSK payload does not affect the label performance greatly

because the DPSK signal does not change the optical signal intensity at the transmitter side and the effect of the PM-to-AM conversion can be neglected. Simulation results have also shown that by detecting the RF power of both the clock tone and SCM label, the CD monitoring range is greatly improved compared with the one using the clock tone power only.

Chapter 6

Conclusions and Future Work

6.1 Conclusions

Chromatic dispersion is a major factor limiting the attainable distance in today's high capacity optical communication systems. It may change with dynamic network reconfigurations and variations in environmental conditions such as temperature. Hence, it is essential to monitor the residual CD of individual channels to ensure that the residual CD does not exceed the designed tolerance. This thesis comprehensively investigates the chromatic dispersion monitoring for next generation optical networks. The new proposed CD monitoring techniques are mainly based on the RF power detection. When an RF signal is intensity modulated to an optical carrier, the detected RF power at the photodetector is varied with the accumulated chromatic dispersion. This phenomenon, known as RF power fading, is exploited to monitor the accumulated dispersion of optical channels. The RF power based CD monitoring techniques are simple and cost-effective to implement. For WDM networks, the RF

tone can be added to the baseband data of multi-channels simultaneously by an external modulator. The RF power can be detected using an RF spectrum analyzer, or an RF filter followed by an RF power detector. Moreover, the technique is irrespective of signal bit rate and coding format.

Chapter 2 gives an overview of chromatic dispersion monitoring. The origin of chromatic dispersion is introduced first. And then dispersion compensation techniques are discussed briefly for illustrating the necessity of CD monitoring. Two conventional CD measurement methods are discussed. The existing chromatic dispersion monitoring techniques are surveyed.

An improved chromatic dispersion monitoring technique based on the RF power ratio detection and dispersion offset insertion has been proposed in Chapter 3. In this technique, two RF tones are added at the transmitter and a dispersion offset is inserted just before the photodetector within the monitoring module for CD monitoring purpose. CD is monitored by tracking the RF power ratio of two tones. The operational principle of the CD induced RF power variation is introduced. Both experiments and simulation have been carried out to examine the monitoring performance of the proposed technique in terms of monitoring range and accuracy (sensitivity). The experimental results have shown that the RF power ratio technique can eliminate the dispersion monitoring errors induced by the loss or gain of the optical channel. The thesis has also experimentally demonstrated that, by simply inserting a dispersion offset just before the photodetector within the monitoring module, this improved technique can monitor both the positive and negative CD caused by optical fibers and other optical components in WDM systems. The

experimental results have shown that the monitoring range can be greater than 1150 ps/nm and the sensitivity can be as high as 0.064 dB/ps/nm by selecting appropriate dispersion offsets and suitable RF frequencies. While the high RF power may induce high power penalty for baseband data, the low RF power cannot be measured accurately, resulting in high monitoring errors and small monitoring range. The investigations on the effects of the modulation index have revealed that the modulation index should be greater than 10% but less than 20% so as to acquire a larger monitoring range with a small power penalty (smaller than 1 dB). Moreover, an RF tone removal scheme is presented to reduce the power penalty. By adding two RF notch filters at the frequencies of RF tones at the baseband data receiver, it has been shown that the impairment induced by the two RF tones can be made small enough and acceptable for practical WDM systems even at high modulation index. The thesis has also investigated the monitoring errors induced by PMD and SPM. The investigations have shown that the use of a dispersion offset can effectively reduce the PMD-induced monitoring error, and the SPM may significantly affect the monitoring accuracy if the launched optical power is greater than +6 dBm.

Chapter 4 gives a detailed investigation and analysis of the impacts of other signal degradation effects such as PMD, SPM, XPM and chirp on RF tone based chromatic dispersion monitoring. In addition to CD, other optical impairments may also cause RF power variation, leading to CD monitoring error. Among those impairments, PMD is an important CD monitoring error source. Both theoretical and experimental studies have revealed that the RF power detection based CD monitoring technique may suffer a large monitoring error in the presence of PMD. A novel and practical DSB/SSB RF power ratio detection technique is proposed for suppressing the PMD

induced CD monitoring error. In the proposed CD monitoring scheme, one RF tone is added at the transmitter. The light is split into two branches in the monitoring module. A FBG filter which can remove one sideband is inserted before the photodetector of one branch. The DSB/SSB RF power ratio between the two branches is measured for dispersion monitoring. The experimental results have shown that the monitoring error induced by PMD can be eliminated by optically sideband filtering and DSB/SSB RF power ratio detection. Moreover, simulation results have demonstrated that this method could partially cancel the CD monitoring error induced by SPM and XPM effects when the accumulated CD is around zero. Furthermore, it is shown that if a dispersion offset is inserted in the CD monitoring module and two RF tones are used, the modulator chirp induced CD monitoring error can be considerably suppressed or eliminated. The impacts from other impairments such as SBS, SRS and XGM are also discussed in this chapter. In intensity modulated baseband optical transmission systems without SOAs, the impacts from these effects to CD monitoring are very small and negligible for the high frequency RF tones.

Chapter 5 investigates chromatic dispersion monitoring for DPSK systems. Adding an RF tone to the DPSK data and detecting its power together with the regenerated clock tone, a new dispersion monitoring method is proposed for DPSK systems. By utilizing the RF tone with different frequencies, flexible CD monitoring sensitivity and large range can be acquired. Experimental and simulation results have shown that the technique can significantly improve the CD monitoring capability compared with the one using the clock tone power only, especially the monitoring range. The RF tone induced power penalty to DPSK signal is also investigated. The impact of RF tone frequency on the power penalty shows that by simply selecting the RF frequency

close to half of the DPSK data-rate frequency, the RF tone induced power penalty to DPSK signal can be significantly suppressed without using any additional RF filter. Moreover, a new transmitter configuration is proposed which can simultaneously generate an RF tone together with DPSK signal using only a single DE-MZM. This new transmitter configuration is further extended to the application in optical label switching (OLS) systems. It is shown that this new transmitter can be used to generate a DPSK payload and a subcarrier label simultaneously. Simulation has been resorted to evaluate the transmission performance of the DPSK/SCM OLS system. Both DPSK payload and SCM label signals experience good BER performance. The simulation has shown that the SCM label can be exploited for CD monitoring as well. Simulation results have demonstrated that by measuring the RF power of both the SCM label and the clock tone, the CD monitoring range can be greatly improved compared with the one using the clock tone power only.

6.2 Recommendations for Future Work

Though a number of CD monitoring approaches have been reported and investigated based on different technologies recently, there are still a number of ways where the present work may be extended. In the following, some of these possibilities are summarized, which may be considered for further extending the research reported by us in this thesis.

In Chapter 4, a technique was proposed to suppress the CD monitoring error induced by PMD and chirp. Its performance was investigated theoretically and

experimentally. However, its application to suppressing the CD monitoring errors induced by SPM and XPM effects is only verified by simulations. Moreover, the technique cannot completely cancel the CD monitoring errors induced by SPM and XPM effects, and its effectiveness is affected by the residual CD. Therefore, an improved technique, which can fully suppress the CD monitoring errors induced by SPM and XPM effects for any accumulated dispersion values, needs to be studied. In [124] and [125], Ramos et al provided a closed expression of the frequency transfer function of SMF considering both CD and SPM effects. This analytical model may be used for exploring a new technique which can further suppress the CD monitoring errors induced by SPM and XPM effects. The experimental verification of this application is also required. Furthermore, the possibility of using an improved RF power based technique monitoring more parameters such as fiber nonlinearities will be explored.

The CD monitoring technique based on the power detection of RF tone and clock tone for DPSK systems has been presented in Section 5.2, where the DPSK signal is generated by a phase modulator. There is another means to generate DPSK signal using a Mach-Zehnder modulator (MZM) which is biased at the transmission null point with an alternating current (AC) coupled data stream [104]. However, due to the residual intensity modulation, the clock tone power of the DPSK signal generated by MZM is different from the one generated by a phase modulator. Therefore, it would be important to evaluate the generated RF power difference between two modulation methods and its induced CD monitoring errors. Moreover, it is necessary to study a technique to eliminate such CD monitoring errors. Taking the ratio of

clock tone power and RF tone power may be a possible solution and worthy of further studies.

Recently, RZ/CSRZ-DPSK, differential quadrature phase-shift keying (DQPSK) [126], and minimum-shift keying (MSK) [127] et al have been demonstrated as effective modulation formats to manage signal impairment and increase channel density or spectral efficiency. But their corresponding CD monitoring technique has not been explored yet. The feasibility of applying RF power techniques in those advanced modulation formats for CD monitoring may also be investigated and verified in the future. The investigation may help to find an optimal format independent CD monitoring approach.

Another aspect that could be interesting to study is the optical performance monitoring with all optical techniques. In this thesis, to detect the RF power of the pilot tone or clock tone, it is necessary to convert an optical signal to an electrical signal first. With the increasing channel bit-rate, the cost of high bandwidth electrical devices increases rapidly. Hence, optical performance monitoring methods in all optical domain may be valuable for next generation optical networks with high channel data-rates. As reviewed in Section 2.4.4, some techniques using optical nonlinear effects have been reported for CD monitoring. However, they can be used to monitor CD only and their CD monitoring sensitivity is low for NRZ signals. With the development of the fiber nonlinearity, the optical sampling technique for optical performance monitoring becomes possible [128]. Another future work is to investigate optical sampling technique which could reconstruct signal waveform in the optical domain. From the reconstructed waveform, not only CD, but also more

objectives such as OSNR and BER can be monitored without high bandwidth electrical devices.

Bibliography

[1] T. Li, "Advances in Optical Fiber Communications: An Historical Perspective," *Selected Areas in Communications, IEEE Journal on*, vol. 1, pp. 356-372, 1983.

[2] G. P. Agrawal, *Fiber-Optic Communication Systems*, 3rd ed. New York: Wiley-Interscience, 2002.

[3] IDC, "Worldwide Bandwidth End-User Forecast and Analysis, 2003-2007: More is Still Not Enough," Feb. 2003.

[4] http://www.lightreading.com/document.asp?doc_id=29062.

[5] http://www.telegeography.com/press/releases/2005-08-23.php.

[6] http://telephonyonline.com/iptv/news/BellSouth_VOD_costs_030706/.

[7] M. Yoneyama, Y. Miyamoto, T. Otsuji, A. Hirano, H. Kikuchi, T. Ishibashi, and H. Miyazawa, "Fully electrical 40-Gbit/s TDM system prototype and its application to 160-Gbit/s WDM transmission," in Proceedings Optical Fiber Communication Conference, 1999, and the International Conference on Integrated Optics and Optical Fiber Communication. OFC/IOOC '99. Technical Digest, 128-130 vol.3, 1999.

[8] P. J. Winzer, G. Raybon, and M. Duelk, "107-Gb/s optical ETDM transmitter for 100G Ethernet transport," in Proceedings Optical Communication, 2005. ECOC 2005. 31st European Conference on, 1-2 vol.6, 2005.

[9] A. I. Siahlo, A. T. Clausen, L. K. Oxenlowe, J. Seoane, and P. Jeppesen, "640 Gb/s OTDM transmission and demultiplexing using a NOLM with commercially available highly non-linear fiber," in Proceedings Lasers and Electro-Optics, 2005. (CLEO). Conference on, 883-885 Vol. 2, 2005.

[10] J.-X. Cai, D. G. Foursa, C. R. Davidson, Y. Cai, G. Domagala, H. Li, L. Liu, W. W. Patterson, A. N. Pilipetskii, M. Nissov, and N. S. Bergano, "A DWDM demonstration of 3.73 Tb/s over 11,000 km using 373 RZ-DPSK channels at 10 Gb/s," in Proceedings Optical Fiber Communications Conference, 2003. OFC 2003, PD22-P1-3 vol.3, 2003.

[11] Y.-S. Hurh, G.-S. Hwang, J.-Y. Jeon, K.-G. Lee, K.-W. Shin, S. S. Lee, K. Y. Yi, and J.-S. Lee, "1-Tb/s (100 × 12.4 Gb/s) transmission of 12.5-GHz-spaced ultradense WDM channels over a standard single-mode fiber of 1200 km," *Photonics Technology Letters, IEEE*, vol. 17, pp. 696-698, 2005.

[12] D. van den Borne, S. L. Jansen, E. Gottwald, P. M. Krummrich, G. D. Khoe, and H. de Waardt, "1.6-b/s/Hz Spectrally Efficient 40 × 85.6-Gb/s Transmission Over 1,700 km of SSMF Using POLMUX-RZ-DQPSK," in Proceedings Optical Fiber Communication Conference, 2006 and the 2006 National Fiber Optic Engineers Conference, 1-3, 2006.

[13] D. C. Kilper, R. Bach, D. J. Blumenthal, D. Einstein, T. Landolsi, L. Ostar, M. Preiss, and A. E. Willner, "Optical performance monitoring," *Lightwave Technology, Journal of*, vol. 22, pp. 294-304, 2004.

[14] I. P. Kaminow and T. Li, *Optical fiber telecommunications IV*, vol. B. Systems and impairments. San Diego: Academic Press, 2002.

[15] H. C. Ji, J. H. Lee, and Y. C. Chung, "Evaluation on system outage due to statistically distributed chromatic dispersion of optical fiber," in Proceedings Optical Fiber Communication (OFC 2004), Paper ThU1, 2004.

[16] H. C. Ji, J. H. Lee, and Y. C. Chung, "Evaluation on system outage probability due to temperature variation and statistically distributed chromatic dispersion of optical fiber," *Lightwave Technology, Journal of*, vol. 22, pp. 1893-1898, 2004.

[17] W. Hatton and M. Nishimura, "Temperature dependence of chromatic dispersion in single mode fibers," *Lightwave Technology, Journal of*, vol. 4, pp. 1552-1555, 1986.

[18] G. Keiser, *Optical fiber communications*, third ed. Boston: McGraw-Hill, 2000.

[19] P. Henry, "Lightwave primer," *Quantum Electronics, IEEE Journal of*, vol. 21, pp. 1862-1879, 1985.

[20] L. Gruner-Nielsen and B. Edvold, "Status and future promises for dispersion compensating fibres," in Proceedings Optical Communication, 2002. ECOC 2002. 28th European Conference on, 1-2, 2002.

[21] http://www.fujikura.co.jp/optde/pdf/20dcm06.pdf, "Slope compensation dispersion compensation fiber modules (SC-DCF module)."

[22] K. O. Hill and G. Meltz, "Fiber Bragg grating technology fundamentals and overview," *Lightwave Technology, Journal of*, vol. 15, pp. 1263-1276, 1997.

[23] C. R. Giles, "Lightwave applications of fiber Bragg gratings," *Lightwave Technology, Journal of*, vol. 15, pp. 1391-1404, 1997.

[24] A. D. Kersey, M. A. Davis, H. J. Patrick, M. LeBlanc, K. P. Koo, C. G. Askins, M. A. Putnam, and E. J. Friebele, "Fiber grating sensors," *Lightwave Technology, Journal of*, vol. 15, pp. 1442-1463, 1997.

[25] N. M. Litchinitser, B. J. Eggleton, and D. B. Patterson, "Fiber Bragg gratings for dispersion compensation in transmission: theoretical model and design criteria for nearly ideal pulse recompression," *Lightwave Technology, Journal of*, vol. 15, pp. 1303-1313, 1997.

[26] K. O. Hill, B. Malo, F. Bilodeau, D. C. Johnson, and J. Albert, "Bragg gratings fabricated in monomode photosensitive optical fiber by UV exposure through a phase mask," *Applied Physics Letters*, vol. 62, pp. 1035-1037, 1993.

[27] H. C. Ji, J. H. Lee, and Y. C. Chung, "System outage probability due to dispersion variation caused by seasonal and regional temperature variations," in Proceedings Optical Fiber Communication (OFC'05), 235-237, 2005.

[28] A. E. Willner, K.-M. Feng, S. Lee, J. Peng, and H. Sun, "Tunable compensation of channel degrading effects using nonlinearly chirped passive fiber Bragg gratings," *Selected Topics in Quantum Electronics, IEEE Journal of*, vol. 5, pp. 1298-1311, 1999.

[29] H. Ooi, K. Nakamura, Y. Akiyama, T. Takahara, T. Terahara, Y. Kawahata, H. Isono, and G. Ishikawa, "40-Gb/s WDM transmission with virtually imaged phased array (VIPA) variable dispersion compensators," *Lightwave Technology, Journal of*, vol. 20, pp. 2196-2203, 2002.

[30] "Agilent 86037C chromatic dispersion test solution, Product Overview," Agilent Technology.

[31] B. Christensen, J. Mark, G. Jacobsen, and E. Bodtker, "Simple dispersion measurment technique with high resolution," *Electronics Letters*, vol. 29, pp. 132, 1993.

[32] C. Peucheret, F. Liu, and R. J. S. Pedersen, "Measurement of small dispersion values in optical components," *Electronics Letters*, vol. 35, pp. 409-411, 1999.

[33] A. Sano, Y. Miyamoto, S. Kuwahara, and H. Toba, "Adaptive dispersion equalization by monitoring relative phase shift between spacing-fixed WDM signals," *Lightwave Technology, Journal of*, vol. 19, pp. 336-344, 2001.

[34] T. E. Dimmick, G. Rossi, and D. J. Blumenthal, "Optical dispersion monitoring technique using double sideband subcarriers," *Photonics Technology Letters, IEEE*, vol. 12, pp. 900-902, 2000.

[35] G. Rossi, T. E. Dimmick, and D. J. Blumenthal, "Optical performance monitoring in reconfigurable WDM optical networks using subcarrier multiplexing," *Lightwave Technology, Journal of*, vol. 18, pp. 1639-1648, 2000.

[36] Q. Yu, L.-S. Yan, Z. Pan, and A. E. Willner, "Chromatic dispersion monitor for WDM systems using vestigial-sideband optical filtering," in Proceedings Optical Fiber Communication Conference and Exhibit, 2002. OFC 2002, 197-199, 2002.

[37] Q. Yu, Z. Pan, L.-S. Yan, and A. E. Willner, "Chromatic dispersion monitoring technique using sideband optical filtering and clock phase-shift detection," *Lightwave Technology, Journal of*, vol. 20, pp. 2267-2271, 2002.

[38] A. Hirano, S. Kuwahara, Y. Miyamoto, and K. Murata, "Dispersion accommodation scheme comparing relative bit-phase of two SSB signals generated from spectrally filtered CS-RZ signal," *Electronics Letters*, vol. 38, pp. 580-582, 2002.

[39] S. M. R. M. Nezam, J. E. McGeehan, and A. E. Willner, "Chromatic dispersion monitoring using partial optical filtering and phase-shift detection of bit rate and doubled half bit rate frequency components," in Proceedings Optical Fiber Communication Conference, 2004. OFC 2004, 3 pp. vol.2, 2004.

[40] B. Fu and R. Hui, "Fiber chromatic dispersion and polarization-mode dispersion monitoring using coherent detection," *Photonics Technology Letters, IEEE*, vol. 17, pp. 1561-1563, 2005.

[41] F. Heismann, "Origin of clock-frequency components in NRZ-formatted optical signals," *Photonics Technology Letters, IEEE*, vol. 15, pp. 912-914, 2003.

[42] Z. Pan, Q. Yu, Y. Xie, S. A. Havstad, A. E. Willner, D. S. Starodubov, and J. Feinberg, "Chromatic dispersion monitoring and automated compensation for NRZ and RZ data using clock regeneration and fading without adding signaling," in Proceedings Optical Fiber Communication (OFC'01), WH5-1-WH5-3, 2001.

[43] T. Inui, T. Komukai, M. Nakazawa, K. Suzuki, K. R. Tamura, K. Uchiyama, and T. Morioka, "Adaptive dispersion slope equalizer using a nonlinearly chirped fiber Bragg grating pair with a novel dispersion detection technique," *Photonics Technology Letters, IEEE*, vol. 14, pp. 549-551, 2002.

[44] S.-M. Kim and C.-H. Lee, "The efficient clock-extraction methods of NRZ signal for chromatic dispersion monitoring," *Photonics Technology Letters, IEEE*, vol. 17, pp. 1100-1102, 2005.

[45] Y. Yamabayashi, M. Tomizawa, and Y. Sato, "Single-wavelength dispersion measurement for multiple-fiber section connected with narrow-band optical amplifiers," *Instrumentation and Measurement, IEEE Transactions on*, vol. 45, pp. 218-224, 1996.

[46] K. J. Park, C. J. Youn, J. H. Lee, and Y. C. Chung, "Performance comparisons of chromatic dispersion-monitoring techniques using pilot tones," *Photonics Technology Letters, IEEE*, vol. 15, pp. 873-875, 2003.

[47] M. N. Petersen, Z. Pan, S. Lee, S. A. Havstad, and A. E. Willner, "Online chromatic dispersion monitoring and compensation using a single inband subcarrier tone," *Photonics Technology Letters, IEEE*, vol. 14, pp. 570-572, 2002.

[48] S. Ohteru and N. Takachio, "Optical signal quality monitor using direct Q-factor measurement," *Photonics Technology Letters, IEEE*, vol. 11, pp. 1307-1309, 1999.

[49] N. Hanik, A. Gladisch, C. Caspar, and B. Strebel, "Application of amplitude histograms to monitor performance of optical channels," *Electronics Letters*, vol. 35, pp. 403-404, 1999.

[50] I. Shake and H. Takara, "Averaged Q-factor method using amplitude histogram evaluation for transparent monitoring of optical signal-to-noise ratio degradation in optical transmission system," *Lightwave Technology, Journal of*, vol. 20, pp. 1367-1373, 2002.

[51] I. Shake and H. Takara, "Chromatic dispersion dependence of asynchronous amplitude histogram evaluation of NRZ signal," *Lightwave Technology, Journal of*, vol. 21, pp. 2154-2161, 2003.

[52] I. Shake, H. Takara, and S. Kawanishi, "Simple measurement of eye diagram and BER using high-speed asynchronous sampling," *Lightwave Technology, Journal of*, vol. 22, pp. 1296-1302, 2004.

[53] H. Chen, A. W. Poon, and X.-R. Cao, "Transparent monitoring of rise time using asynchronous amplitude histograms in optical transmission systems," *Lightwave Technology, Journal of*, vol. 22, pp. 1661-1667, 2004.

[54] N. Kikuchi, S. Hayase, K. Sekine, and S. Sasaki, "Performance of chromatic dispersion monitoring using statistical moments of asynchronously sampled waveform histograms," *Photonics Technology Letters, IEEE*, vol. 17, pp. 1103-1105, 2005.

[55] S. D. Dods and T. B. Anderson, "Optical performance monitoring technique using delay tap asynchronous waveform sampling," in Proceedings Optical Fiber Communication Conference, 2006 and the 2006 National Fiber Optic Engineers Conference. Paper OThP5, 2006.

[56] A. R. Chraplyvy, R. W. Tkach, L. L. Buhl, and R. C. Alferness, "Phase modulation to amplitude modulation conversion of CW laser light in optical fibers," *Electronics Letters*, vol. 22, pp. 409-410, 1986.

[57] Z. Li, C. Lu, Y. Wang, and G. Li, "In-Service Signal Quality Monitoring and Multi-Impairment Discrimination Based on Asynchronous Amplitude Histogram Evaluation for NRZ-DPSK Systems," *Photonics Technology Letters, IEEE*, vol. 17, pp. 1998-2000, 2005.

[58] Z. Li and G. Li, "In-line performance monitoring for RZ-DPSK signals using asynchronous amplitude histogram evaluation," *Photonics Technology Letters, IEEE*, vol. 18, pp. 472-474, 2006.

[59] Z. Li and G. Li, "Chromatic dispersion and polarization-mode dispersion monitoring for RZ-DPSK signals based on asynchronous amplitude-histogram evaluation," *Lightwave Technology, Journal of*, vol. 24, pp. 2859-2866, 2006.

[60] P. S. Westbrook, B. J. Eggleton, T. Her, G. Raybon, and S. Hunsche, "Application of self-phase modulation and optical filtering to measurement of

residual chromatic dispersion," in Proceedings Optical Fiber Communication Conference and Exhibit, 2002. OFC 2002, 335-336, 2002.

[61] S. Li and D. V. Kuksenkov, "A novel dispersion monitoring technique based on four-wave mixing in optical fiber," *Photonics Technology Letters, IEEE*, vol. 16, pp. 942-944, 2004.

[62] T. Luo, C. Yu, Z. Pan, Y. Wang, J. E. McGeehan, M. Adler, and A. E. Willner, "All-optical chromatic dispersion monitoring of a 40-Gb/s RZ signal by measuring the XPM-generated optical tone power in a highly nonlinear fiber," *Photonics Technology Letters, IEEE*, vol. 18, pp. 430-432, 2006.

[63] S. Wielandy, M. Fishteyn, and B. Zhu, "Optical performance monitoring using nonlinear detection," *Lightwave Technology, Journal of*, vol. 22, pp. 784-793, 2004.

[64] A. Djupsjobacka, "Residual chirp in integrated-optic modulators," *Photonics Technology Letters, IEEE*, vol. 4, pp. 41-43, 1992.

[65] F. Koyama and K. Iga, "Frequency chirping in external modulators," *Lightwave Technology, Journal of*, vol. 6, pp. 87-93, 1988.

[66] X. Yi, C. Lu, F. Wei, W. D. Zhong, and Y. Wang, "A new method for chromatic dispersion measurement of WDM components using photonic microwave technique," *Transactions on Electronics, IEICE*, vol. E86-C, pp. 1359-1365, 2003.

[67] G. Meslener, "Chromatic dispersion induced distortion of modulated monochromatic light employing direct detection," *Quantum Electronics, IEEE Journal of*, vol. 20, pp. 1208-1216, 1984.

[68] M. Murakami, T. Imai, and M. Aoyama, "A remote supervisory system based on subcarrier overmodulation for submarine optical amplifier systems," *Lightwave Technology, Journal of*, vol. 14, pp. 671-677, 1996.

[69] L. Boivin and G. J. Pendock, "Receiver sensitivity for optically amplified RZ signals with arbitrary duty cycle," in Proceedings Optical Amplifiers and Their Applications (OAA'99), Paper ThB4, pp. 106-109, 1999.

[70] P. J. Winzer, M. Pfennigbauer, M. M. Strasser, and W. R. Leeb, "Optimum filter bandwidths for optically preamplified NRZ receivers," *Lightwave Technology, Journal of*, vol. 19, pp. 1263-1273, 2001.

[71] F. Devaux, Y. Sorel, and J. F. Kerdiles, "Simple measurement of fiber dispersion and of chirp parameter of intensity modulated light emitter," *Lightwave Technology, Journal of*, vol. 11, pp. 1937-1940, 1993.

[72] Y. Hamazumi and M. Koga, "Transmission capacity of optical path overhead transfer scheme using pilot tone for optical path network," *Lightwave Technology, Journal of*, vol. 15, pp. 2197-2205, 1997.

[73] K.-P. Ho and J. M. Kahn, "Methods for crosstalk measurement and reduction in dense WDM systems," *Lightwave Technology, Journal of*, vol. 14, pp. 1127-1135, 1996.

[74] E. Kong, F. Tong, K. P. Ho, L. K. Chen, and C. K. Chan, "Pilot-tone based optical-path supervisory scheme for optical cross-connects," *Electronics Letters*, vol. 35, pp. 1481-1483, 1999.

[75] E. Kong, F. Tong, K.-P. Ho, L.-K. Chen, and C.-K. Chan, "An optical-path supervisory scheme for optical cross-connects using pilot-tones," in Proceedings Lasers and Electro-Optics, 1999. CLEO/Pacific Rim '99. The Pacific Rim Conference on, 1281-1282 vol.4, 1999.

[76] K.-U. Chu, C.-H. Lee, and S.-Y. Shin, "Scalable optical-path supervisory scheme using pilot tones and channel equalisers," *Electronics Letters*, vol. 36, pp. 817-818, 2000.
[77] F. Heismann, M. T. Fatehi, S. K. Korotky, and J. J. Veselka, "Signal tracking and performance monitoring in multi-wavelength optical networks," in Proceedings Optical Communication, 1996. ECOC '96. 22nd European Conference on, 47-50 vol.3, 1996.
[78] http://www.vpisystems.com.
[79] http://www.omniyig.com, "MR2661D Band Reject Yig Filter datasheet."
[80] E. L. Goldstein, L. Eskildsen, C. Lin, and Y. Silberberg, "Polarization statistics of crosstalk-induced noise in transparent lightwave networks," *Photonics Technology Letters, IEEE*, vol. 7, pp. 1345-1347, 1995.
[81] H. Schmuck, "Effect of polarisation-mode-dispersion in fibre-optic millimetre-wave systems," *Electronics Letters*, vol. 30, pp. 1503-1504, 1994.
[82] M.-S. Kao and J. Wu, "Effect of polarization mode dispersion on a coherent optical system with pilot carrier," *Lightwave Technology, Journal of*, vol. 11, pp. 303-308, 1993.
[83] R. Hui, C. Allen, and K. Demarest, "PMD-insensitive SCM optical receiver using polarization diversity," *Photonics Technology Letters, IEEE*, vol. 14, pp. 1632-1634, 2002.
[84] J. Capmany, B. Ortega, A. Martinez, D. Pastor, M. Popov, and P. Y. Fonjallaz, "Multiwavelength single sideband modulation for WDM radio-over-fiber systems using a fiber grating array tandem device," *Photonics Technology Letters, IEEE*, vol. 17, pp. 471-473, 2005.
[85] J. Capmany, D. Pastor, P. Munoz, B. Ortega, S. Sales, and A. Martinez, "Multiwavelength optical SSB generation for dispersion mitigation in WDM fibre radio systems using AWG multiplexer," *Electronics Letters*, vol. 38, pp. 1194-1196, 2002.
[86] L. Meflah, B. Thomsen, J. Mitchell, and P. Bayvel, "Chromatic dispersion monitoring of a multi-channel 40 Gbit/s system for dynamically reconfigurable networks," in Proceedings Optical Communication, 2005. ECOC 2005. 31st European Conference on, 935-936 vol.4, 2005.
[87] S. M. R. M. Nezam, Y.-W. Song, C. Yu, J. E. McGeehan, A. B. Sahin, and A. E. Willner, "First-order PMD monitoring for NRZ data using RF clock regeneration techniques," *Lightwave Technology, Journal of*, vol. 22, pp. 1086-1093, 2004.
[88] K. J. Park, J. H. Lee, C. J. Youn, and Y. C. Chung, "A simultaneous monitoring technique for polarization-mode dispersion and group-velocity dispersion," in Proceedings Optical Fiber Communication Conference and Exhibit, 2002. OFC 2002, 199-200, 2002.
[89] I. P. Kaminow and T. Li, *Optical fiber telecommunications IV*, vol. A. Components. San Diego: Academic Press, 2002.
[90] http://products.jdsu.com/assets/public/pdf/CQF935_708_20030312.pdf.
[91] K. J. Park, C. J. Youn, J. H. Lee, and Y. C. Chung, "Chromatic dispersion monitoring technique in WDM network," in Proceedings Optical Fiber Communication Conference and Exhibit, 2002. OFC 2002, 735-737, 2002.
[92] K. J. Park, C. J. Youn, J. H. Lee, and Y. C. Chung, "Effect of self-phase modulation on group-velocity dispersion measurement technique using PM-AM conversion," *Electronics Letters*, vol. 38, pp. 1247-1248, 2002.

[93] C. Youn, "Effects of SPM and PMD on chromatic dispersion monitoring techniques using pilot tones," in Proceedings Optical Fiber Communications Conference, 2003. OFC 2003, 403-404 vol.1, 2003.

[94] G. L. Li and P. K. L. Yu, "Optical intensity modulators for digital and analog applications," *Lightwave Technology, Journal of*, vol. 21, pp. 2010-2030, 2003.

[95] H. Kim and A. H. Gnauck, "Chirp characteristics of dual-drive Mach-Zehnder modulator with a finite DC extinction ratio," *Photonics Technology Letters, IEEE*, vol. 14, pp. 298-300, 2002.

[96] H. Nagata, N. F. O'Brien, W. R. Bosenberg, G. L. Reiff, and K. R. Voisine, "DC-Voltage-induced thermal shift of bias point in $LiNbO_3$ optical Modulators," *Photonics Technology Letters, IEEE*, vol. 16, pp. 2460-2462, 2004.

[97] P. Jiang and A. C. O'Donnell, "$LiNbO_3$ Mach-Zehnder modulators with fixed negative chirp," *Photonics Technology Letters, IEEE*, vol. 8, pp. 1319-1321, 1996.

[98] A. Liu, G. J. Pendock, and R. S. Tucker, "Chromatic dispersion monitoring using time-multiplexed in-band RF tones," in Proceedings Optical Fiber Communication (OFC'05), Paper OThH6, 2005.

[99] Y. Aoki, K. Tajima, and I. Mito, "Input power limits of single-mode optical fibers due to stimulated Brillouin scattering in optical communication systems," *Lightwave Technology, Journal of*, vol. 6, pp. 710-719, 1988.

[100] H. S. Chung, S. K. Shin, H. G. Woo, and Y. C. Chung, "Effects of stimulated Raman scattering on pilot-tone based WDM supervisory technique," in Proceedings Optical Fiber Communication (OFC'00), 185-187 vol.2, 2000.

[101] Z. Gao, M. Chen, J. Jin, and S. Xie, "Theoretical and experimental analysis of the effect of stimulated Raman scattering on pilot-tone detection technique in dense wavelength-division multiplexing transmission system," *Optical Engineering*, vol. 44, pp. 015001-1 - 015001-5, 2005.

[102] H. S. Chung, S. K. Shin, K. J. Park, H. G. Woo, and Y. C. Chung, "Effects of stimulated Raman scattering on pilot-tone-based WDM supervisory technique," *Photonics Technology Letters, IEEE*, vol. 12, pp. 731-733, 2000.

[103] Y. Sun, A. A. M. Saleh, J. L. Zyskind, D. L. Wilson, A. K. Srivastava, and J. W. Sulhoff, "Time dependent perturbation theory and tones in cascaded erbium-doped fiber amplifier systems," *Lightwave Technology, Journal of*, vol. 15, pp. 1083-1087, 1997.

[104] A. H. Gnauck and P. J. Winzer, "Optical phase-shift-keyed transmission," *Lightwave Technology, Journal of*, vol. 23, pp. 115-130, 2005.

[105] C. Xu, X. Liu, and X. Wei, "Differential phase-shift keying for high spectral efficiency optical transmissions," *Selected Topics in Quantum Electronics, IEEE Journal of*, vol. 10, pp. 281-293, 2004.

[106] X. Wei, A. H. Gnauck, D. M. Gill, X. L. A.-X. Liu, U.-V. K. A.-U.-V. Koc, S. C. A.-S. Chandrasekhar, G. R. A.-G. Raybon, and J. L. A.-J. Leuthold, "Optical $\pi/2$-DPSK and its tolerance to filtering and polarization-mode dispersion," *Photonics Technology Letters, IEEE*, vol. 15, pp. 1639-1641, 2003.

[107] U.-V. Koc and X. Wei, "Combined effect of polarization-mode dispersion and chromatic dispersion on strongly filtered $\pi/2$-DPSK and conventional DPSK," *Photonics Technology Letters, IEEE*, vol. 16, pp. 1588-1590, 2004.

[108] T. Miyano, M. Fukutoku, K. Hattori, and H. Ono, "Suppression of degradation induced by SPM/XPM + GVD in WDM transmission using a bit synchronous

intensity modulated DPSK Signal," in Proceedings OptoElectronics and Communication Conference (OECC 2000), 580-581, 2000.

[109] N. Liu, W. D. Zhong, P. Shum, C. Lu, and Y. X. Wang, "Improved chromatic dispersion monitoring technique," *Optics Communications*, vol. 259, pp. 553-561, 2006.

[110] N. Liu, W.-D. Zhong, Y. J. Wen, C. Lu, L. Cheng, and Y. Wang, "PMD and chirp effects suppression in RF tone-based chromatic dispersion monitoring," *Photonics Technology Letters, IEEE*, vol. 18, pp. 673-675, 2006.

[111] Z. Pan, Y. Wang, Y. Song, R. Motaghian, S. Havstad, and A. E. Willner, "Monitoring chromatic dispersion and PMD impairments in optical differential phase shift-keyed (DPSK) systems," in Proceedings Optical Fiber Communication (OFC'03), 402-403 vol.1, 2003.

[112] S. B. Jun, H. Kim, P. K. J. Park, J. H. Lee, and Y. C. Chung, "Pilot-tone-based WDM monitoring technique for DPSK systems," *Photonics Technology Letters, IEEE*, vol. 18, pp. 2171-2173, 2006.

[113] J. J. O. Pires and J. R. F. de Rocha, "Performance analysis of DPSK direct detection optical systems in the presence of interferometric intensity noise," *Lightwave Technology, Journal of*, vol. 10, pp. 1722-1730, 1992.

[114] Y. J. Wen, A. Nirmalathas, and D.-S. Lee, "RZ/CSRZ-DPSK and chirped NRZ signal generation using a single-stage dual-electrode Mach-Zehnder modulator," *Photonics Technology Letters, IEEE*, vol. 16, pp. 2466-2468, 2004.

[115] G. H. Smith, D. Novak, and Z. Ahmed, "Technique for optical SSB generation to overcome dispersion penalties in fibre-radio systems," *Electronics Letters*, vol. 33, pp. 74-75, 1997.

[116] D. J. Blumenthal, B.-E. Olsson, G. Rossi, T. E. Dimmick, L. Rau, M. Masanovic, O. Lavrova, R. Doshi, O. Jerphagnon, J. E. Bowers, V. Kaman, L. A. Coldren, and J. Barton, "All-optical label swapping networks and technologies," *Lightwave Technology, Journal of*, vol. 18, pp. 2058-2075, 2000.

[117] X. Liu, Y. Su, X. Wei, J. Leuthold, and R. C. Giles, "Optical-label switching based on DPSK/ASK modulation format with balanced detection for DPSK Payload," in Proceedings European Conference on Optical Communication (ECOC'03), 306-307, 2003.

[118] N. Chi, L. Xu, J. Zhang, P. V. Holm-Nielsen, C. Peucheret, C. Mikkelsen, H. Ou, J. Seoane, and P. Jeppesen, "Orthogonal optical labeling based on a 40 Gbit/s DPSK payload and a 2.5 Gbit/s IM label," in Proceedings Optical Fiber Communication (OFC'04), Paper FO6, 2004.

[119] T. Flarup, C. Peucheret, J. J. V. Olmos, Y. Geng, J. Zhang, I. T. Monroy, and P. Jeppesen, "Labeling of 40 Gbit/s DPSK payload using in-band subcarrier multiplexing," in Proceedings Optical Fiber Communication (OFC'05), Paper OWB7, 2005.

[120] I. T. Monroy, J. J. V. Olmos, M. G. Larrode, T. Koonen, and C. D. Jimenez, "In-band 16-QAM and multi-carrier SCM modulation to label DPSK payload signals for IP packet routing," *Optics Express*, vol. 14, pp. 1000-1005, 2006.

[121] I. T. Monroy, J. J. V. Olmos, A. M. J. Koonen, F. M. Huijskens, H. d. Waardt, and G.-D. Khoe, "Optical label switching by using differential phase shift keying and in-band subcarrier multiplexing modulation format," *Optical Engineering*, vol. 43, pp. 1476-1477, 2004.

[122] W.-R. Peng, Y.-C. Lu, J.-H. Chen, and S. Chi, "ASK/RZ-DPSK labelled signal generation using only one Mach-Zehnder modulator," in Proceedings European Conference on Optical Communication (ECOC'05), 105-106, 2005.

[123] W.-R. Peng, Y.-C. Lu, J. Chen, and S. Chi, "Encoding ASK labeled CSRZ-DPSK payload by using only one dual-drive Mach-Zehnder modulator with enhanced label performance," *Photonics Technology Letters, IEEE*, vol. 17, pp. 2227-2229, 2005.

[124] F. Ramos, J. Marti, V. Polo, and J. M. Fuster, "On the use of fiber-induced self-phase modulation to reduce chromatic dispersion effects in microwave/millimeter-wave optical systems," *Photonics Technology Letters, IEEE*, vol. 10, pp. 1473-1475, 1998.

[125] F. Ramos and J. Marti, "Frequency transfer function of dispersive and nonlinear single-mode optical fibers in microwave optical systems," *Photonics Technology Letters, IEEE*, vol. 12, pp. 549-551, 2000.

[126] H. G. Weber, S. Ferber, M. Kroh, C. Schmidt-Langhorst, R. Ludwig, V. Marembert, C. Boerner, F. Futami, S. Watanabe, and C. Schubert, "Single channel 1.28 Tbit/s and 2.56 Tbit/s DQPSK transmission," in Proceedings Optical Communication, 2005. ECOC 2005. 31st European Conference on, 3-4 vol.6, 2005.

[127] J. Mo, Y. J. Wen, Y. Dong, Y. Wang, and C. Lu, "Optical minimum-shift keying format and its dispersion tolerance," in Proceedings Optical Fiber Communication Conference, 2006 and the 2006 National Fiber Optic Engineers Conference. OFC 2006, 3 pp., 2006.

[128] M. Westlund, P. A. Andrekson, H. Sunnerud, J. Hansryd, and J. Li, "High-performance optical-fiber-nonlinearity-based optical waveform monitoring," *Lightwave Technology, Journal of*, vol. 23, pp. 2012-2022, 2005.

Author's Related Publications

Journal Papers:

1. N. Liu, W.D. Zhong, P. Shum, C. Lu, and Y. Wang, "Improved chromatic dispersion monitoring technique," Optics Communications, vol. 259, pp. 553-561, March 2006 (related to Chapter 3).

2. N. Liu, W.D. Zhong, Y.J. Wen, C. Lu, L. Cheng, and Y. Wang, "PMD and chirp effects suppression in RF tone based chromatic dispersion monitoring," *Photonics Technology Letters, IEEE*, vol. 18, pp. 673-675, March 2006 (related to Chapter 4).

3. N. Liu, W.D. Zhong, and Y.J. Wen, "Simultaneous differential phase-shift keying payload and subcarrier multiplexed label generation using a single modulator and its application to dispersion monitoring," *Optical Engineering*, vol. 46, pp. 095010 1-5, September 2007. (related to Chapter 5).

4. N. Liu, W.D. Zhong, Y.J. Wen, and Z. Li, "New transmitter configuration for subcarrier multiplexed DPSK systems and its applications to chromatic dispersion monitoring," *Optics Express*, vol. 15, pp. 839-844, February 2007 (related to Chapter 5).

Conference Papers:

1. N. Liu, W.D. Zhong, P. Shum, C. Lu, and Y. Wang, "Investigation of an improved chromatic dispersion monitoring technique," in Proc. International Conference on Optical Communications and Networks (ICOCN 2004), 2004 (related to Chapter 3).

2. N. Liu, W.D. Zhong, X. Yi, Y. Wang, and C. Lu, "Chromatic dispersion monitoring using the power ratio of two RF tones with a dispersion offset," in

Proc. Optical Fiber Communication (OFC 2004), 2004, Paper MF81 (related to Chapter 3).

3. N. Liu, W.D. Zhong, L. Cheng, Y.J. Wen, Y. Wang, and C. Lu, "Suppression of PMD and chirp effects in chromatic dispersion monitoring," in Proc. Asia-Pacific Optical Communications (APOC 2005), 2005, Paper 6021-06 (related to Chapter 4).

4. N. Liu, W.D. Zhong, Y.J. Wen, and Y. Wang, "PMD-insensitive chromatic dispersion monitoring," in Proc. Eur. Conf. Optical Communication (ECOC 2005), 2005, pp. 503-504, Paper We4.P.001 (related to Chapter 4).

5. N. Liu, W.D. Zhong, Y.J. Wen, “Simultaneous generation of DPSK and RF tone using a single DE-MZM for CD monitoring,” in Proc. OptoElectronics and Communication Conference (OECC 2006), 2006, Paper 7C2-4 (related to Chapter 5).